United States
Environmental Protection
Agency

Atmospheric Research and
Exposure Assessment Laboratory
Research Triangle Park, NC 27711

EPA/600/3-90/025
January 1990

Research and Development

PROJECT REPORT

FLOW AND DISPERSION OF POLLUTANTS WITHIN TWO-DIMENSIONAL VALLEYS

Summary Report on Joint Soviet-American Study

EPA/600/3-90/025
January 1990

FLOW AND DISPERSION OF POLLUTANTS WITHIN TWO-DIMENSIONAL VALLEYS

Summary Report on Joint Soviet-American Study

by

LEON H. KHURSHUDYAN

Main Geophysical Observatory
Leningrad, U.S.S.R.

WILLIAM H. SNYDER

Atmospheric Sciences Modeling Division
Atmospheric Research and Exposure Assessment Laboratory
U.S. Environmental Protection Agency
Research Triangle Park, NC 27711

IGOR V. NEKRASOV

Institute of Mechanics
State University of Moscow
Moscow, U.S.S.R.

ROBERT E. LAWSON, Jr.

ROGER S. THOMPSON
and
FRANCIS A. SCHIERMEIER

Atmospheric Sciences Modeling Division
Atmospheric Research and Exposure Assessment Laboratory
U.S. Environmental Protection Agency
Research Triangle Park, NC 27711

Atmospheric Research and Exposure Assessment Laboratory
Office of Research and Development
U.S. Environmental Protection Agency
Research Triangle Park, NC 27711

DISCLAIMER

This report has been reviewed by the Atmospheric Research and Exposure Assessment Laboratory, U.S. Environmental Protection Agency, and the Main Geophysical Observatory, Leningrad, U.S.S.R., and approved for publication. Mention of trade names or commercial products does not constitute endorsement or recommendation for use.

William H. Snyder and Robert E. Lawson, Jr. are physical scientists and Francis A. Schiermeier is a meteorologist in the Atmospheric Sciences Modeling Division, U.S. Environmental Protection Agency, Research Triangle Park, NC. They are on assignment from the National Oceanic and Atmospheric Administration, U.S. Department of Commerce.

PREFACE

In May 1972, the governments of the United States of America and the Union of Soviet Socialist Republics signed an Agreement on Cooperation in the Field of Environmental Protection. This cooperation was aimed at solving the most important aspects of the problems of the environment and was devoted to working out measures to prevent pollution, to study pollution and its effect on the environment, and to develop the basis for controlling the impact of human activities on nature.

For implementation of this Agreement, a United States/Soviet Union Joint Committee on Cooperation in the Field of Environmental Protection was established, consisting of ten Working Groups. Under the proviso for exchange of scientists, experts, and research scholars, two Soviet scientists have spent four months conducting joint research in the Fluid Modeling Facility of the EPA Atmospheric Research and Exposure Assessment Laboratory in Research Triangle Park, North Carolina. The scientists represented the A. I. Voeikov Main Geophysical Observatory in Leningrad and Moscow State University in Moscow.

The research activities reported herein were conducted under the auspices of the United States/Soviet Union Working Group 02.01-10 on Air Pollution Modeling, Instrumentation, and Measurement Methodology; Project 02.01-11 on Air Pollution Modeling and Standard Setting.

Alexander S. Zaitsev	Francis A. Schiermeier
Soviet Union Co-Chairman	United States Co-Chairman
Working Group 02.01-10	Working Group 02.01-10

ABSTRACT

Wind-tunnel experiments and a theoretical model concerning the flow structure and pollutant diffusion over two-dimensional valleys of varying aspect ratio are described and compared. Three model valleys were used, having small, medium, and steep slopes. Measurements of mean and turbulent velocity fields were made upstream, within, and downwind of each of these valleys. Concentration distributions were measured downwind of tracer sources placed at an array of locations within each of the valleys. The data are displayed as maps of terrain amplification factors, defined as the ratios of maximum ground-level concentrations in the presence of the valleys to the maxima observed from sources of the same height located in flat terrain. Maps are also provided showing the distance to locations of the maximum ground-level concentrations. The concentration patterns are interpreted in terms of the detailed flow structure measured in the valleys. These data were also compared with results of a mathematical model for treating flow and dispersion over two-dimensional complex terrain. This model used the wind-tunnel measurements to generate mean flow fields and eddy diffusivities, and these were applied in the numerical solution of the diffusion equation. Measured concentration fields were predicted reasonably well by this model for the valley of small slope and somewhat less well for the valley of medium slope. Because flow separation was observed within the steepest valley, the model was not applied in this case.

CONTENTS

PREFACE iii

ABSTRACT iv

FIGURES vi

TABLES vii

ACKNOWLEDGEMENTS viii

1. INTRODUCTION 1

2. APPARATUS, INSTRUMENTATION AND MEASUREMENT TECHNIQUES 5

   2.1 Wind Tunnel 5
   2.2 The Models 5
   2.3 Velocity Measurements 6
   2.4 The Source 17
   2.5 Concentration Measurements 21

3. PRESENTATION AND DISCUSSION OF EXPERIMENTAL RESULTS 26

   3.1 Boundary-Layer Structure in Flat Terrain 26
      3.1.1 Velocity 26
      3.1.2 Concentration 26
   3.2 Flow Structure over the Valleys 33
   3.3 Concentration Measurements in the Valleys 46

4. NUMERICAL MODEL AND COMPARISONS WITH EXPERIMENTAL RESULTS 57

   4.1 Calculations of Dispersion over Flat Terrain 57
   4.2 Calculations of Dispersion near Valleys 63
      4.2.1 Generation of flow fields 63
      4.2.2 Calculation of eddy diffusivities 69
      4.2.3 Calculation of pollutant spreading and terrain amplification factors 72

5. CONCLUSIONS 79

6. REFERENCES 81

FIGURES

Number		Page
1.	Construction details of models.	7
2.	Shapes of valleys.	10
3.	Typical calibration curve of hot-wire anemometer.	13
4.	Sketch of pulsed-wire anemometer.	14
5.	Typical calibration curve of pulsed-wire anemometer.	16
6.	Diagram of wind-tunnel setup, source, and flow-measurement apparatus.	18
7.	Concentration profiles measured downwind of sources with different flow rates. H_s = 29 mm, x = 234 mm, U_∞ = 4 m s^{-1}.	19
8.	Details of spring-loaded sampling rake.	22
9.	Surface longitudinal concentration profile measured with spring-loaded sampling rake.	23
10.	Calibration of flame ionization detectors.	24
11.	Structure of the flat-terrain boundary layer.	27
12.	Longitudinal surface concentration profiles in flat terrain.	31
13.	Maximum ground-level concentration as a function of source height.	32
14.	Surface longitudinal concentration profile in flat terrain, scaled up 1250:1 from wind tunnel measurements, compared with Gaussian plume predictions using Pasquill-Gifford stabilities C and D and Hosker-Gifford-Smith stability D with z_o = 40 cm. H_s = 146 m (177 mm in wind tunnel).	34
15.	Longitudinal mean velocity profiles over the valleys.	35
16.	Longitudinal turbulence intensity profiles over the valleys.	36
17.	Reynolds stress distributions over the valleys.	37
18.	Streamline patterns derived from experimental measurements over the valleys.	39
19.	Probability density distribution of longitudinal velocity fluctuations measured at half the valley height above valley 3.	40
20.	Probability density distributions of longitudinal velocity fluctuations at various elevations above the center of valley 3.	42
21.	Probability density distributions of longitudinal velocity fluctuations at various elevations above the center of valley 5.	43
22.	Probability density distributions of longitudinal velocity fluctuations at various elevations above the center of valley 8.	44

23. Comparison of surface concentration profiles from sources placed within the valleys with one from a source of the same height in flat terrain. $H_s = h$. 47

24. Comparison of surface concentration profiles from sources placed within the valleys with one from a source of the same height in flat terrain. $H_s = h/2$. 50

25. Contours of constant terrain amplification factor derived from experimental measurements. 52

26. Distance in valley depths from the valley center to the location of maximum ground-level concentration. Flat-terrain values are indicated as dotted lines. 54

27. Lateral concentration distributions measured 6 H_s downwind of stacks of height h/4 placed in the center of each of the three valleys. 55

28. Vertical profile of eddy diffusivity k_m in flat terrain. 60

29. Growth of lateral plume width in flat terrain: comparison with interpolation (Eq. 11). 62

30. Dependence of χ_{mx} on source height H_s in flat terrain. 64

31. Dependence of x_{mx} on source height H_s in flat terrain. 65

32. Relation between χ_{mx} and x_{mx} in flat terrain. 66

33. Vertical profile of diffusivity k_m over valley 8. 73

34. Vertical profile of diffusivity k_m over valley 5. 74

35. Contours of constant terrain amplification factor derived from calculations. 77

TABLES

Number Page

1. Values of mean longitudinal velocity (m s^{-1}) near valley 8. 70

2. Values of mean longitudinal velocity (m s^{-1}) near valley 5. 70

3. Values of TAF for sources near valley 8. 76

4. Values of TAF for sources near valley 5. 76

ACKNOWLEDGEMENTS

The cooperation of the entire staff at the Fluid Modeling Facility is gratefully acknowledged. The authors are particularly indebted to Mr. Paul K. Bookman (NSI Technology Services Corporation) for the construction and innumerable installations of the model valleys, to Mr. Michael S. Shipman (NSI) for his innovative programming for the collection and processing of experimental data as well as for his assistance in running the numerical model, and to Mr. Lewis A. Knight, whose years of travail came to fruition as an operational automated instrument carriage in the wind tunnel for the collection of experimental data.

The authors especially express their gratitude to Ms. Anna L. Cook for her continuous help in innumerable ways and for preparing the manuscripts.

1. INTRODUCTION

This report presents preliminary results of the Joint Soviet-American Work Program for studying air flow and dispersion of pollutants released within two-dimensional valleys. This study is a natural complement to earlier work by Khurshudyan *et al.* (1981, hereafter referred to as RUSHIL), wherein similar measurements were made of the flow structure and dispersion of pollutants over two-dimensional hills. An extensive data set was collected in a wind tunnel on the flow structure and concentration fields resulting from sources placed within three valleys with different width-to-depth ratios. In addition to furthering basic understanding of the physics, one of the main purposes of the experimental study was to test the performance of a diffusion model for calculating maximum ground-level concentrations (glcs) resulting from elevated point sources placed within the valleys. The work was conducted within the Fluid Modeling Facility of the U.S. Environmental Protection Agency in Research Triangle Park, NC.

Investigations of air pollution transport and dispersion in the atmosphere within valleys are essential for the protection of air quality, because industrial enterprises and other sources of air pollution locate predominantly within valleys. Although much effort has already been expended in elucidating this problem and establishing guidelines for industry and air pollution control organizations to follow in the prediction of concentrations from sources located within complex terrain, the problem is far from solved. Given the preponderance of populations and industry located within valleys, the lack of concerted research efforts on flow structure and dispersion within valleys is rather surprising, particularly in comparison with the efforts expended on flow and dispersion over hills.

A series of recent (and continuing) field experiments by the U.S Department of Energy, called the ASCOT program (Atmospheric Studies in COmplex Terrain), has focused primarily on the within-valley flow structure under strongly stratified ambient conditions, where the cold air mass within the valley decouples from the flow aloft (see, for example, Porch *et al.*, 1989). Under such conditions, a pollutant released within the valley is transported and diffused within the gravity-driven flow down the valley axis. The basic physics of the problem studied herein are completely different. The problem considered is the atmospheric flow in a direction perpendicular to the axis of a very long (two-dimensional) valley, where the approaching flow is neutrally

stratified and the stratification of the air mass within the valley itself is of no consequence. We imagine the case where a relatively flat plain is "cut" by a river valley (as opposed to a valley formed between two parallel ridges). Whereas the stratified-flow problem has considerable potential for effecting large surface concentrations of pollutants, study of the current neutral-flow problem is not without merit; as will be seen later, the presence of a valley can result in rather large increases in maximum surface concentrations over those that would be observed from the same source (and the same approaching wind conditions) in otherwise flat terrain. The current results suggest that the increase in concentration may range from more than 100% for a gently sloped valley to approximately 1400% for a steep-sloped valley!

We are not aware of any field studies designed or conducted to examine the problem posed above. Mathematical models designed to predict concentrations under such conditions are sparse. One recent model for application to light-and-variable wind conditions and complex boundaries is WYNDvalley (Harrison, 1987; 1988). For regulatory applications, the U.S. Environmental Protection Agency (EPA) does not currently recommend other than screening techniques to deal with sources located in complex terrain. Recent research efforts have been concentrated on flow and dispersion around hills (see for example, Strimaitis *et al.*, 1987). The Complex Terrain Dispersion Model (CTDM) has been released by EPA (Paine *et al.*, 1987) to the user community. In the Soviet Union, however, several theoretical models have been developed: (1) a numerical boundary-layer model for flow over complex terrain coupled with the numerical solution of the diffusion equation (Berlyand and Genikhovich, 1971; Berlyand *et al.*, 1983; Berlyand *et al.*, 1987), (2) a diffusion model in quasi-potential flow (Berlyand, 1975), and (3) the model used in the present study (Berlyand *et al.*, 1975). Practical recommendations for the estimation of air pollution levels in complex terrain in the U.S.S.R. are based upon the predictions of these models, some field studies, and laboratory studies (primarily the previous RUSHIL study). The new Soviet regulatory document, which specifies air pollutant calculation techniques (Hydromet State Committee, 1987), provides estimates of terrain amplification factors for valleys that are generally close to values obtained in the present study.

The primary results of our study are presented in terms of terrain amplification factors (TAFs), defined as the ratios of maximum ground-level concentrations in the presence of the valleys to the maximum glcs from sources

of the same height in the absence of the valleys (in flat terrain). This definition does not involve the locations of the maximum glcs; these maxima will generally occur at very different downwind distances from the source in the two situations (with and without the valley), but it is only the values of the maxima which are compared, wherever they occur. In the U.S.S.R., the TAF is used directly in the regulatory framework. The U.S. EPA, on the other hand, uses a related "excess concentration"; it is related to the TAF through the additive factor of unity; that is, a "zero" excess concentration is equivalent to a TAF of 1.0, and a 40% excess concentration is equivalent to a TAF of 1.4 (EPA, 1985).

Following the lead of Lawson *et al.* (1989), we present the primary results as contour plots of constant TAF. This allows the further introduction of "windows" of excess concentration (Hunt *et al.*, 1979). If a source is far enough upstream of the valley and the pollutant is released at low level, the maximum glc will occur upstream of the valley, so that the effect of the valley will be negligible. If the source is tall enough, the maximum glc will occur far downstream of the valley, so that, again, the effect of the valley will be negligible. If pollutants are released within the valley, however, the TAF will generally exceed unity, and its value will depend upon the source location within the valley. Hence, a region or "window" will exist such that pollutants emitted within that window will result in "excessive" glcs.

Recent fluid modeling studies (Snyder and Britter, 1987; Snyder, 1983; Castro and Snyder, 1982; Khurshudyan *et al.*, 1981), have indicated that increases in concentration (TAFs as large as 15) can result from placement of sources in the vicinity of hills. Lawson *et al.* (1989) have presented "windows" of excess concentration for typical shapes of two- and three-dimensional hills that extended as far as 10 to 15 hill heights upstream and downstream of the hills. The purpose of the current study was to determine to what extent valleys might influence maximum glcs, that is, to establish values and windows of excess concentration for typical valley shapes that might be found in the real world. The valleys chosen were two-dimensional shapes with three different aspect ratios, $n = a/h = 3$, 5, and 8, where a is the valley half-width, and h is the valley depth (height). The valleys will hereafter be referred to according to their aspect ratio; that is, as valley 3, valley 5, and valley 8 for $n = 3$, 5, and 8, respectively. These valley shapes were chosen to represent a fairly typical range of realistic valley shapes. The

maximum slopes were 10° (valley 8), 16° (valley 5), and 26° (valley 3). As will be shown later, the flow structure in these valleys differed rather dramatically from one to the next. In valley 8, the flow did not separate, but nevertheless, the influence of the valley on the TAFs was significant. In valley 3, the flow clearly separated on the upstream slope, and a mean recirculation region was formed inside the valley; this had important influences on the TAFs. In valley 5, the separation might be described as *incipient*; the *mean* flow was downstream everywhere, but instantaneous flow reversals were commonly observed. Thus, pollutants emitted within this flow were frequently wafted back and forth before being transported downstream, and large TAFs were measured within this valley.

Extensive measurements of the flow structure within each of the three valleys were made, and we attempt to interpret the results (the TAF plots) in terms of the flow structure. But the flow-field measurements are of interest in and of themselves. We are not aware of any similar measurements of changes in turbulence intensities or Reynolds stresses as effected by flow distortions within a valley.

Simultaneously with the measurements in the wind tunnel, a theoretical model (Berlyand *et al.*, 1975) was used to calculate terrain amplification factors for sources located within the valleys. This model used wind-tunnel data on the flow structure as input for numerical solution of the turbulent diffusion equation. As will be seen later, the model provides quite reasonable predictions of TAFs for the valley of intermediate slope and somewhat better predictions for the gently-sloped valley. Because the model cannot handle separated flows, it was not applied to the steep-sloped valley.

2. APPARATUS, INSTRUMENTATION, AND MEASUREMENT TECHNIQUES

The detailed features and operational characteristics of the EPA Meteorological Wind Tunnel are described by Snyder (1979). The instrumentation and general laboratory procedures for velocity and concentration measurements are described by Lawson (1984). The microcomputers and programs used for data acquisition and analysis of the wind-tunnel data are described by Shipman (1988). Hence, only the main features of the equipment and special instrumentation or different procedures will be described here.

2.1 Wind Tunnel

The wind tunnel test section is 3.7 m wide, 2.1 m high and 18.3 m long. The air speed in the test section may be varied from 0.5 to 10 m s^{-1}. An instrument carriage, supported on rails along the test-section walls, is capable of positioning a probe or sampling rake by manual or computer-aided control.

An atmospheric boundary layer was simulated by placing a fence (vertical barrier) of 153 mm height at the entrance to the test section and covering the tunnel floor downwind of the fence with rough gravel. The gravel, consisting of stones of approximately 10 mm and smaller diameter, was epoxy-cemented onto plywood floor panels. Previous tests showed that an equilibrium boundary layer (*i.e.*, very slowly developing) that is a reasonable approximation to the neutral atmospheric boundary layer was established at a distance of 7 to 8 m downstream of the fence (Arya and Shipman, 1981; Arya *et al.*, 1981). Additional measurements of the boundary-layer structure and dispersion characteristics were made during the current study.

The ceiling height of the wind tunnel was adjusted to ensure a longitudinal pressure gradient of zero over the flat terrain. It was *not* readjusted when the model valleys were installed.

2.2 The models

Three model valleys were constructed; all had shapes given by the parametric equations:

if $|\xi| \leq a$

$$x = \frac{1}{2}\ \xi \left[1 + \frac{a^2}{\xi^2 + m^2\ (a^2 - \xi^2)} \right],$$

$$z = \frac{-1}{2}\ m \left(a^2 - \xi^2\right)^{1/2} \left[1 - \frac{a^2}{\xi^2 + m^2\ (a^2 - \xi^2)} \right];$$

if $\quad |\xi| > a,\ z = 0\ ;$

where $\quad m = \frac{h}{a} + \left[\left(\frac{h}{a} \right)^2 + 1 \right]^{1/2},$

h = height (depth) of valley, a = half-width of valley, and ξ = arbitrary parameter. x is directed along the approach flow direction (origin at center of valley), and z is directed vertically upward. Since the surface is two-dimensional, the equations do not include the y variable, and the models extended across the width of the test section of the wind tunnel. These valley shapes are smooth, symmetric about the z-axis, and smoothly merge into a flat plane at the points x = ± a. They describe a two-parameter family of surfaces, the parameters being h and the aspect ratio n = a/h.

The valleys constructed for this study had aspect ratios of 3, 5, and 8 (maximum slopes of 26°, 16°, and 10°, respectively). All had heights (depths) of 117 mm and, therefore, half-widths of a = 351 mm, 585 mm, and 936 mm. Figure 1 shows the construction details of the three valleys and Fig. 2 shows the valley shapes and compares the ideal shapes with those measured after they were installed in the wind tunnel. The actual shapes differed from the ideal ones by less than ± 5 mm. All the models were covered with gravel to match the roughness of the wind-tunnel floor. The difference between the ideal and actual shapes shown in Fig. 2 is due primarily to the uncertainty in measuring to the top of the gravel roughness.

The leading edges of all the valleys were placed 8 m downwind of the fence at the entrance to the test section.

2.3 Velocity measurements

Two basic types of instruments were used to measure the flat-terrain boundary layer and the flow structure within the valleys, a hot-wire anemometer (HWA) and a pulsed-wire anemometer (PWA). The HWA is a convenient instrument to use where the flow is reasonably well-behaved, that is, where the turbulence intensities are relatively low (less than, say, 20%), or where the instantaneous velocity vector remains within a cone with a total angle of,

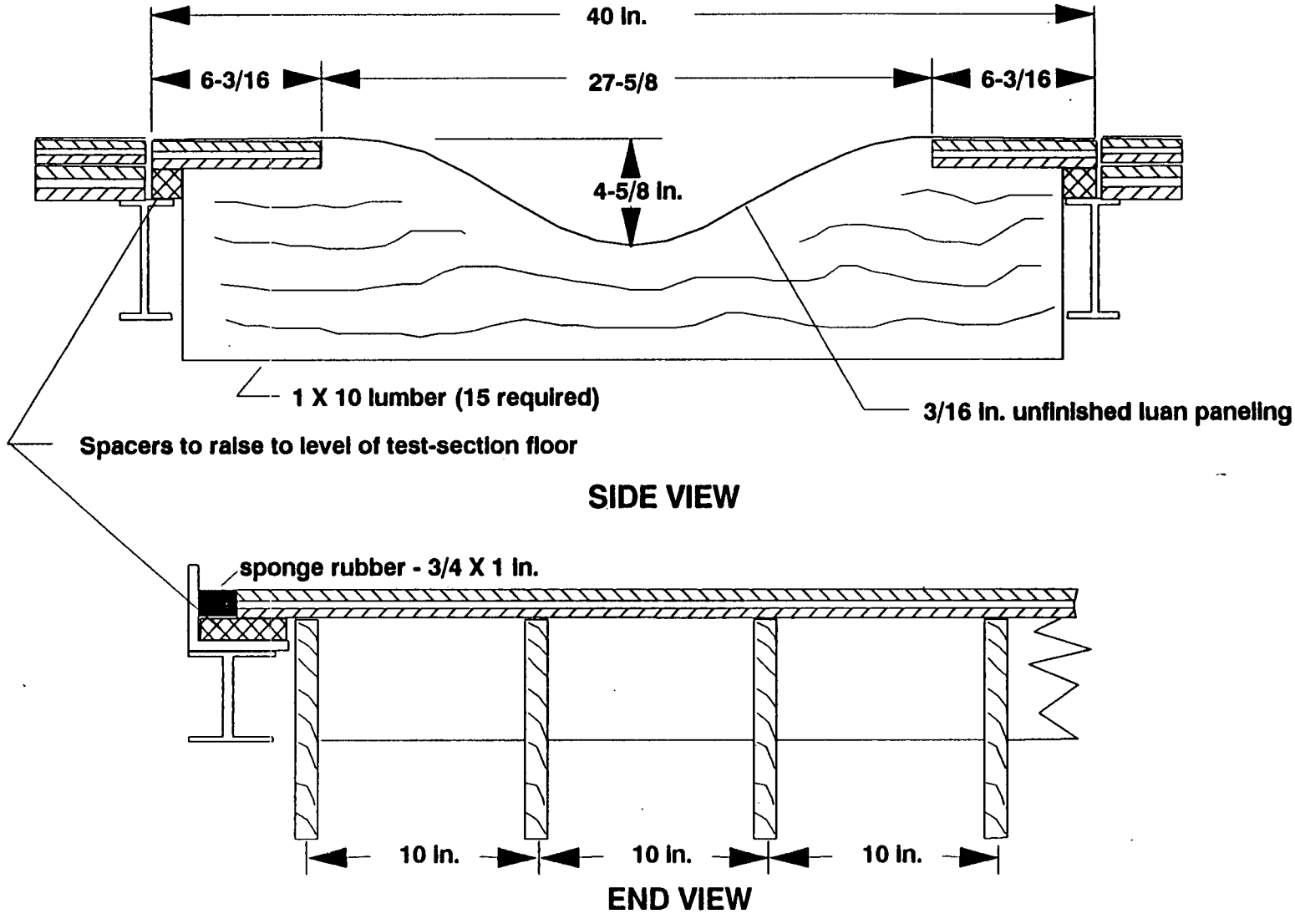

(a) Valley 3

Figure 1. Construction details of models.

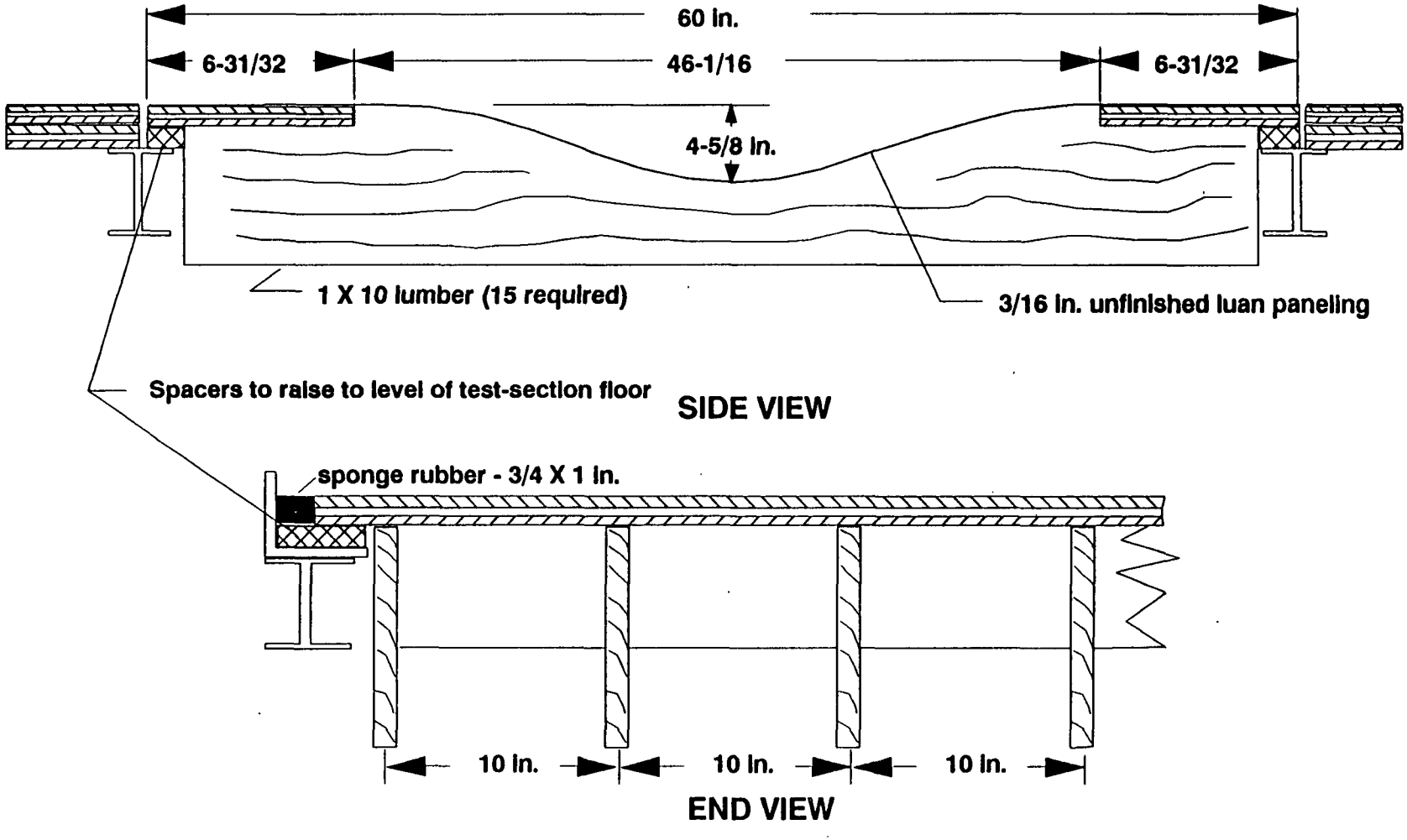

(b) Valley 5

Figure 1. Construction details of models.

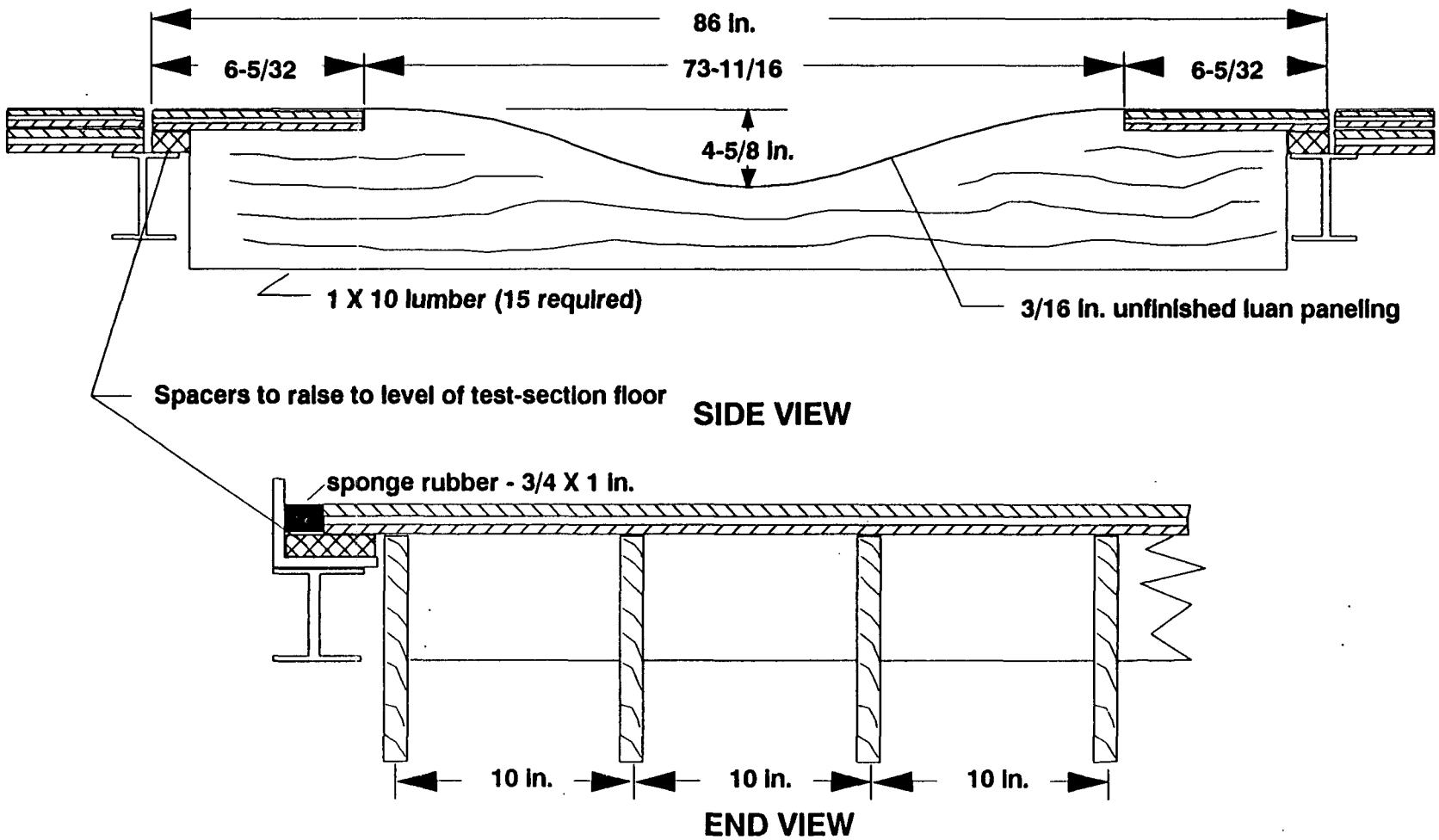

(c) Valley 8

Figure 1. Construction details of models.

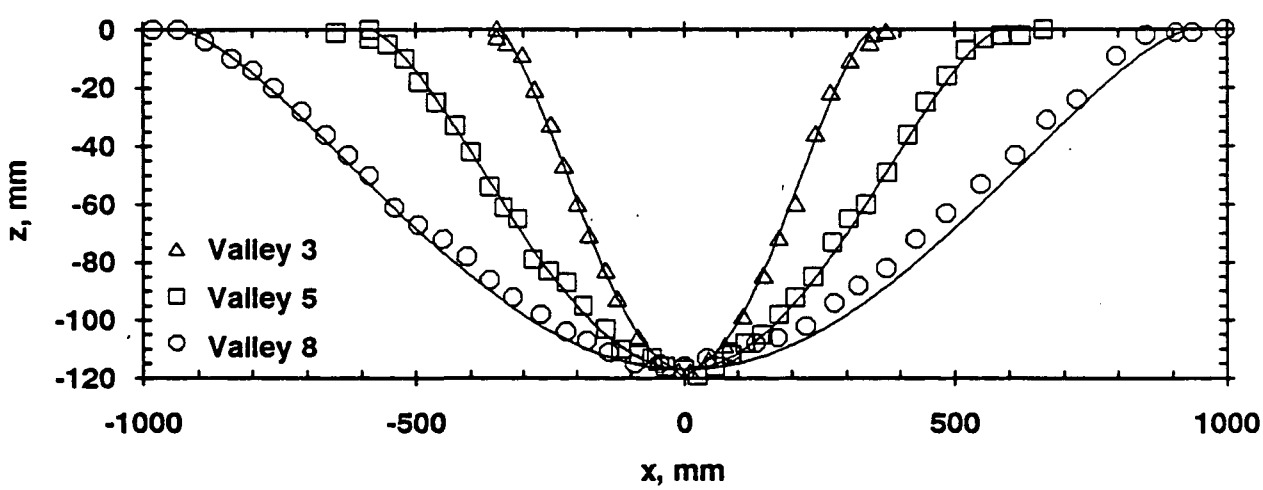

Figure 2. Shapes of valleys. Lines: ideal shapes; symbols: measured shapes.

say, 30°. The PWA, on the other hand, is ideally suited for use in flows of very high turbulence intensities, and even in reversing flows (Bradbury and Castro, 1971). The PWA is less suited for measurements in low-intensity flows, especially for measuring components perpendicular to the mean flow vector. Thus, in valley 8, where indicated turbulence intensities were generally less than 25%, the HWA was used for the bulk of the measurements. In valleys 3 and 5, however, the flows were highly turbulent and reversing, so the HWA measurements within the valley were supplemented with PWA measurements.

The HWA was a model IFA-100 from TSI, Inc. Three types of X-array hot-wire probes were used. The model 1241-T1.5 (end-flow style) was used for a few measurements in the flat terrain. Because of the geometric configuration, this probe was inconvenient to use within the valleys, so the bulk of measurements was made with the model 1243-T1.5 (boundary-layer style) probe. The orientation of this probe is such as to measure the longitudinal and vertical components (u and w) of the flow. A few measurements (primarily in Valley 8) were made with a model 1243L-T1.5 probe. This is also a boundary-layer style probe, but the orientation is such as to measure the longitudinal and lateral components (u and v) of the flow. All of these probes were fabricated using tungsten wire with diameter of 1.5 μm. For a detailed examination of the response of these probes, see Khurshudyan *et al.* (1981).

The analog output signals from the HWA were digitized to 12-bit precision at a rate of 500 Hz. The digitized data were subsequently linearized and processed on a personal computer (80286 microprocessor). A sampling duration of 2 min yielded reasonably repeatable results (generally within ±5% on the measurement of turbulence intensity).

The probes were traversed about the test section of the wind tunnel by using an automated carriage. The carriage control system was also driven by the microcomputer through the use of the software program HOT. Positioning accuracy of the system is ± 1.0 mm.

The hot-wire probes were calibrated against a Pitot-static tube mounted in the free-stream of the wind tunnel above the boundary layer (typically at a height of 1200 mm above the floor). These calibrations were checked at least once each day and recalibrations were made as deemed necessary. Calibrations were made over the velocity range of interest, typically for 6 to 8 points

over the range of 0.5 to 5 m s^{-1}, and "best fit" to King's law

$$E^2 = A + BU^{\alpha},$$

where E = output voltage of anemometer, U = wind speed indicated by the Pitot-static tube (manometer), and A, B and α are constants that were determined through an iterative least-squares procedure. The calibrations were accomplished using the program HCALX, developed inhouse (Shipman, 1988). A typical calibration curve is shown in Fig. 3. Corrections for varying ambient temperatures were made according to the method of Bearman (1971), temperatures being monitored continuously.

The PWA was manufactured by PELA Flow Instruments, Ltd. The principle of operation of the PWA is quite simple. The probe consists of three fine wires, two outside wires being parallel to one another and a central wire being perpendicular to the outer ones (see Fig. 4). The central wire is pulsed with a high current for a few microseconds duration, which raises the temperature of the wire to several hundred degrees Celsius. Thus, a tracer of heated air is released into the flow and is convected away with the instantaneous velocity of the air stream. The two outside wires are the sensors, which are operated as simple resistance thermometers. They are used to measure the time of arrival of the heated air parcel. Under ideal conditions, the time taken for the heated parcel to reach the sensor wire is

$$t = x/|U|\cos\theta,$$

where x is the distance between the pulsed and sensor wires, U is the magnitude of the flow velocity vector, and θ is the angle between the direction normal to the probe (*i.e.*, perpendicular to all three wires) and the instantaneous velocity vector. The use of two sensor wires, one on either side of the pulsed wire, ensures that the flow direction is determined unambiguously.

The PWA probe can be oriented to measure the velocity components in all three coordinate directions. Because of the finite wire lengths, the probe has a yaw response up to about 70°, so that, for reasonable measurements of transverse components of the flow, the turbulence intensity must be relatively high, *e.g.*, above 20 to 25%.

The electronics of the PWA provide for triggering the pulsed wire up to 60 times per second and for measuring the transit time (and direction) of the heat pulse. The instrument provides a 12-bit binary output indicative of the

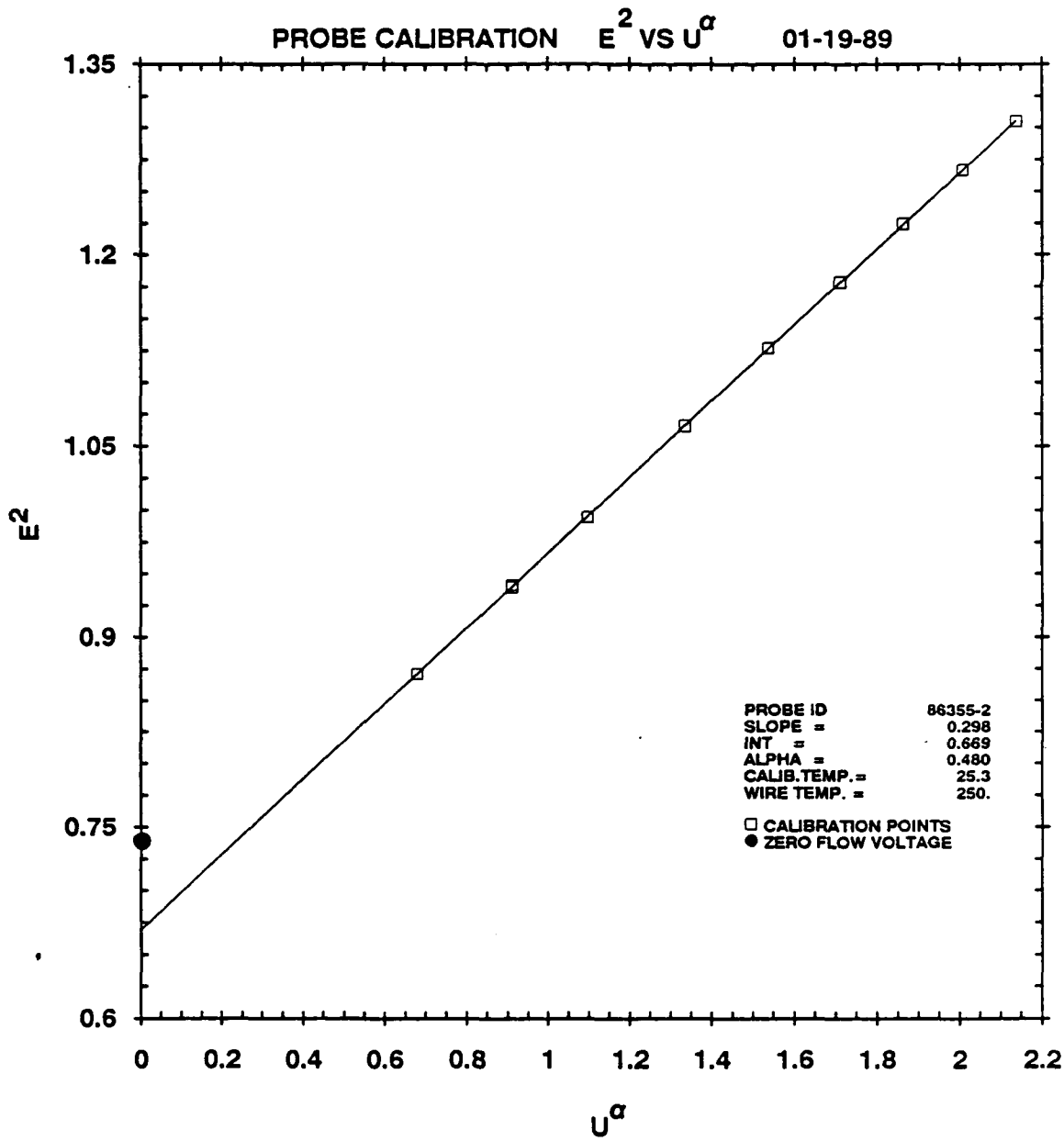

Figure 3. Typical calibration curve of hot-wire anemometer.

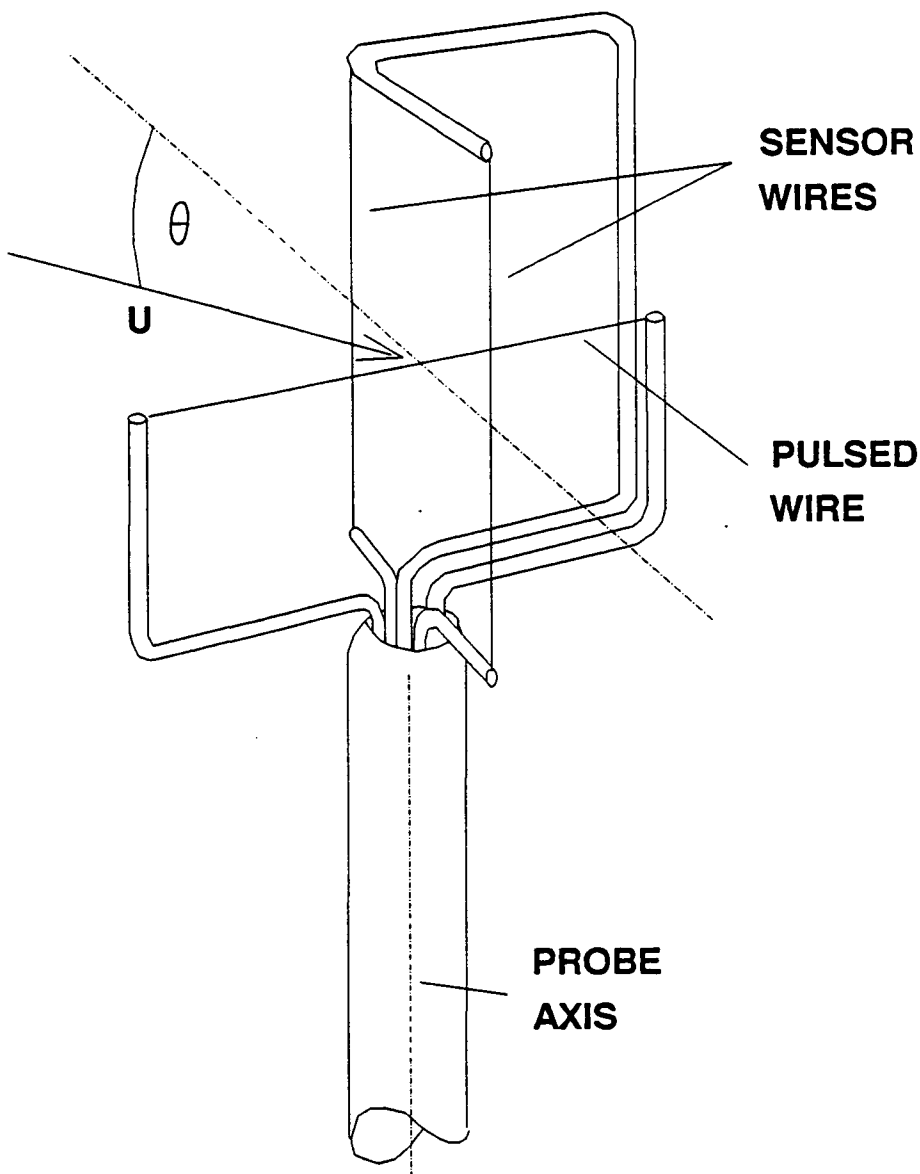

Figure 4. Sketch of pulsed-wire anemometer.

time of flight of the heated air parcel each time the sensor wire is triggered. The PWA was controlled with the personal computer which provided triggering pulses 30 times per second. Calibrations were performed, as with the HWA, against a Pitot-static tube mounted in the free-stream of the wind tunnel, over a typical velocity range of 0.5 to 5 m s^{-1}. These calibration points were "best-fit" with an inhouse software program PWACAL to the equation

$$U = \frac{A}{T} + \frac{B}{T^2} + \frac{C}{T^3} ,$$

where U = wind speed indicated by the Pitot-static tube (manometer), T is the time of flight of the heated air parcel (from the pulsed wire to the sensor wire), and A, B and C are constants that are determined through an iterative least-squares procedure. A typical calibration curve is shown in Fig. 5. As with the HWA, a sampling duration of 2 min was found to yield reasonably stable mean velocity and turbulence intensity values.

To maintain consistency in the measurement of probe elevations above the gravel surface, a square flat plate 10 cm on each side was placed on the gravel surface below the probe; the bottom of the plate was regarded as the origin of the z-coordinate (positive upwards), and probe elevations are reported with reference to this system.

A large amount of information was collected on the flow structure over the valleys. In general, measurements were made at 16 locations (longitudinal positions) from $x/a = -2.0$ to $x/a \geq 5.0$ for each valley. HWA measurements were made with the uw-probe at several longitudinal positions in flat terrain and at all locations for each valley. A complete set of HWA measurements was made with the uv-probe over valley 8 only. Approximately 75 individual profiles were measured with the HWA, each profile consisting of approximately 20 measurement points. Each measurement provided information on the mean velocity, the angle of the mean velocity, two components of turbulence intensity (u and w or u and v), and Reynolds stress.

The HWA measurements were supplemented by PWA measurements within the high-turbulence regions in the valleys. Only the longitudinal component was measured with the PWA in valley 8, but in valleys 5 and 3, all three components were measured (u, v, and w, one at a time), and each of these at between 5 and 9 locations within each valley. Approximately 60 PWA profiles were measured, each profile consisting of approximately 10 points. Each measurement provided information on the mean velocity, the turbulence

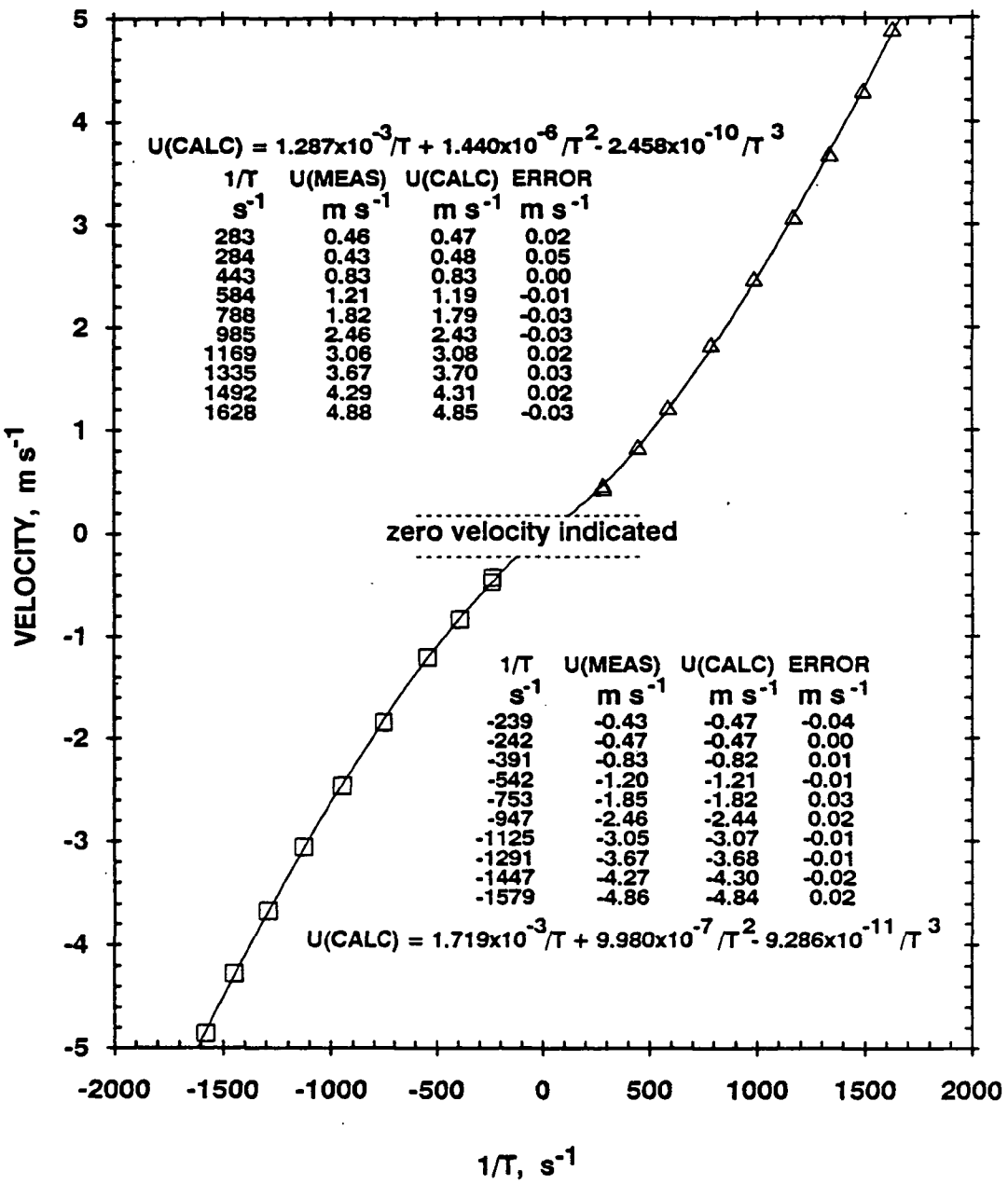

Figure 5. Typical calibration curve of pulsed-wire anemometer.

intensity, and the skewness and kurtosis of the velocity distributions. Additionally, time-series data were recorded at several elevations above each of the valley centers (a total of about 40 time series). These data were analyzed to obtain more detail on the nature of the velocity fluctuations; that is, the probability density distributions were analyzed from each of these time series.

2.4 The source

In accordance with the purposes of the present investigation, the tracer was to be neutrally buoyant and released from a point source. The tracer used was ethane (C_2H_6), which has a molecular weight of 30 and is only slightly heavier than air. In combination with typical flow speeds of 2 to 4 m s^{-1} at the release point and the generally small release rates (typically 4000 cm^3 min^{-1}), this tracer may be regarded as neutrally buoyant.

The ethane was emitted from a "stack" that was adjustable in height. It contained a 90° bend and a perforated hollow plastic sphere of 10 mm diameter, as shown in Fig. 6. This spherical source was used because the wind was not always horizontal (as on the windward sides of the valleys) and possibly in the reverse direction (as in the separated region within the steep valley), and this configuration should provide the closest practical approximation to an ideal point source. Note that in our earlier study (RUSHIL), the source used was constructed of porous stone and was 15 mm in diameter. That source, however, was quite fragile and tended to "plug up" with usage. The present hollow sphere is regarded as an improvement because it is rugged, stable, and smaller in diameter. Approximately 200 holes of 0.1-mm diameter were drilled through the surface to provide for a "uniform" release rate in all directions.

To determine whether the source emission rate had an influence on the downwind concentration field, a special test was run wherein lateral and vertical concentration profiles were measured a short distance downwind of the source, and the source flow rate was varied by a factor of 3. The nondimensional plots of concentration (see next section) are shown in Fig. 7; since the data at the two different emission rates coincide using this nondimensionalization, the emission rate is clearly inconsequential.

The ethane flow rate was monitored continuously using a Meriam laminar flow element (model 50MJ10-1/2) and micromanometer (model 23FB2TM-20, null type) as shown in Fig. 6. The laminar flow element was calibrated (and checked periodically) using a volumetric flow calibrator (Brooks model 1050A

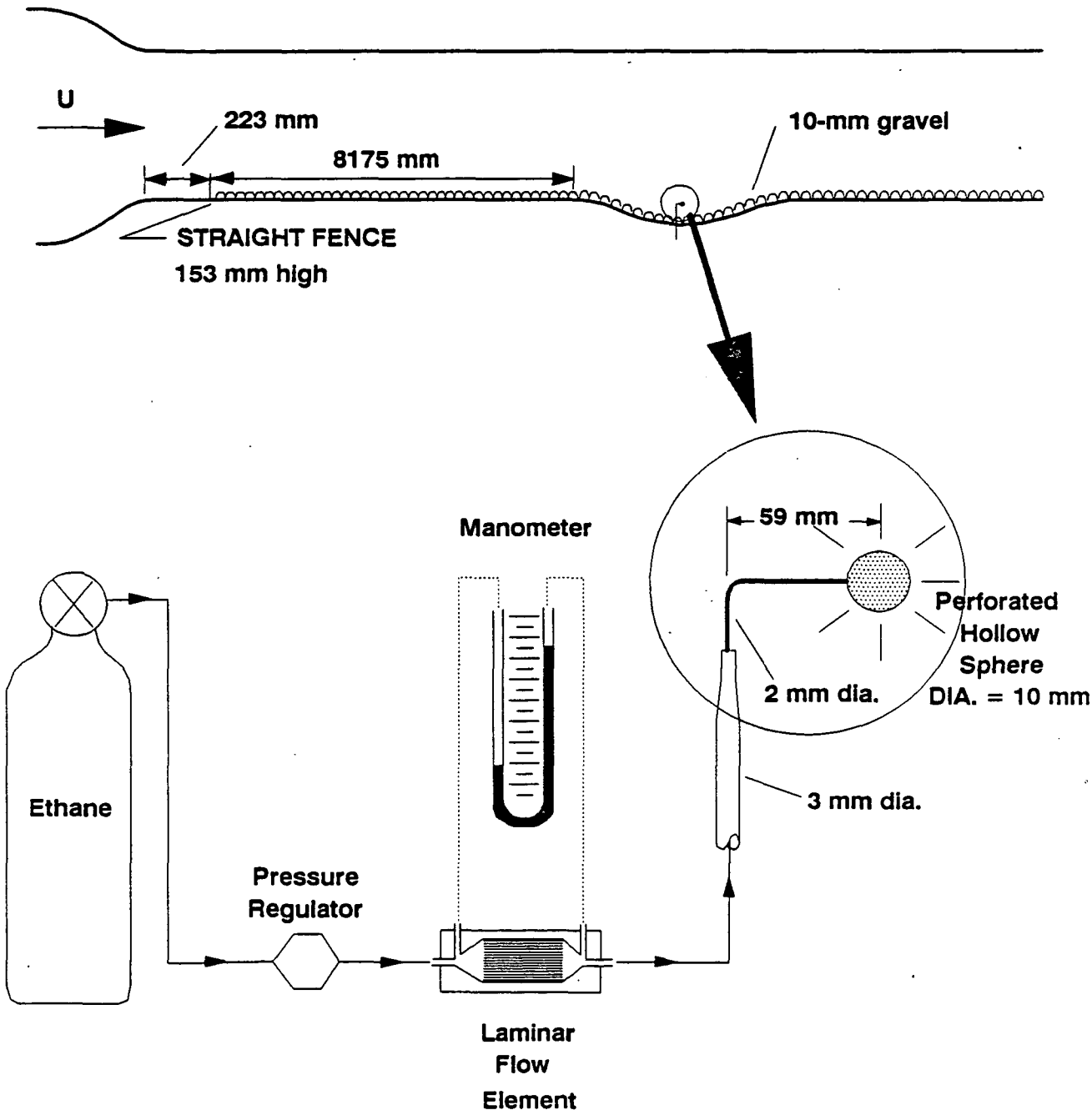

Figure 6. Diagram of wind-tunnel setup, source, and flow-measurement apparatus.

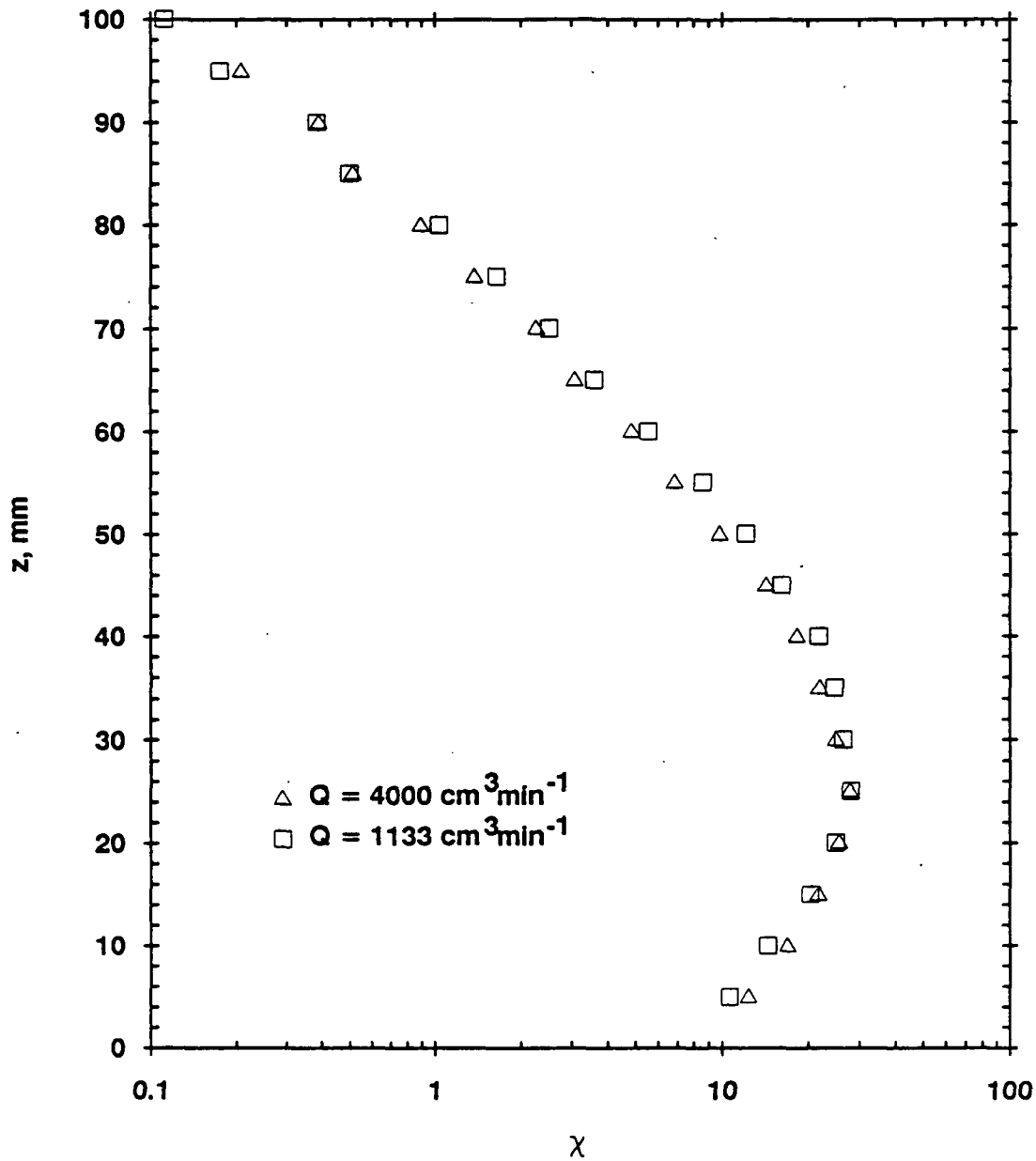

(a) Vertical profiles

Figure 7. Concentration profiles measured downwind of sources with different flow rates. H_s = 29 mm, x_s = 234 mm, U_∞ = 4 m s^{-1}.

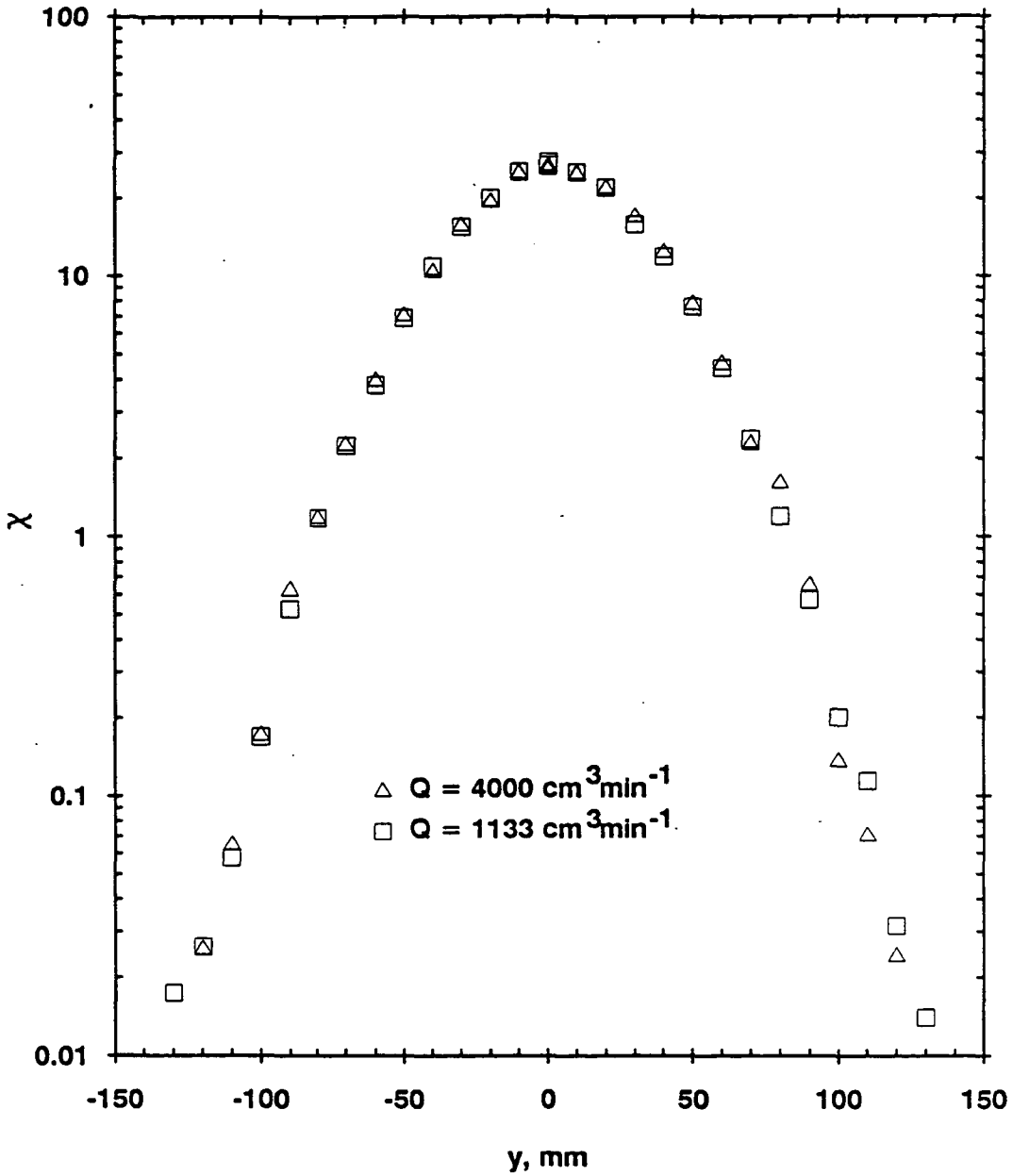

(b) Lateral profiles

Figure 7. Concentration profiles measured downwind of sources with different flow rates. H_s = 29 mm, x_s= 234 mm, U_∞= 4 m s^{-1}.

1J1) which has a rated accuracy of 0.5%. These calibrations were performed *in situ*, *i.e.*, the entire plumbing system was calibrated as used during measurements; the "stack" was enclosed in a sealed container that collected the ethane released from the source and diverted it to the volumetric flow calibrator.

2.5 Concentration Measurements

Concentration profiles were obtained by collecting samples through 1.6-mm OD tubes that were fastened to the instrument carriage. These samples were drawn through Beckman model 400 hydrocarbon analyzers (flame ionization detectors, FIDs) operating in the continuous sampling mode for analysis. Typically, five FIDs were used simultaneously in conjunction with sampling rakes which contained sampling tubes of fixed spacing. As with the velocity measurements, elevations of the tubes above the surface were measured with reference to the bottom of a square plate placed on the gravel surface. For surface concentration measurements, however, a special spring-loaded sampling rake was used with flat circular disks on the bottom of each tube (see Fig. 8) to ensure that the samples were drawn consistently from an elevation of 5 mm above the "tops of the rocks". No probe interference effects were observed during the measurement of surface (streamwise along the ground) profiles, even though sampling tubes were in the wakes of one another during the sampling process (see Fig. 9).

The FIDs were initially calibrated and checked for linear response using certified gases of (nominally) 1.0, 0.5, 0.05, and 0.005% ethane in hydrocarbon-free air from Scott Environmental Technology, Inc. A typical calibration curve is shown in Fig. 10.

The "span" (full scale) and "zero" settings were adjusted before beginning measurements and checked after finishing measurements each day. Background (room) hydrocarbon level measurements were made at the beginning and end of each profile. The computer program HCA subtracted a background level from each sample measurement by assuming a linear change in background with time between sequential background measurements. Typical background levels were 5 ppm at the beginning and 30 ppm at the end of the day.

The output signals from the FIDs were digitized at the rate of 20 Hz (each unit) and processed on the personal computer. With 2-min sampling times, reasonably repeatable values of concentration were obtained, generally within ± 5% on mean concentrations. The HCA program controlled the sampling

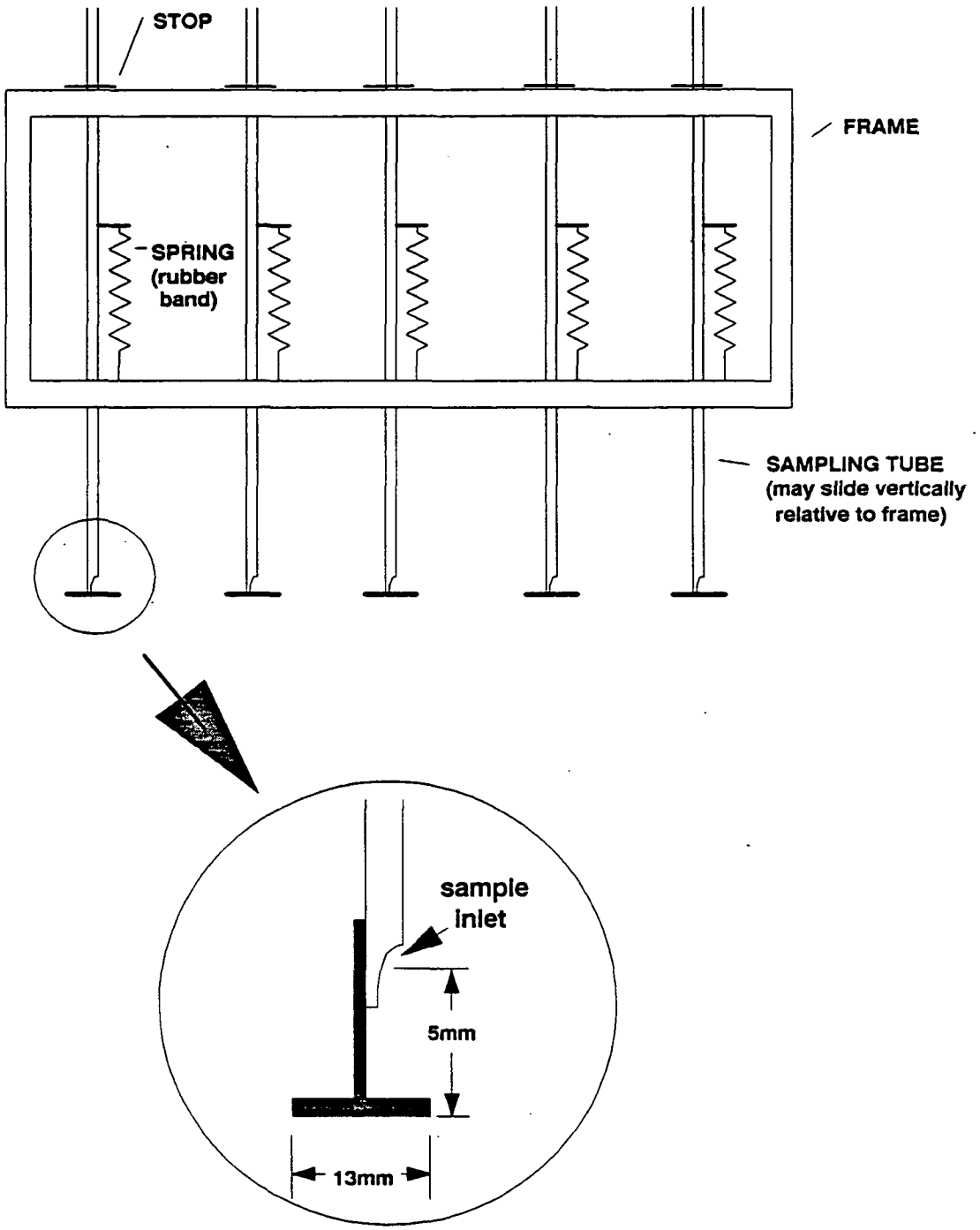

Figure 8. Detail of spring-loaded sampling rake.

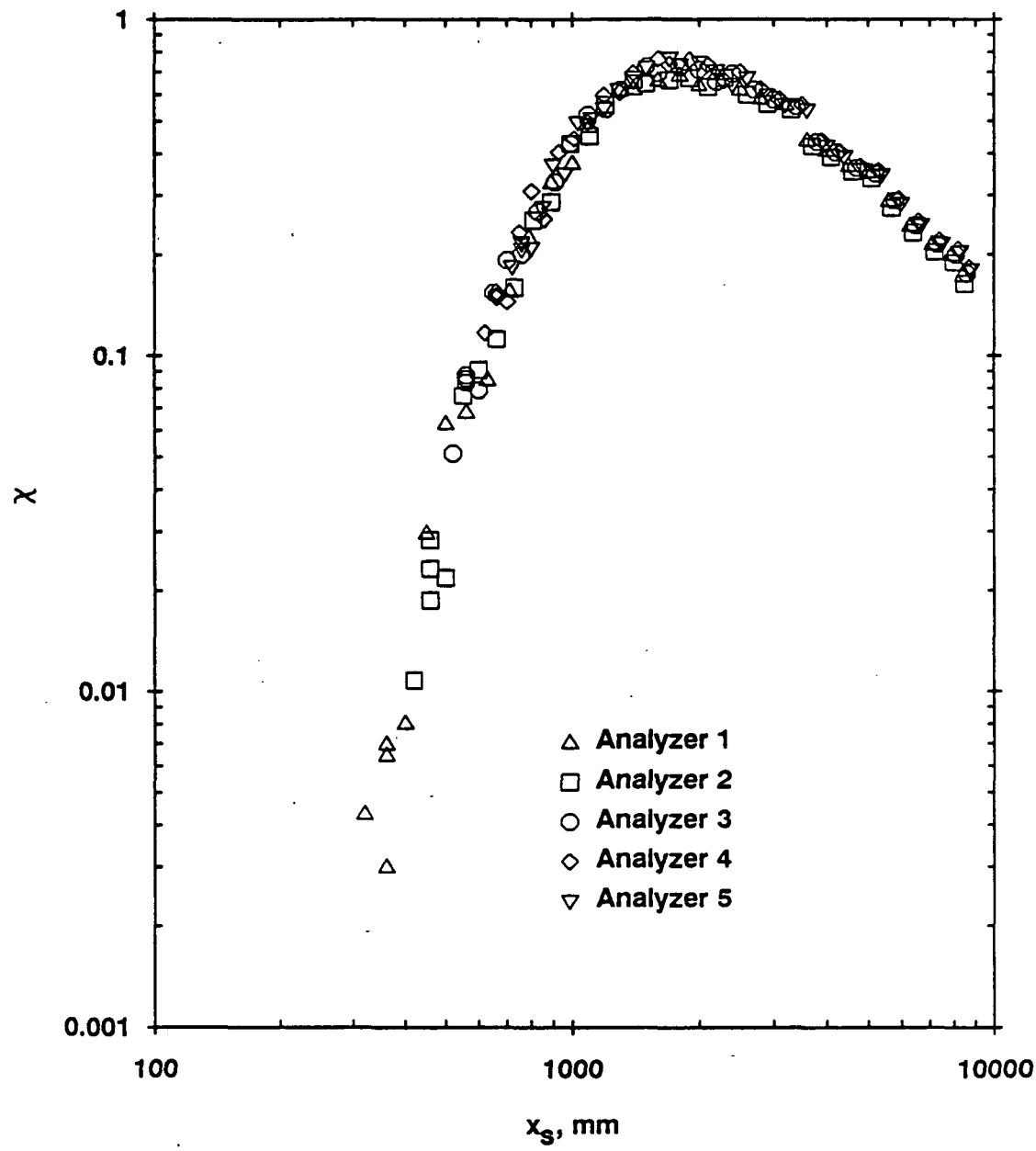

Figure 9. Surface longitudinal concentration profile measured with spring-loaded sampling rake.

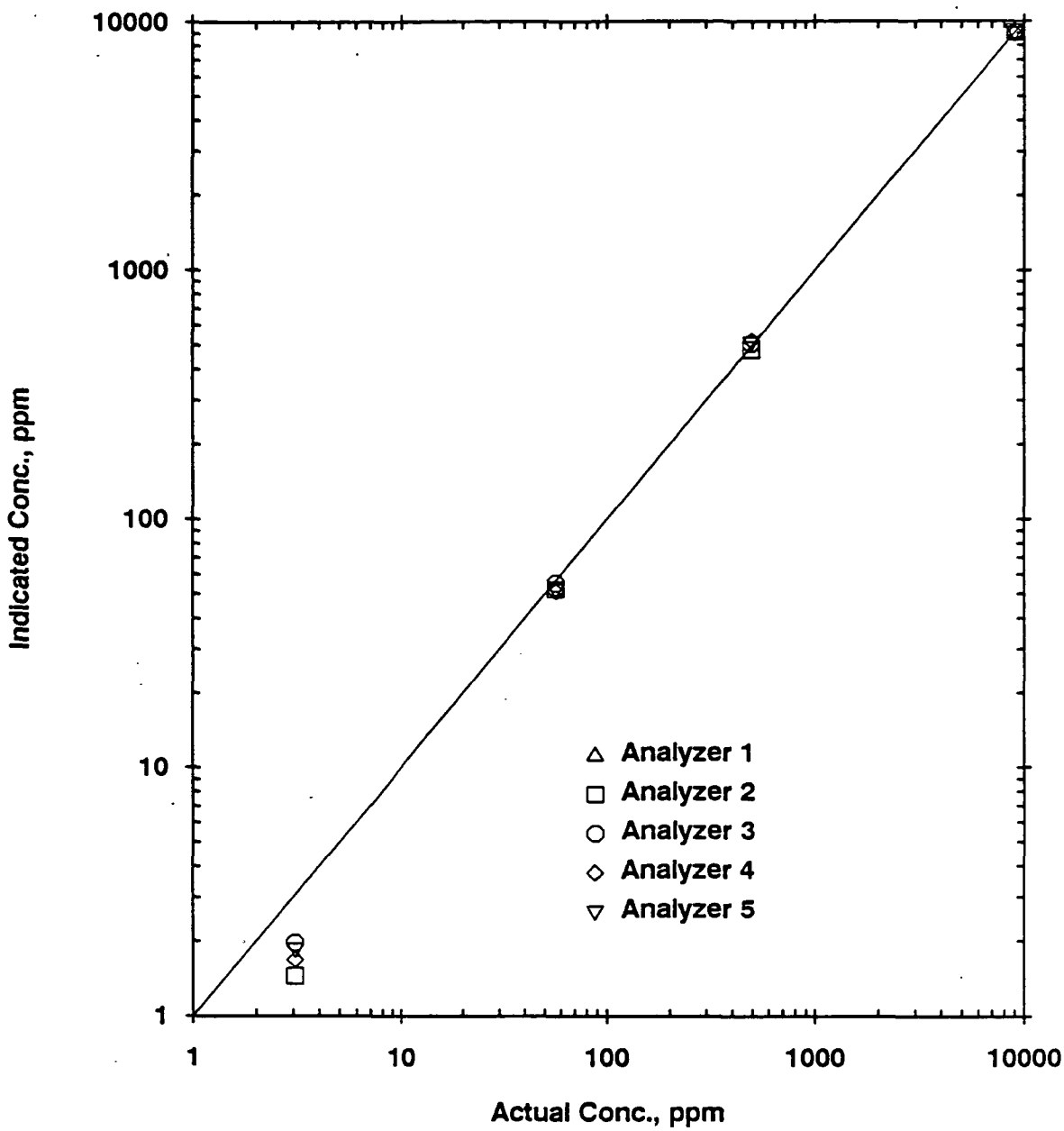

Figure 10. Calibration of flame ionization detectors.

and range-switching of the FIDs and rake positioning through the instrument carriage. It also processed the data (scaling, averaging, *etc.*) and stored the data from each of the instruments in separate files. These files contain all possible information collected, including "span", "zero" and background readings. HCA optionally permits these "raw" files to be stripped of this superfluous information and merged together to form a "merged" profile.

The "corrected" concentrations (*i.e.*, with background subtracted) were normalized as follows:

$$\chi = CU_{\infty}H^2/Q \ ,$$

where χ is the normalized concentration (used in all graphs), C is the corrected concentration (in ppm by volume), U_{∞} is the free-stream wind speed (nominally 4 m s^{-1}), H is a convenient length scale (H = 234 mm was used throughout this study for ease in comparison with earlier RUSHIL data), and Q is the ethane flow rate (cm^3 min^{-1}).

A large number of concentration profiles (approximately 170) were measured. Primary stack heights H_s were 29, 59, 117, and 176 mm (H_s/h = 0.25, 0.50, 1.0, and 1.50, respectively). Primary stack positions were at the upstream edge (x/a = -1.0), center (x/a = 0.0) and downstream edge (x/a = 1.0) of each valley. Full surface concentration profiles were measured with each of these stack heights and locations within each valley (and in flat terrain). Abbreviated surface profiles, sufficient to determine the value and location of the maximum ground-level concentration were made at intermediate stack heights and locations. Lateral and vertical concentration profiles were measured at only a few downwind positions for a very limited number of stack positions and heights.

3. PRESENTATION AND DISCUSSION OF EXPERIMENTAL RESULTS

3.1 Boundary-Layer Structure in Flat Terrain

Sufficient measurements were made of the flat-terrain boundary-layer structure and its dispersive characteristics to ascertain that it was similar to that used during the RUSHIL study and also a reasonable simulation of the neutral atmospheric boundary layer. The free-stream wind speed was 4 m s^{-1}, and the ceiling height was adjusted to obtain a zero longitudinal pressure gradient.

3.1.1 Velocity

Figure 11 shows local mean speed u normalized by the freestream speed U_∞, turbulence intensity (σ_u/u, σ_w/u), and Reynolds-stress ($-\overline{u'w'}/u_*^2$) distributions measured at various positions within the flat-terrain boundary layer, and compares these with measurements made in the RUSHIL study. The boundary-layer structure appears to be near-equilibrium beyond the 8-m position (downwind of the trip fence and the approximate location of the upstream edge of the valleys), as relatively small changes are observed. Also, the measurements match those made during the RUSHIL study reasonably well. The friction velocity and roughness length are approximately 0.19 m s^{-1} and 0.16 mm, respectively. These are essentially the same as the RUSHIL values.

3.1.2 Concentration

Surface longitudinal profiles of ethane concentration were measured downwind of the source for 8 source heights H_s. These profiles are compared with RUSHIL data (available for 6 source heights) in Fig. 12. Generally, the values and locations of maximum surface concentration match the RUSHIL data within approximately 10%. The differences may be attributed to the somewhat different source configuration (smaller diameter hollow sphere compared with a porous stone in the RUSHIL study) and, possibly, to the difficulty in measuring the precise height of the source; for example, an uncertainty of ±3 mm in the measurement of the stack height (above the rough gravel surface) could easily result in the differences observed. In Fig. 13, the maximum ground-level concentration is plotted as a function of source height; this is also compared with the RUSHIL data. The concentration clearly decreases as the inverse square of the stack height. The comparison with the RUSHIL data is excellent.

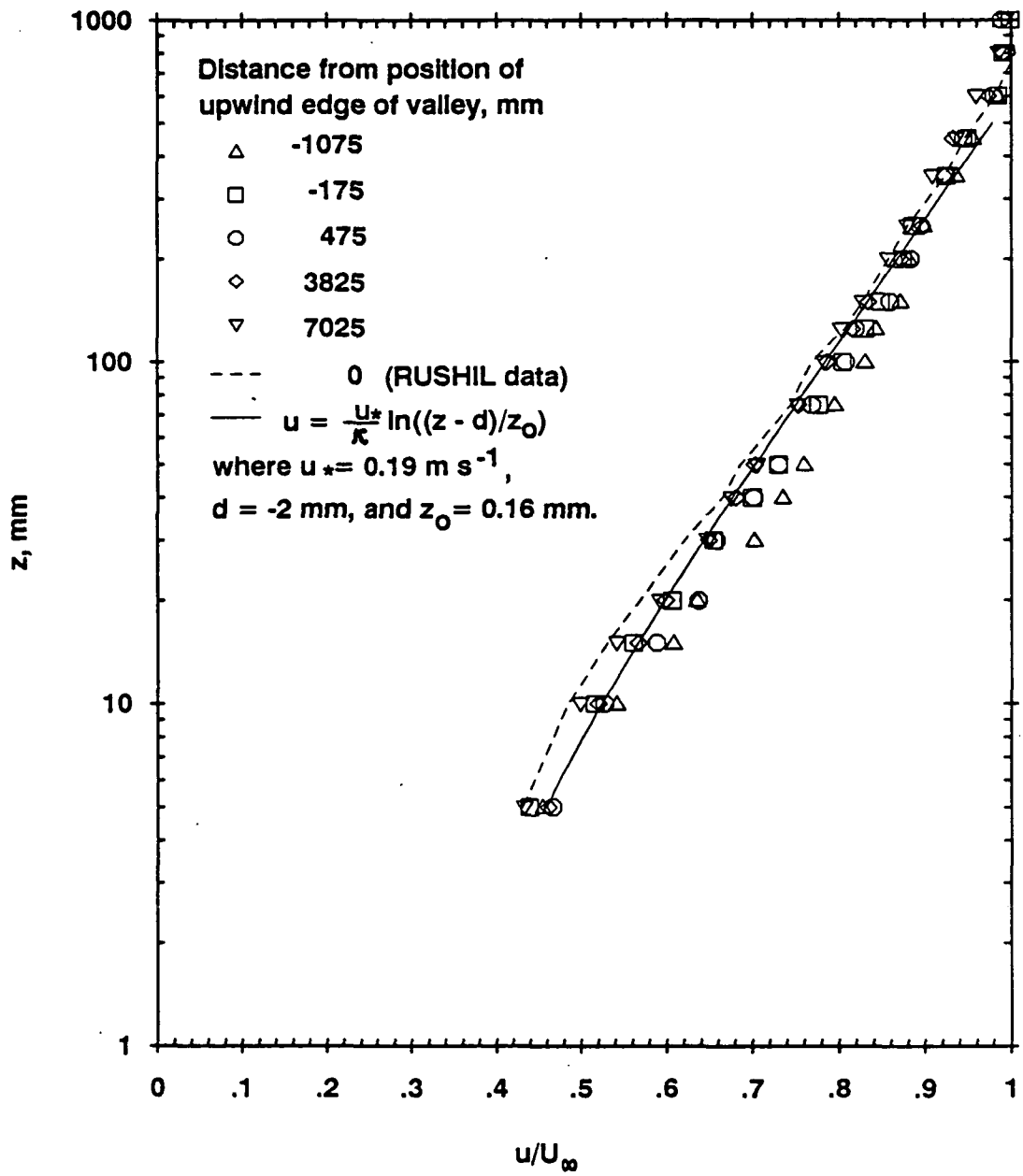

(a) Mean velocity profiles

Figure 11. Structure of the flat-terrain boundary layer.

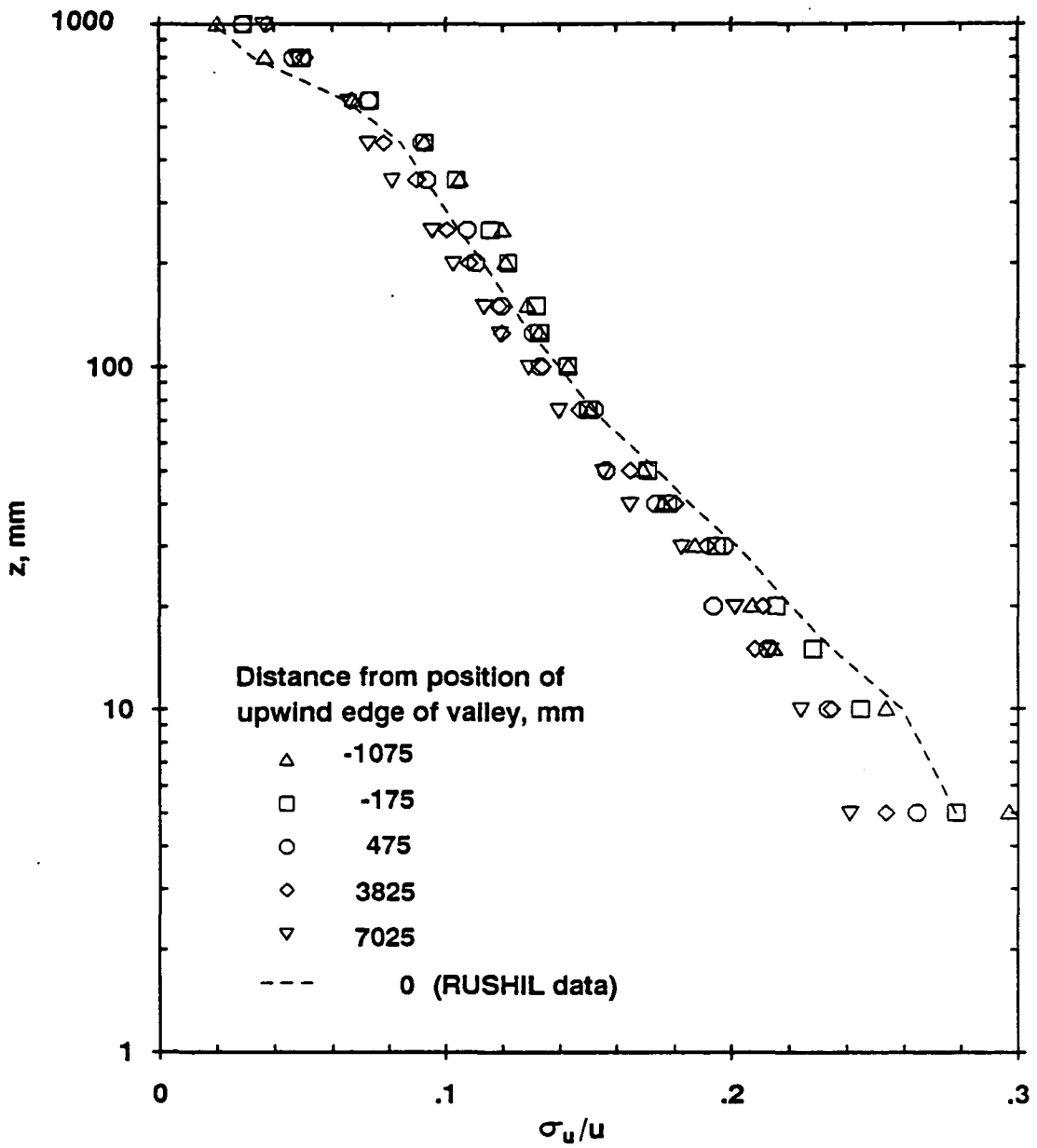

(b) Longitudinal turbulence intensity profiles

Figure 11. Structure of the flat-terrain boundary layer.

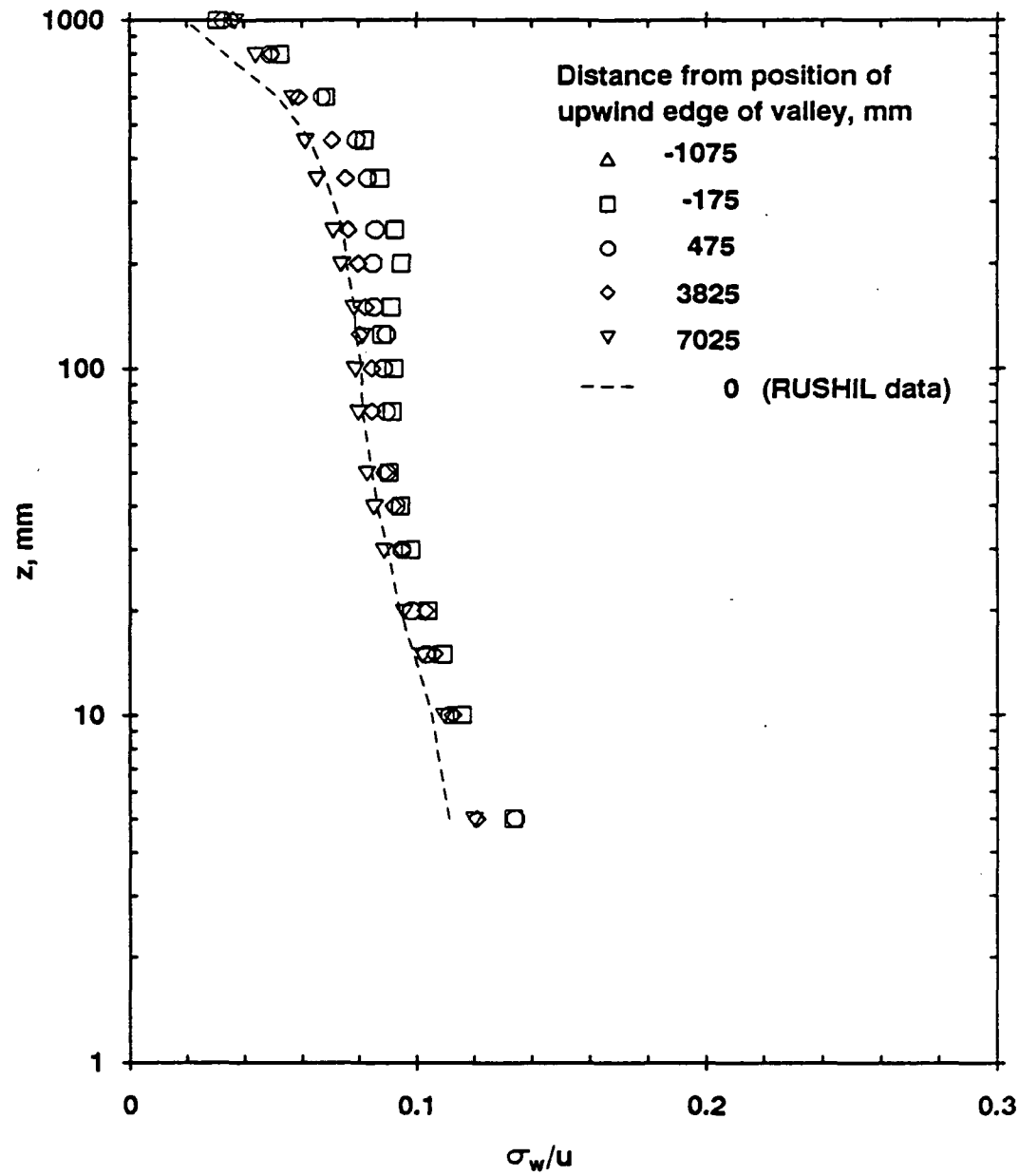

(c) Vertical turbulence intensity profiles

Figure 11. Structure of the flat-terrain boundary layer.

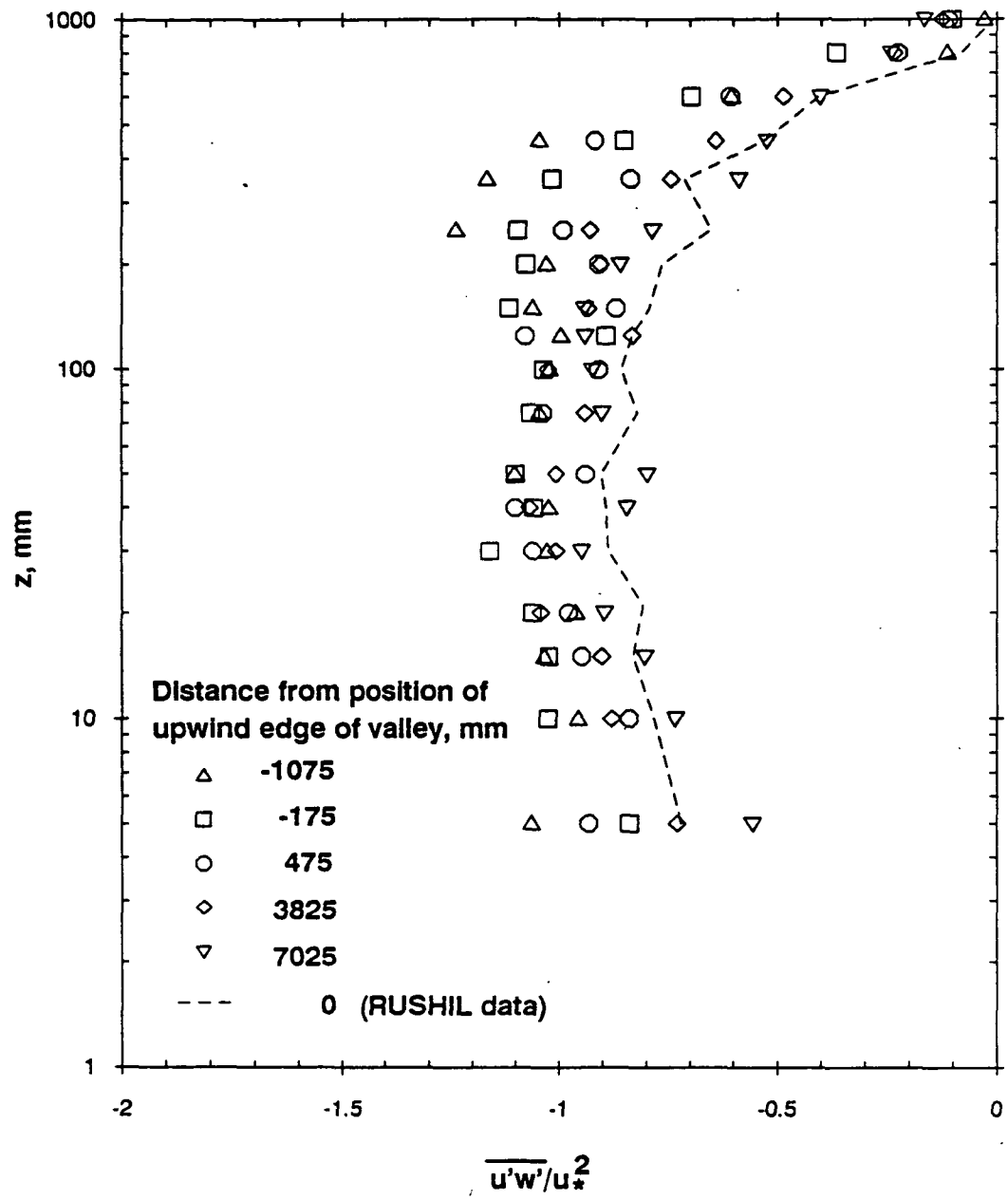

(d) Reynolds stress distributions

Figure 11. Structure of the flat-terrain boundary layer.

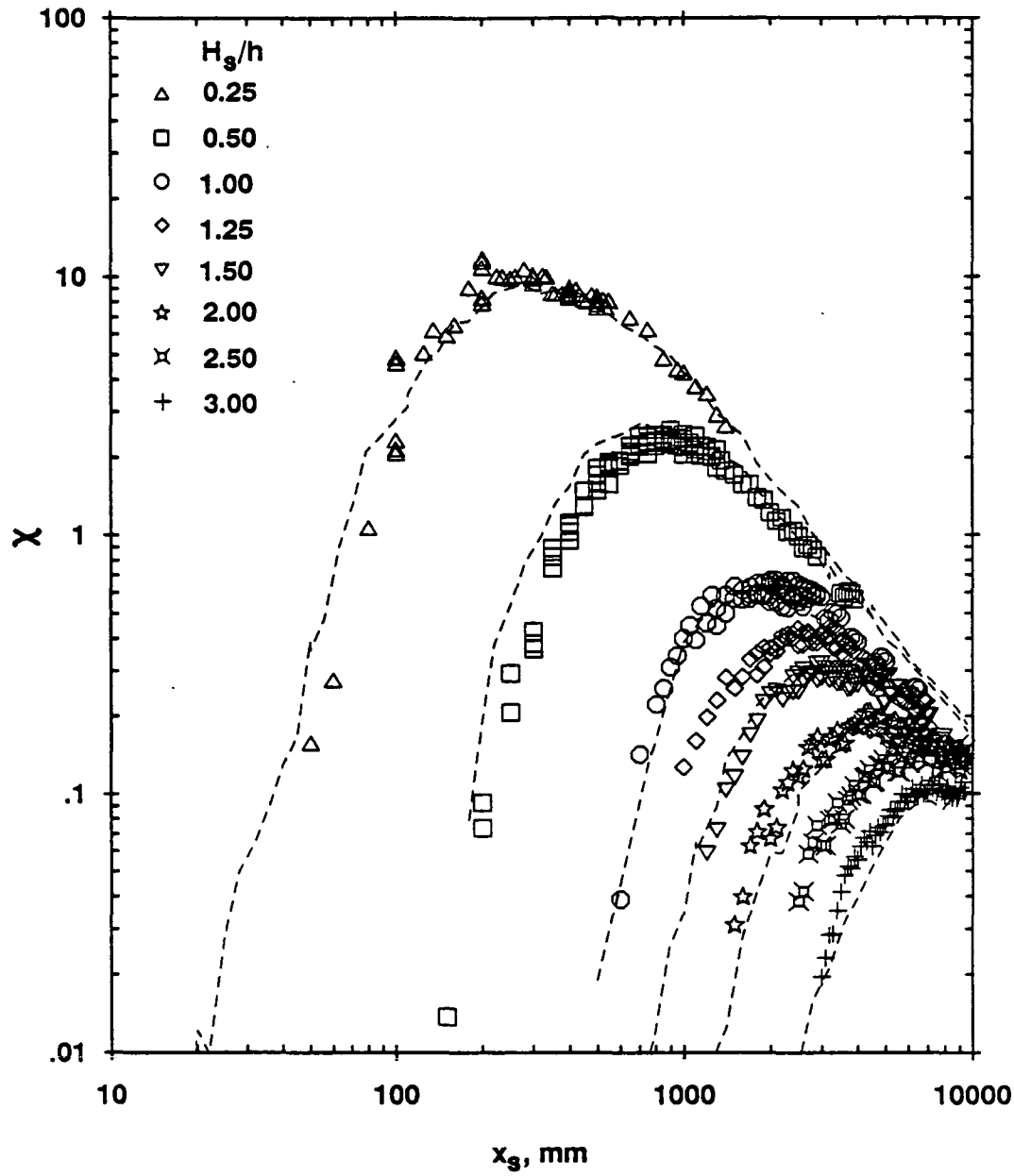

Figure 12. Longitudinal surface concentration profiles in flat terrain. Dashed lines are RUSHIL data.

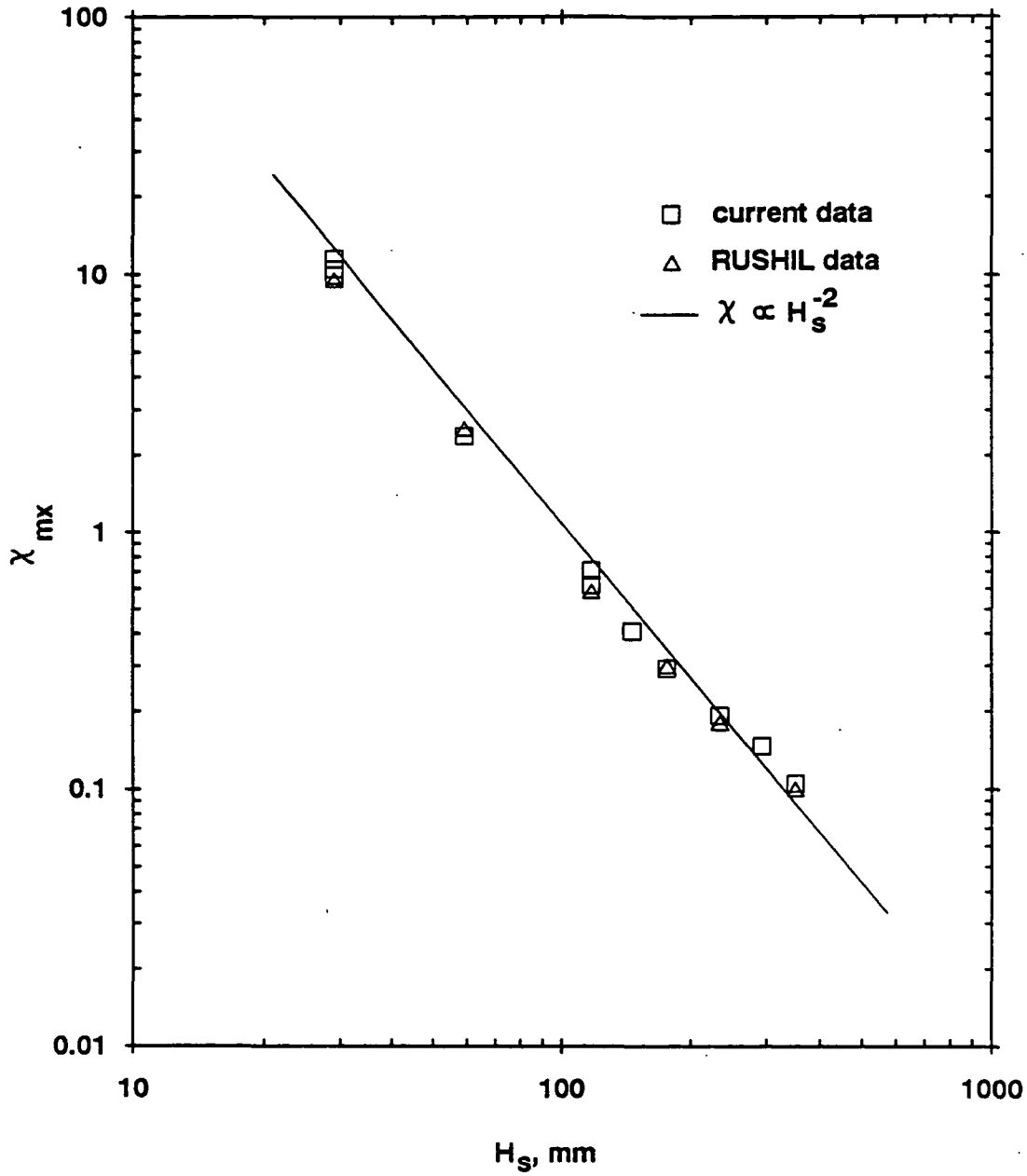

Figure 13. Maximum ground-level concentration as a function of source height.

On the basis of these comparisons of flow structure and dispersion characteristics, we were confident that the boundary layer was the same in every substantial way as that used in the RUSHIL study. Figure 13, then, served as the flat terrain or reference data for later evaluations of TAFs.

A comparison is also made between the dispersion characteristics in this simulated atmospheric boundary layer and those estimated using Pasquill-Gifford stability categories C and D (Turner, 1970), as shown in Fig. 14. The Pasquill-Gifford stability C describes a slightly convective atmosphere and is used here for comparison only; the wind tunnel models neutral flow. A scale factor of 1:1250 was used in this comparison. As is common with wind-tunnel simulations, the dispersion was approximated as between stability classes C and D near the source, but farther downstream, it was closely approximated by stability class D. Also shown is the dispersion scheme suggested by Hosker (1974), Gifford (1975), and Smith (1973) for stability class D and a 40 cm roughness length (scaling up the wind tunnel roughness length gives z_o = 20 cm, but their scheme uses discrete values and 40 cm is the next largest choice). This scheme uses a distance-dependent roughness-length correction and allows much larger values of roughness length than the Pasquill-Gifford approach; it matches the wind-tunnel data much better than the Pasquill-Gifford scheme. In summary, we conclude that the wind tunnel boundary layer provides a reasonable simulation of the dispersion characteristics of the neutral atmospheric boundary layer.

3.2 Flow Structure over the Valleys

Figures 15 through 17 show vertical profiles of longitudinal mean velocity, turbulence intensity, and Reynolds stress, respectively, over the three valleys. Although not all are shown, 16 profiles were measured for each valley, spanning the range from one valley half-width (a) upstream to at least 6a downstream. Note that these profiles contain a mixture of hot-wire and pulsed-wire data. Because the hot-wire data are inaccurate at high-turbulence intensities and the pulsed-wire data are inaccurate at low intensities (at least for components perpendicular to the mean flow), the profiles taken with each instrument were merged by selecting the most accurate data for each range. Some region of overlap was allowed, as may be evident in the figures. Also, the Reynolds stresses have been converted to the "natural" coordinate system, that is, parallel and perpendicular to the mean streamlines in

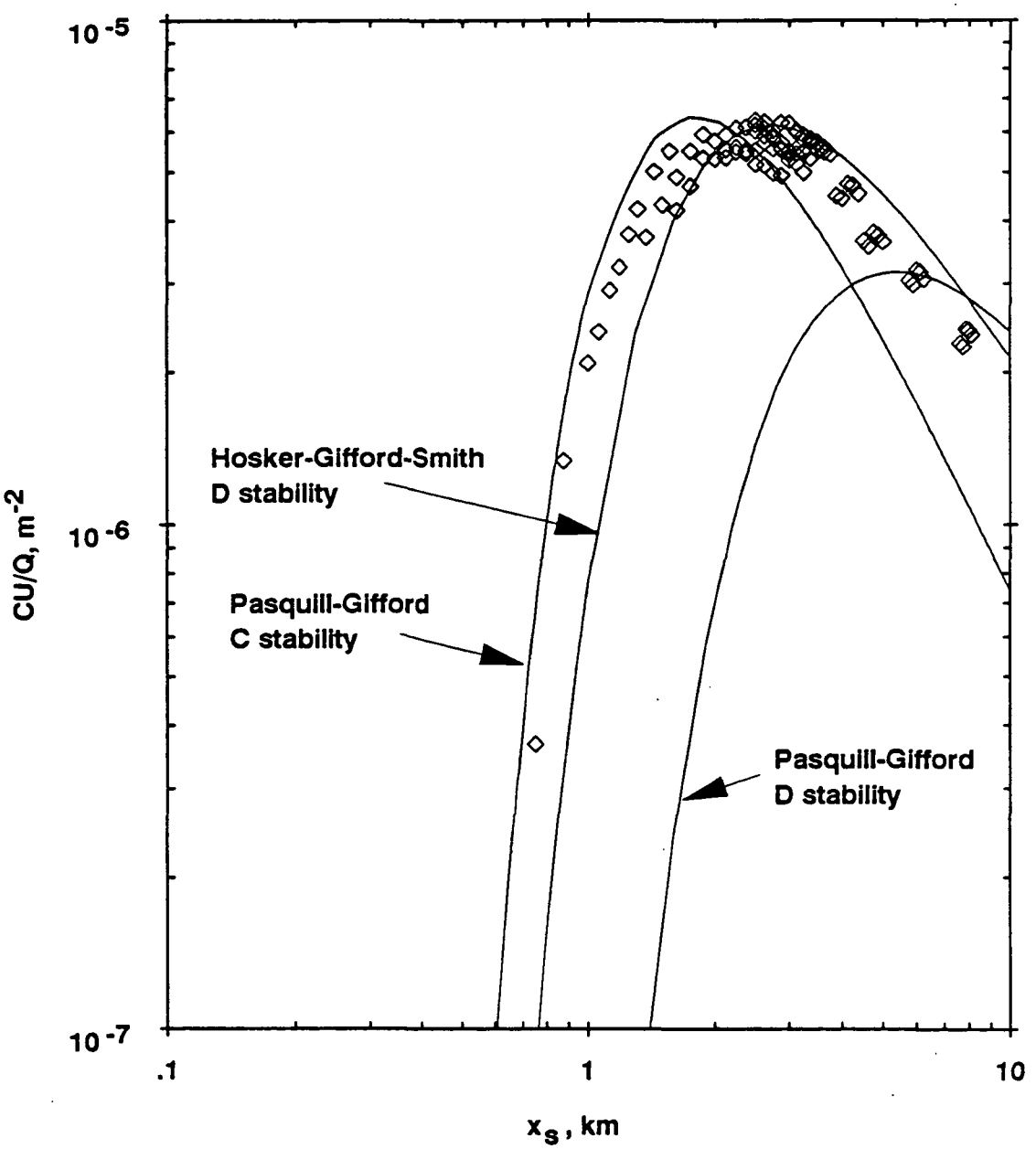

Figure 14. Surface longitudinal concentration profile in flat terrain, scaled up 1250:1 from wind-tunnel measurements, compared with Gaussian plume predictions using Pasquill-Gifford stabilities C and D and Hosker-Gifford-Smith stability D with z_o = 40 cm. H_s = 146 m (117 mm in wind tunnel).

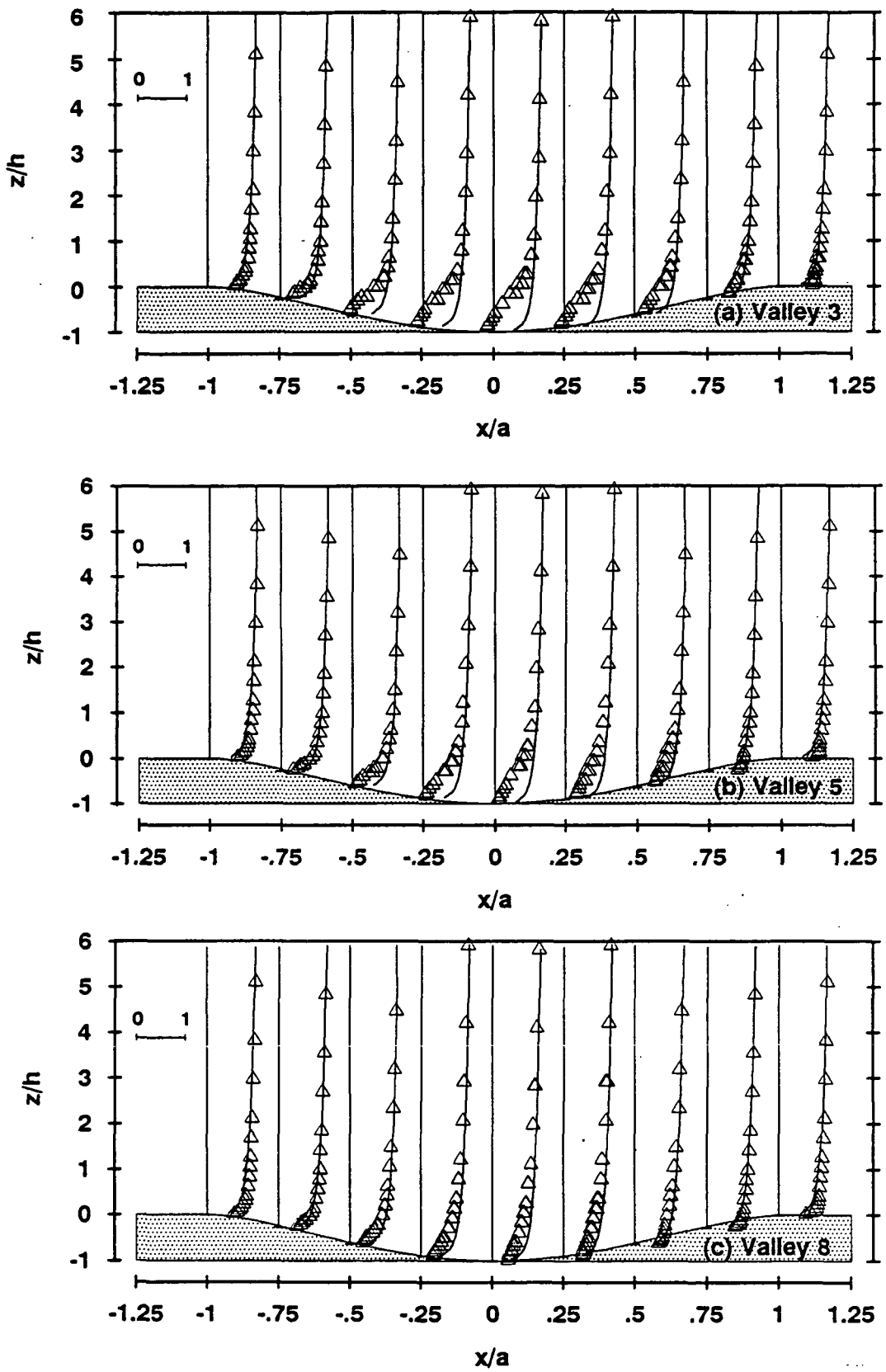

Figure 15. Longitudinal mean velocity profiles over the valleys (u/U_∞). Solid lines are flat-terrain profiles.

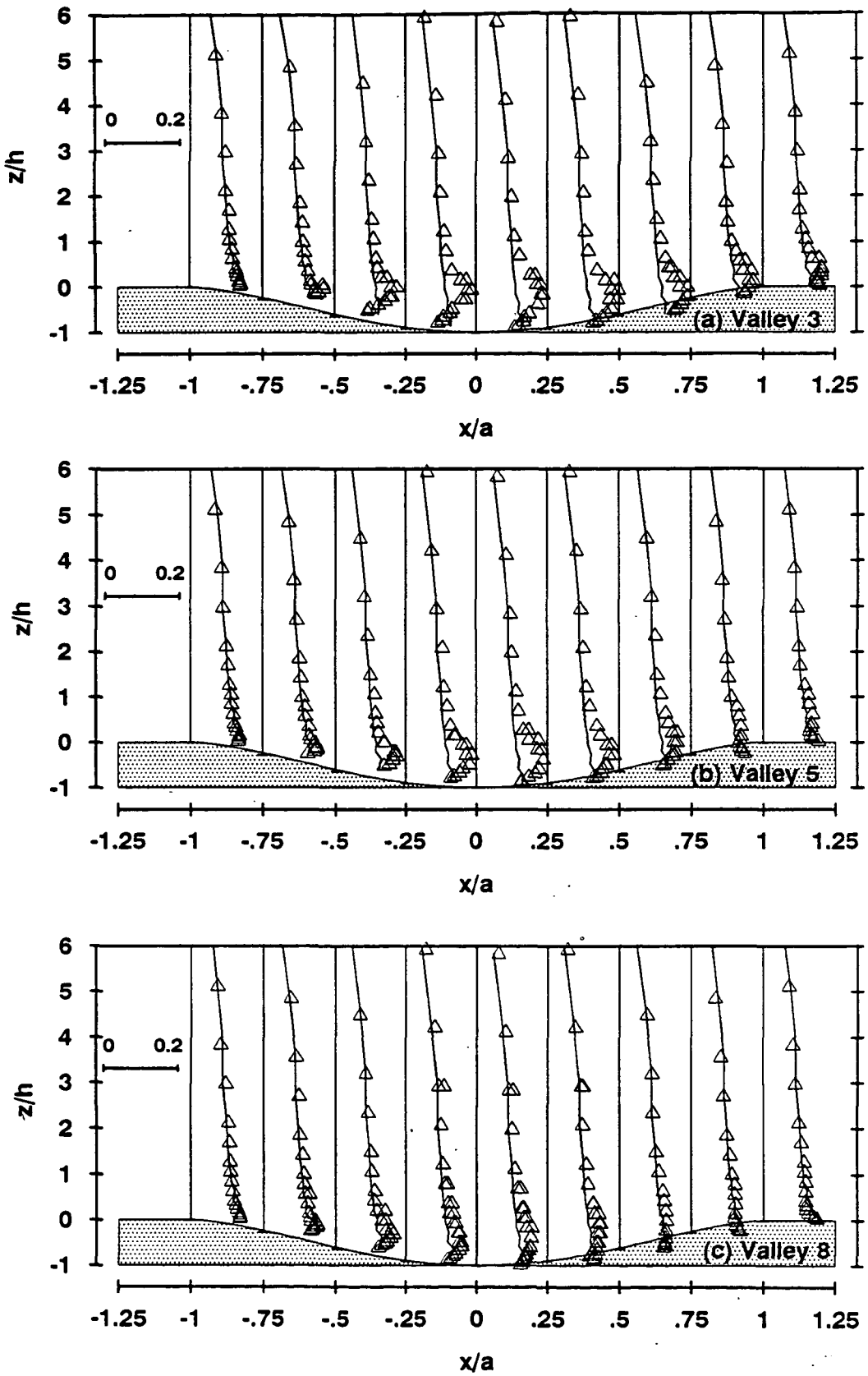

Figure 16. Longitudinal turbulence intensity profiles over the valleys (σ_u/U_∞). Solid lines are flat-terrain profiles.

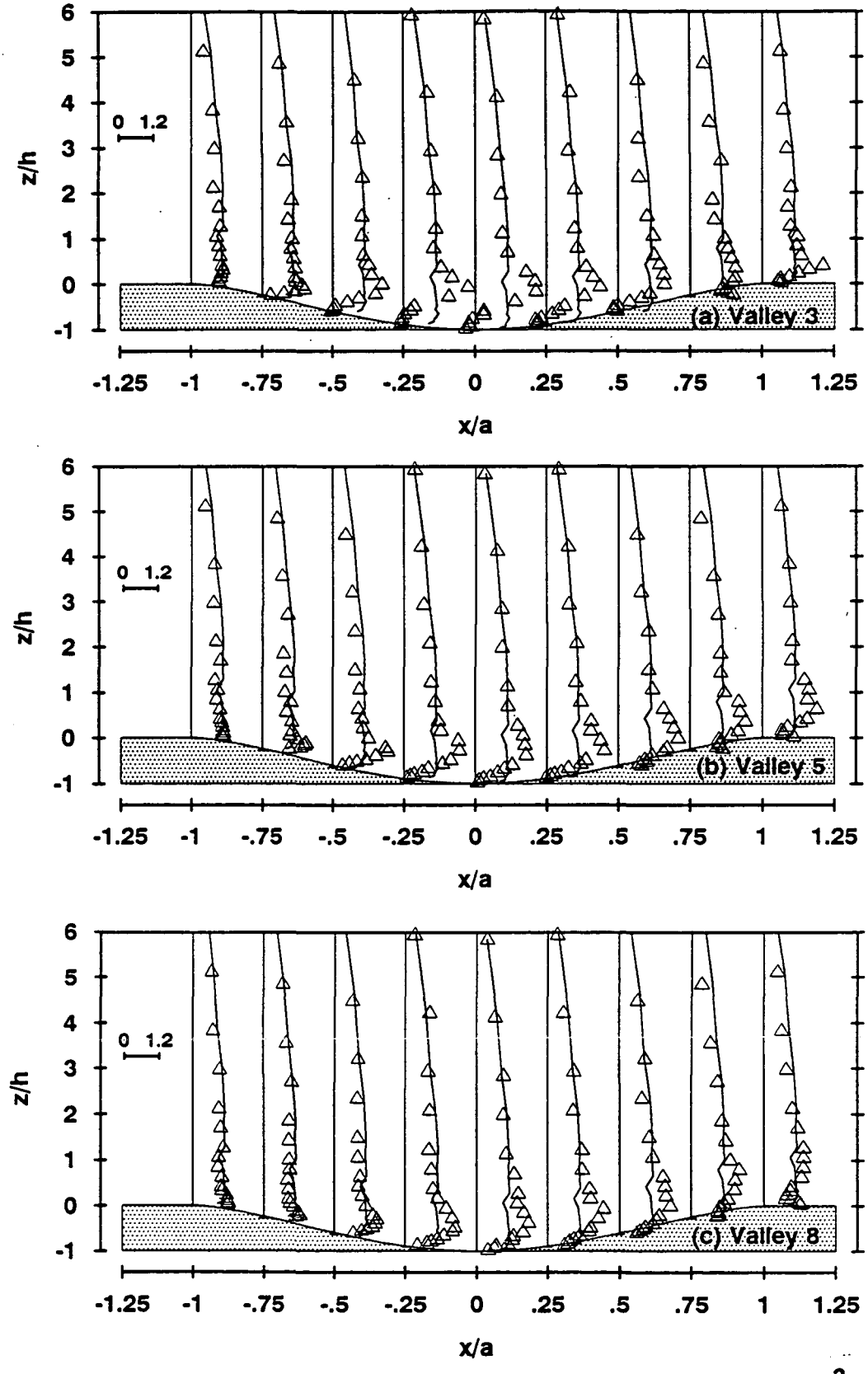

Figure 17. Reynolds-stress distributions over the valleys ($-\overline{u'w'} \times 10^3/U_\infty^2$). Solid lines are flat-terrain profiles.

accordance with the angle of the mean velocity vector. The profiles measured in flat terrain are shown for reference as solid lines in the figures.

Mean streamlines were calculated from the mean velocity measurements. For valleys 5 and 8, mass-consistent wind fields were computed using the model that is described in Section 4. For valley 3, the mean velocity profiles were simply integrated to find the elevations of specific values of the stream functions. These streamline patterns are displayed in Fig. 18.

At first glance, the streamline pattern over valley 8 is reminiscent of potential flow, but closer examination reveals it is clearly asymmetrical, with the lower streamlines being considerably closer to the surface on the downwind slope than on the upwind one. The streamline pattern over valley 5 is clearly asymmetrical and, because the streamlines diverge strongly away from the surface, it is clear that the velocity is reduced remarkably at the valley center; indeed, it appears that a stagnation region exists in the valley bottom. In valley 3, the streamline pattern clearly shows a recirculation region, with separation occurring a short distance down the upwind slope and reattachment occurring about halfway up the downwind slope from the valley center. The three valley shapes thus result in three fundamentally different flow patterns. We believe these basic flow structures are fairly typical and cover the range of patterns to be observed at full scale, albeit in neutral stratification.

It is instructive to examine the detailed characteristics of the velocity fluctuations within the valleys. Figure 19 shows the probability density distribution (or function -- PDF) of the longitudinal velocity fluctuations at half the valley height above the center of valley 3. This was measured with the pulsed-wire anemometer. Several interesting features are to be noted from these figures:

1. A best-fit Gaussian distribution is shown for comparison (on a logarithmic scale, the Gaussian distribution appears parabolic). The measured data are obviously slightly skewed, but for many practical purposes, the data may be considered to have a Gaussian distribution. The skewness and kurtosis are 0.18 and 2.85, respectively; these may be compared with Gaussian values of 0 and 3.0.
2. The distribution shows that the mean velocity is positive but the instantaneous velocity is negative perhaps 40% of the time. Thus, whereas flow reversals in the sense of the mean flow do not occur (at this position), instantaneous reversals occur frequently. The local turbulence intensity σ_u/u is very large, over 170%!
3. Abnormalities are observed at the points close to zero velocity. This is due to a hardware limitation of the PWA. If the speed of the heat pulse

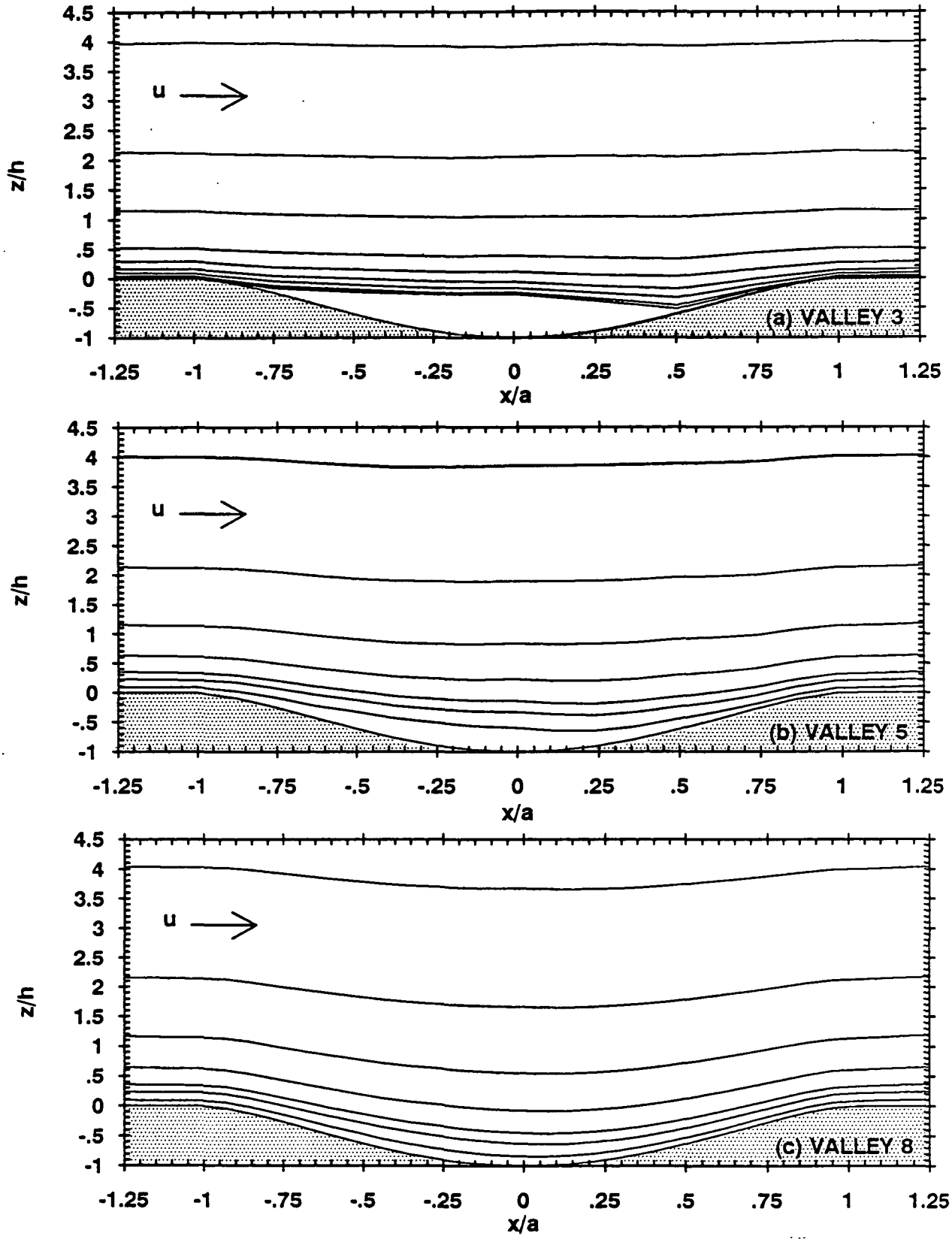

Figure 18. Streamline patterns derived from experimental measurements over the valleys. Note that the vertical scales are exaggerated.

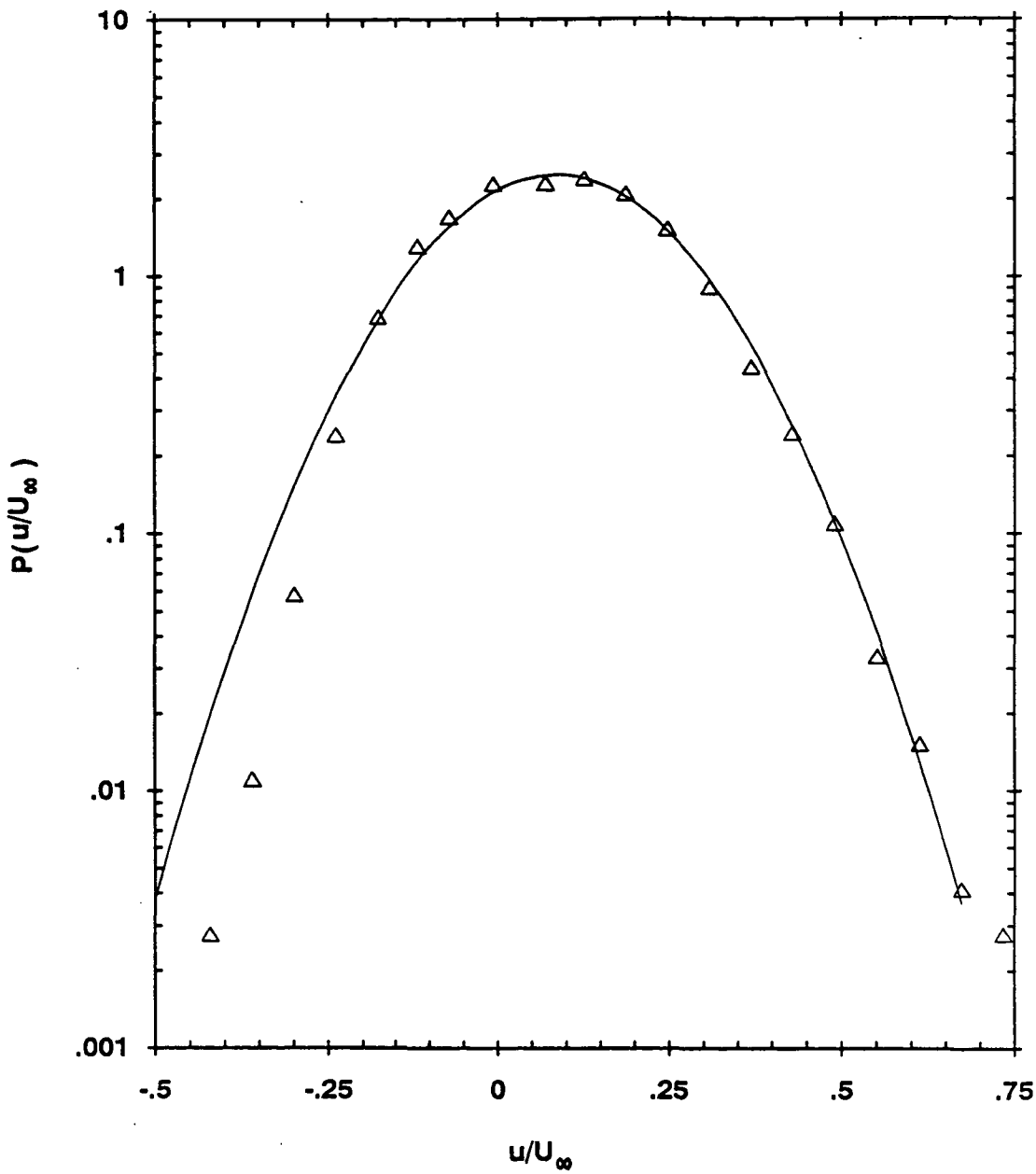

Figure 19. Probability density distribution of longitudinal velocity fluctuations measured at half the valley height above the center of valley 3.

is too low, it will not reach the sensor wire before the clock overflows, or the heat will diffuse such that the sensor wire will not detect it. In either event, very low velocities (typically less than 0.15 m s^{-1} -- positive or negative) will be indicated as zero velocities. This region is shown on the calibration curve in Fig. 5. Depending upon how the sorting slots are distributed about zero velocity, the results will be distorted. These abnormalities could be reduced somewhat by clever data manipulation, but no attempt was made to do so here.

Figure 20 shows the PDFs of the longitudinal velocity fluctuations at 5 elevations above the center of valley 3. The following characteristics of the flow are illustrated:

1. The *mean* velocities are negative at the two lowest elevations, h/8 and h/4, very close to zero at h/2, and some flow reversals occur even at the valley top h.

2. The magnitude of the velocity fluctuations, as evidenced by the *widths* of the distributions, is largest at the top of the valley. (This was also evident from the vertical intensity profiles, but is more dramatically illustrated here.) This is the position where the shear in the mean flow is largest (see Fig. 11a).

3. The reversed flow at the lowest elevation is quite steady, with only occasional ($\simeq$10% of the time) positive velocities indicated there.

Figures 21 and 22 show similar distributions measured above the centers of valleys 5 and 8. At the lowest levels within valley 5, the mean velocities were quite small, but instantaneous flow reversals were very common (up to 40% of the time at z/h = 0.13). A few reversals occurred at elevations as high as the valley top h in valley 5. A very few reversals (<1% of the time) were also observed in valley 8 between the surface and z = 0.4h.

Taken together, all of these data have important implications for the behavior of pollutants released within these valleys. Two primary features of two-dimensional neutral flow affect ground-level concentrations (glcs): the displacement of the mean streamlines and the changes in turbulence. The displacement of streamlines determines how near to the surface the centerline of a plume will reach. The convergence and divergence of the streamlines affect the plume width (a) directly and (b) indirectly through their distorting effects on the velocity gradients, which in turn affect the turbulence. The turbulence itself, of course, spreads and diffuses the plume. All of these effects can either increase or decrease surface concentrations. Note that, because the flow is two-dimensional, the mean streamlines remain in vertical planes. However, the longitudinal and vertical turbulence intensities are greatly increased through the flow distortions and, because of

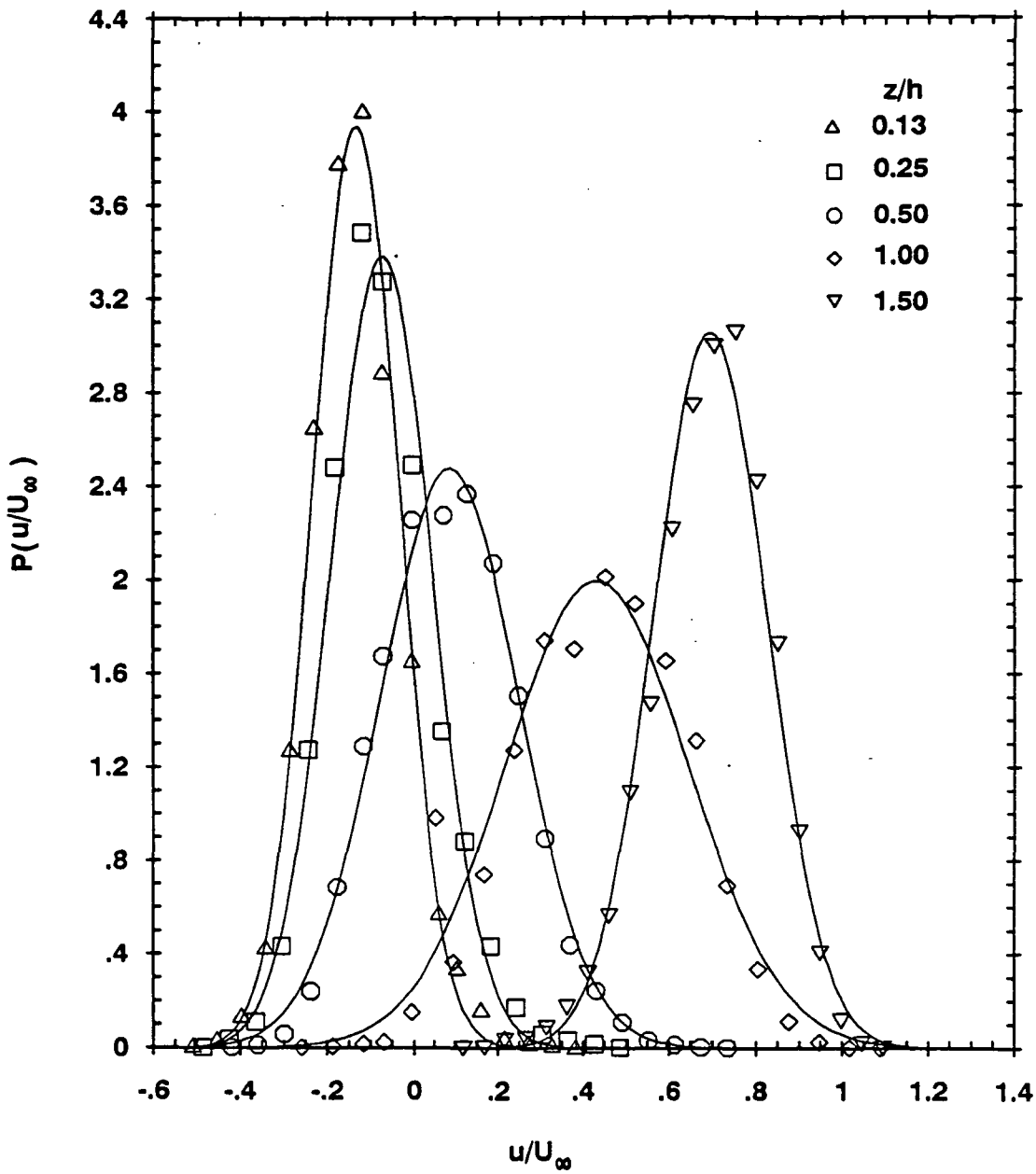

Figure 20. Probability density distributions of longitudinal velocity fluctuations at various elevations above the center of valley 3.

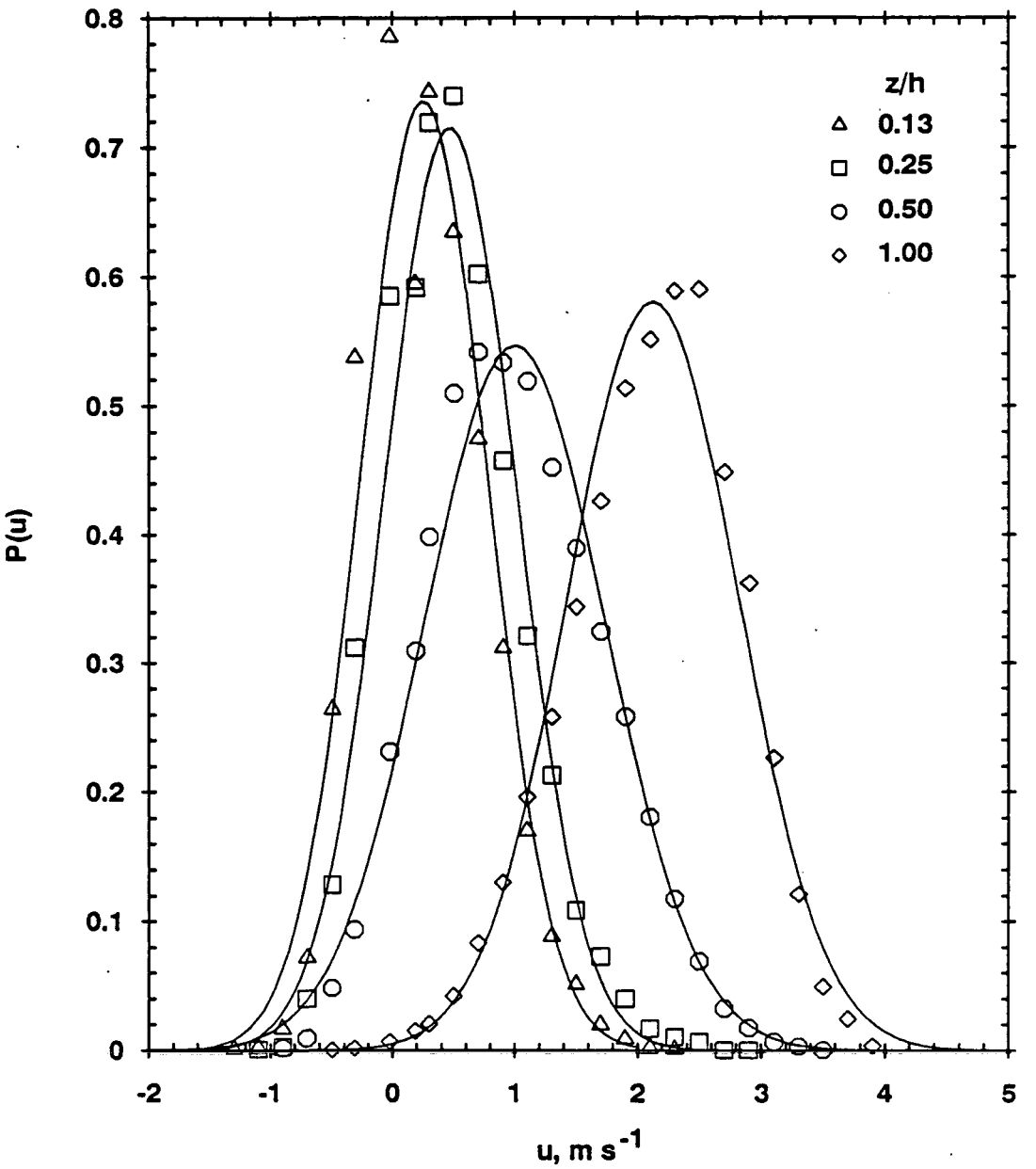

Figure 21. Probability density distributions of longitudinal velocity fluctuations at various elevations above the center of valley 5.

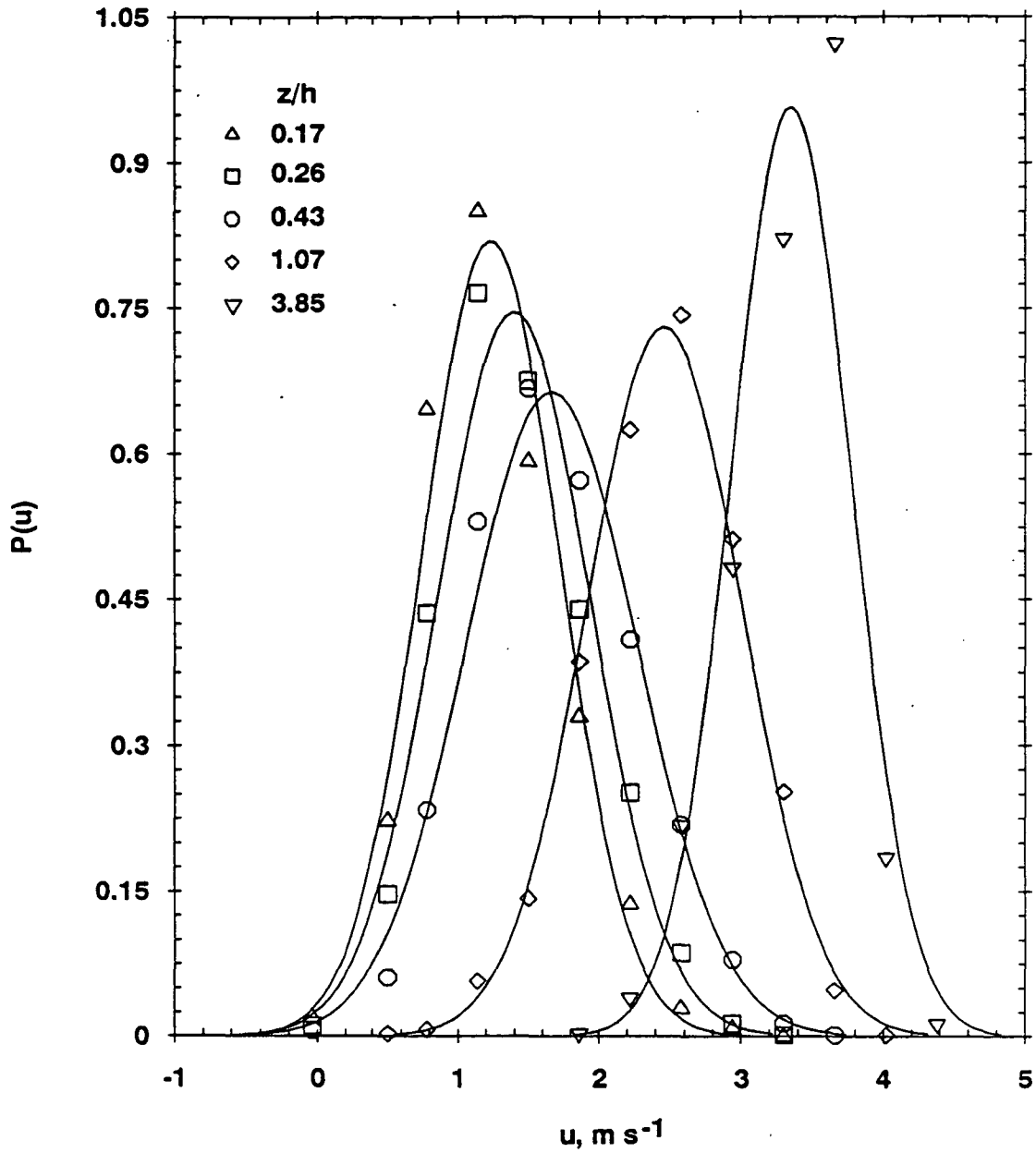

Figure 22. Probability density distributions of longitudinal velocity fluctuations at various elevations above the center of valley 8.

the tendency of turbulence to distribute its energy equally in all directions (return toward isotropy), the lateral turbulence intensities will also be greatly increased.

It is useful to examine in some detail the flow structure within the three valleys with a view toward anticipating the behavior of pollutants released within them. Consider first the mean streamline pattern over valley 8 (Fig. 18c). Because it displays the smallest flow distortions of the three valleys, we may expect the smallest changes (from flat terrain) in maximum surface concentrations, (*i.e.*, TAFs closest to 1.0). Because the mean streamlines begin to diverge at the upstream edges of the valleys, we might expect maximum glcs from sources placed there to be less than those observed in flat terrain (TAFs less than unity). On the upwind slope, the mean streamlines diverge so that plumes released there would be transported farther from the surface. However, because the turbulence is increased, these plumes would be diffused more rapidly to the surface. With these counteracting tendencies, it is difficult to speculate on the net effects except to state that we would not expect the largest TAFs to occur with sources located in this position. For sources placed above the valley center, it is easily seen that the streamlines transport the plumes closer to the surface and the enhanced turbulence rapidly diffuses a plume to the surface. Hence, we may expect the largest TAFs from sources placed in the valley center. For sources placed at the downwind edge of the valley, we again observe the counteracting effects of streamline divergence but increased turbulence, and we expect the TAFs to be near unity again. Note that enhanced lateral diffusion will diminish surface concentrations along the plume axis, but increase the area of coverage in the lateral direction.

For valleys 5 and 3, we may expect roughly the same behavior from sources placed near the upstream and downstream edges of the valleys, *i.e.*, TAFs near unity. For low sources above the center of valley 5, however, we observe very small mean transport speeds and very common flow reversals. We may expect the plumes to be wafted back and forth while being diffused strongly in the lateral and vertical directions before eventually being transported downstream. Thus, we may expect quite large TAFs for low sources near the center of valley 5.

In valley 3, the streamline patterns show a definite recirculation region that extends to nearly 75% of the valley depth. Plumes released on the separation/reattachment streamline will be transported directly to the

surface. We may thus expect very large TAFs from such releases. Plumes released well below the separation/reattachment streamline, say in the reversed flow region around h/4, would be transported upstream in a more routine manner, with the plume axis remaining nearly parallel to the surface. Because of the very large turbulence intensities and relatively low transport speeds, we may still expect large TAFs (but not as large as those from the higher sources).

The general features of these flows are remarkably similar to those observed on the lee sides of the hills in the RUSHIL study. As mentioned earlier, those hills had exactly inverse shapes (and slopes) as the present valleys. And as with the valleys, hill 8 exhibited no separation, hill 5 exhibited *incipient* separation (*i.e.*, instantaneous flow reversals were observed approximately 40% of the time, but the mean flow was always downstream), and hill 3 exhibited clear separation with mean-flow reversals at low elevations.

3.3 Concentration Measurements in the Valleys

Figure 23 illustrates some typical comparisons between surface concentration profiles measured from sources placed within the valleys and those from sources of the same height in flat terrain. In all cases, the stack height H_s was equal to the valley depth h. x_s denotes the distance from the source. In Fig. 23a, the source was located at the upstream edge of each valley, and the changes in the maximum glcs induced by the valleys are small, less than 15% in all cases. This figure shows that the *location* of the maximum glc is beyond the downstream edge of the valley in each case and that, where the maximum glc is higher, its location is closer to the source and *vice versa*.

In Fig. 23b, the source was located at the valley center. The increased concentrations caused by the valleys are dramatic and TAFs range from about 2.5 in valley 8 to about 15 in valley 3. Also, as the concentration increases, the distance to the maximum decreases. Indeed, the location of the maximum in valley 3 is only 2 stack heights downstream, compared with about 15 stack heights in flat terrain. This is obviously because the plume is released very near to the separation/reattachment streamline.

When the source was placed at the downstream edge of the valley (Fig. 23c), virtually no change in the maximum glc was observed.

One more case is illustrated in Fig. 24, where the source location was half the valley height above the valley center. The location of the maximum

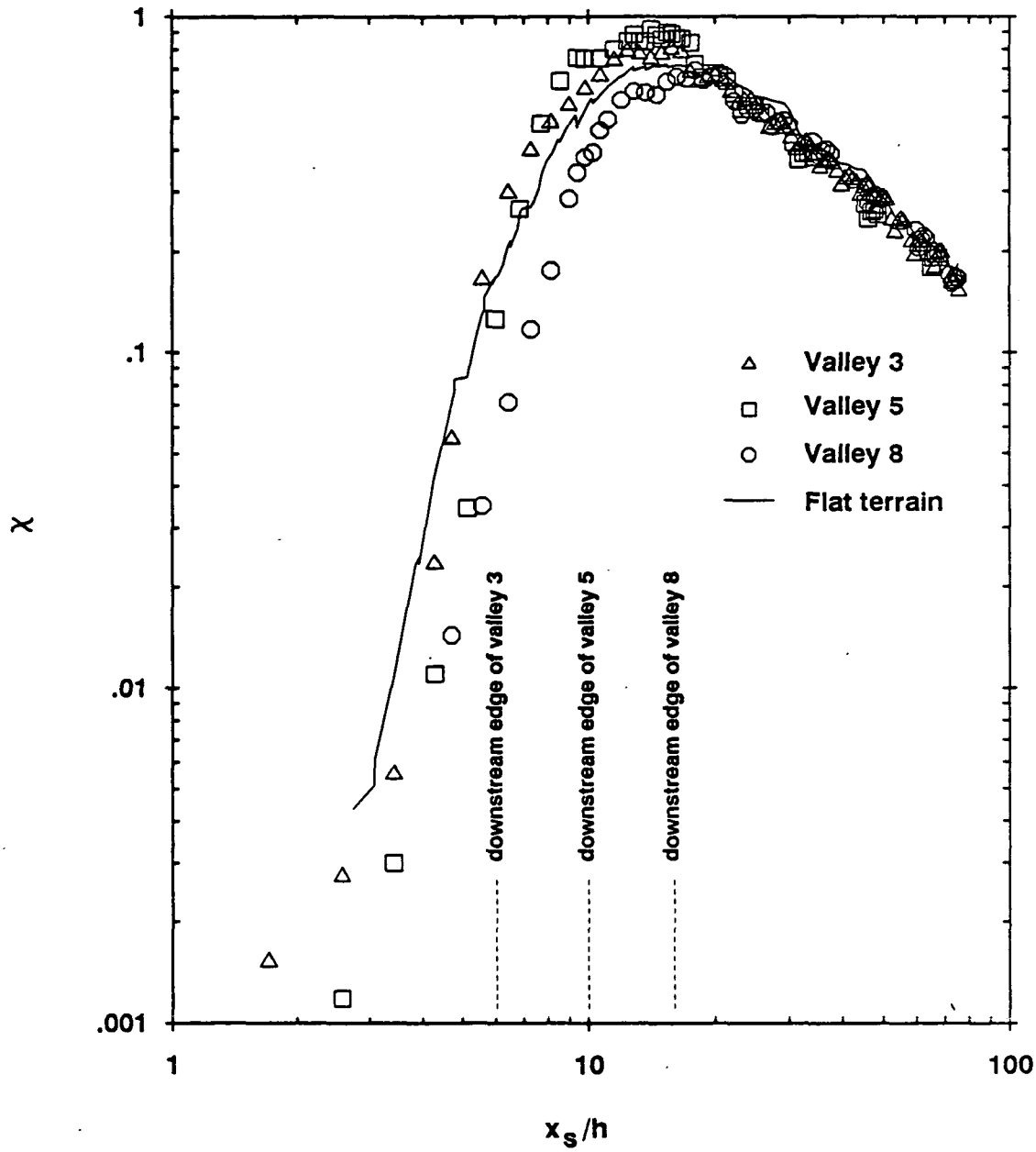

(a) Source located at upstream edge of valleys

Figure 23. Comparison of surface concentration profiles from sources placed within the valleys with one from a source of the same height in flat terrain. $H_S = h$.

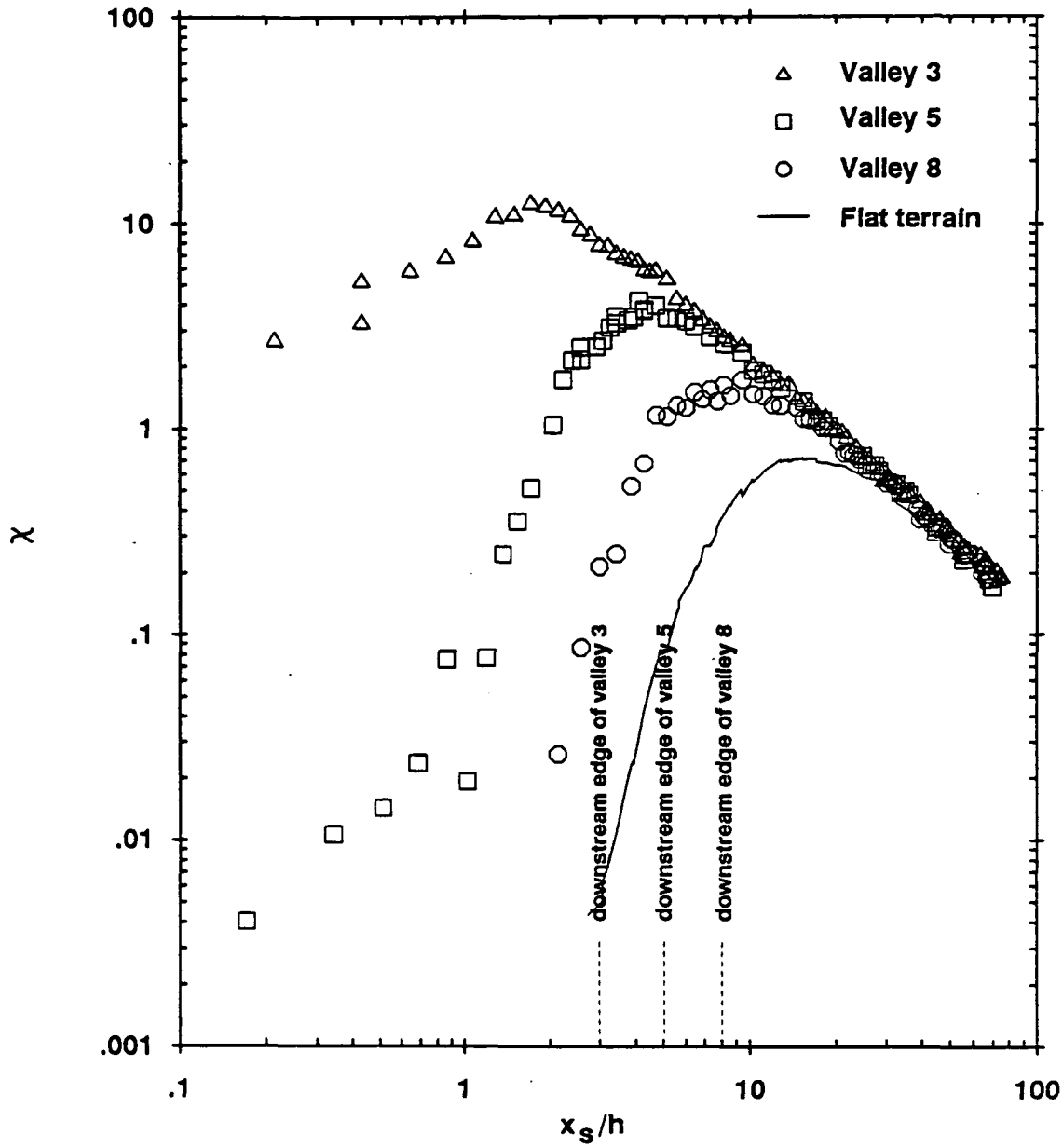

(b) Source located at center of valleys

Figure 23. Comparison of surface concentration profiles from sources placed within the valleys with one from a source of the same height in flat terrain. $H_s = h$.

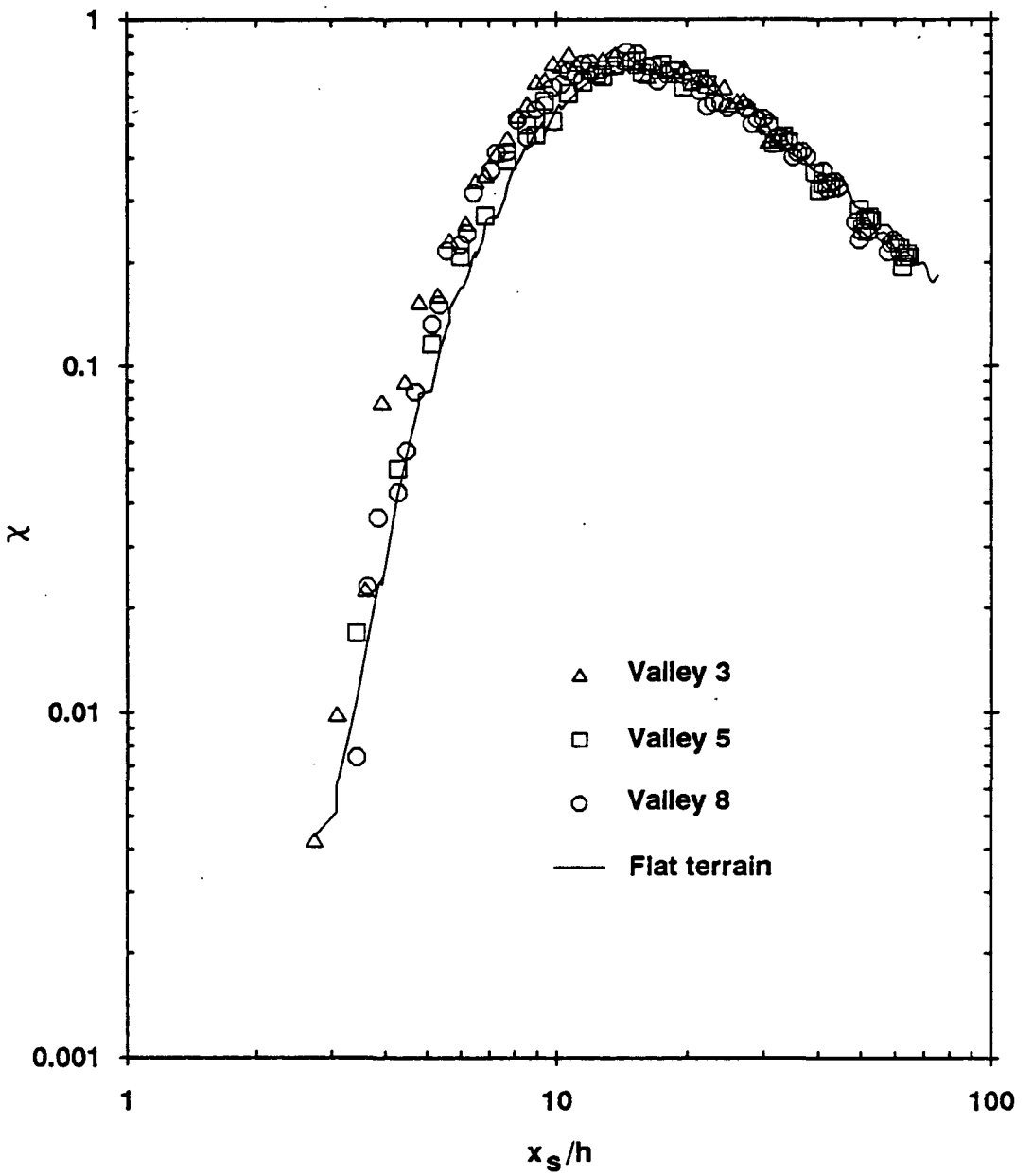

(c) Source located at downstream edge of valleys

Figure 23. Comparison of surface concentration profiles from sources placed within the valleys with one from a source of the same height in flat terrain. $H_s = h$.

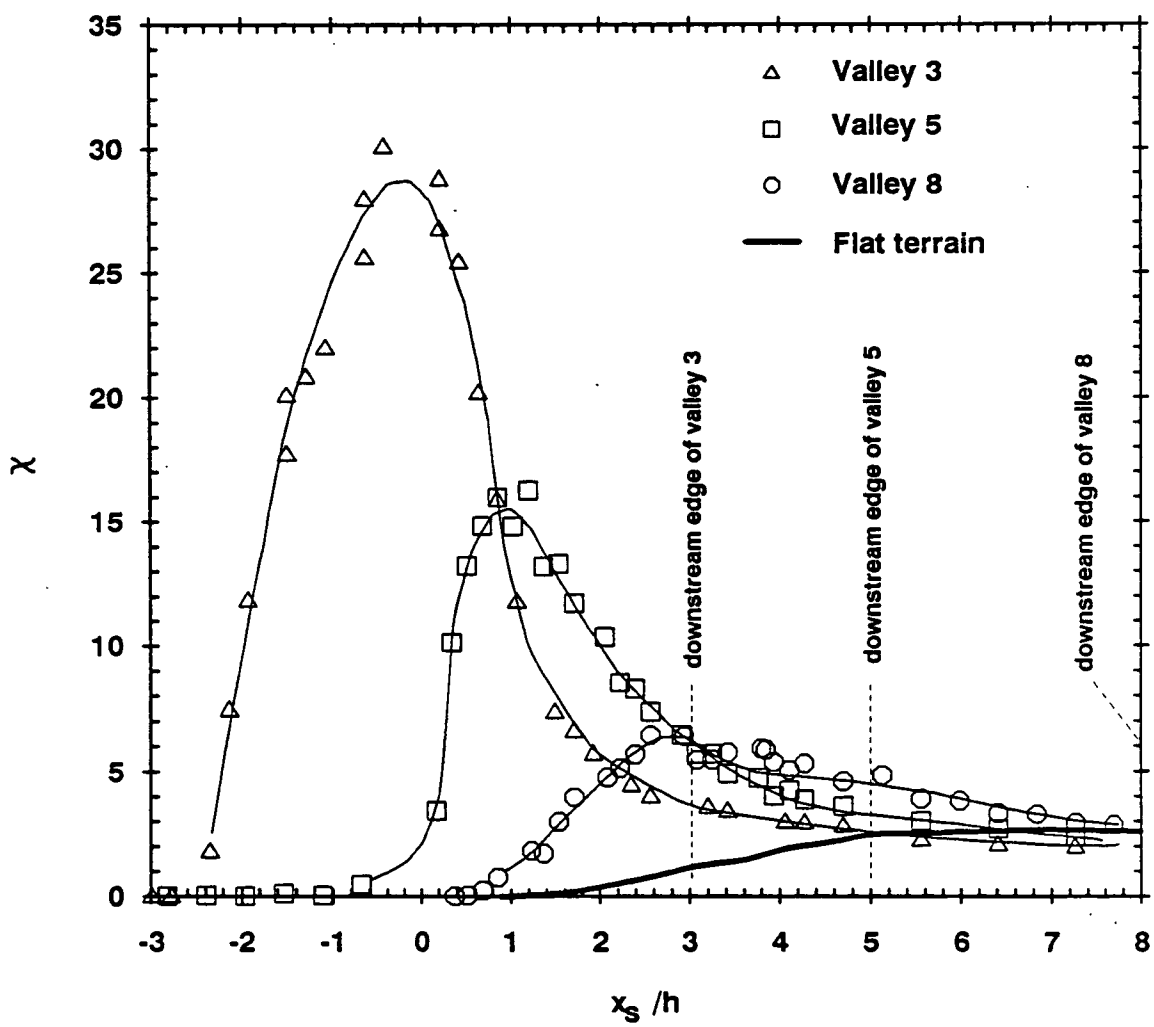

Figure 24. Comparison of surface concentration profiles from sources placed within the valleys with one from a source of the same height in flat terrain. $H_s = h/2$. Source position is at the center of the valley (x/a = 0).

for valley 3 was actually slightly upwind of the source, and the TAF is about 12. For valley 5, the location of the maximum glc was downstream, but very close -- about 2 stack heights away -- and the TAF is about 6.

Measurements such as these were made at an array of source locations and heights in the vicinity of each of the three valleys, and the TAFs were determined for each location. Maps of these TAFs are shown in Fig. 25, where isopleths of constant TAF have been drawn. The first impression is that the patterns are symmetrical about the vertical centerline, but closer examination reveals some asymmetry. Nevertheless, the near-symmetry and the overall similarity in shape amongst the three valleys is quite surprising in view of the very different flow patterns observed. In contrast, the magnitudes of the maximum TAFs differ widely, from 2.5 in valley 8 to 15 in valley 3. These differences, of course, reflect the effects of the different flow structures. The location of the maximum TAF seems to be independent of valley shape, occurring above the valley center in each case (but see Section 4: the theoretical model predicts maximum TAFs a short distance upwind of the center of valley 8, at a position where no experimental measurements were made). The TAFs display rather broad peaks on the vertical centerline -- between h/2 and h, the TAFs vary by only 10 to 20%.

Contours with TAF values of 1.4, 2, 4, *etc.*, have been drawn where appropriate. Note that these contours form "windows" within which the maximum glc exceeds the glc that occurs in flat terrain by 40%, 100%, 300%, *etc.* The longitudinal extent of the window of 40% excess concentration extends over approximately 60% of the width of valley 8, 80% of the width of valley 5, and more than 90% of the width of valley 3. The vertical extent of the 40% window is 1.5, 2.0, and 2.5 valley heights above the valley *top* for valleys 8, 5, and 3, respectively.

At first the vertical extent of the 40% windows may appear excessively large. For example, the height of a stack placed near the center of valley 5 would have to equal 3 valley heights in order to meet a 40% excess criterion. A very rough estimate will show, however, that this is quite reasonable. We assume that for very tall stacks, the only effect of the valley is to reduce the effective stack height H_s by the valley height h. Because the maximum glcs may generally be considered inversely proportional to the square of the stack height, the TAF may be calculated as

$$A = \chi_{mx}/\chi^{o}_{mx} = H_s^2/(H_s - h)^2 ,$$

Where χ_{mx} is the maximum normalized glc and χ^{o}_{mx} is the maximum normalized glc

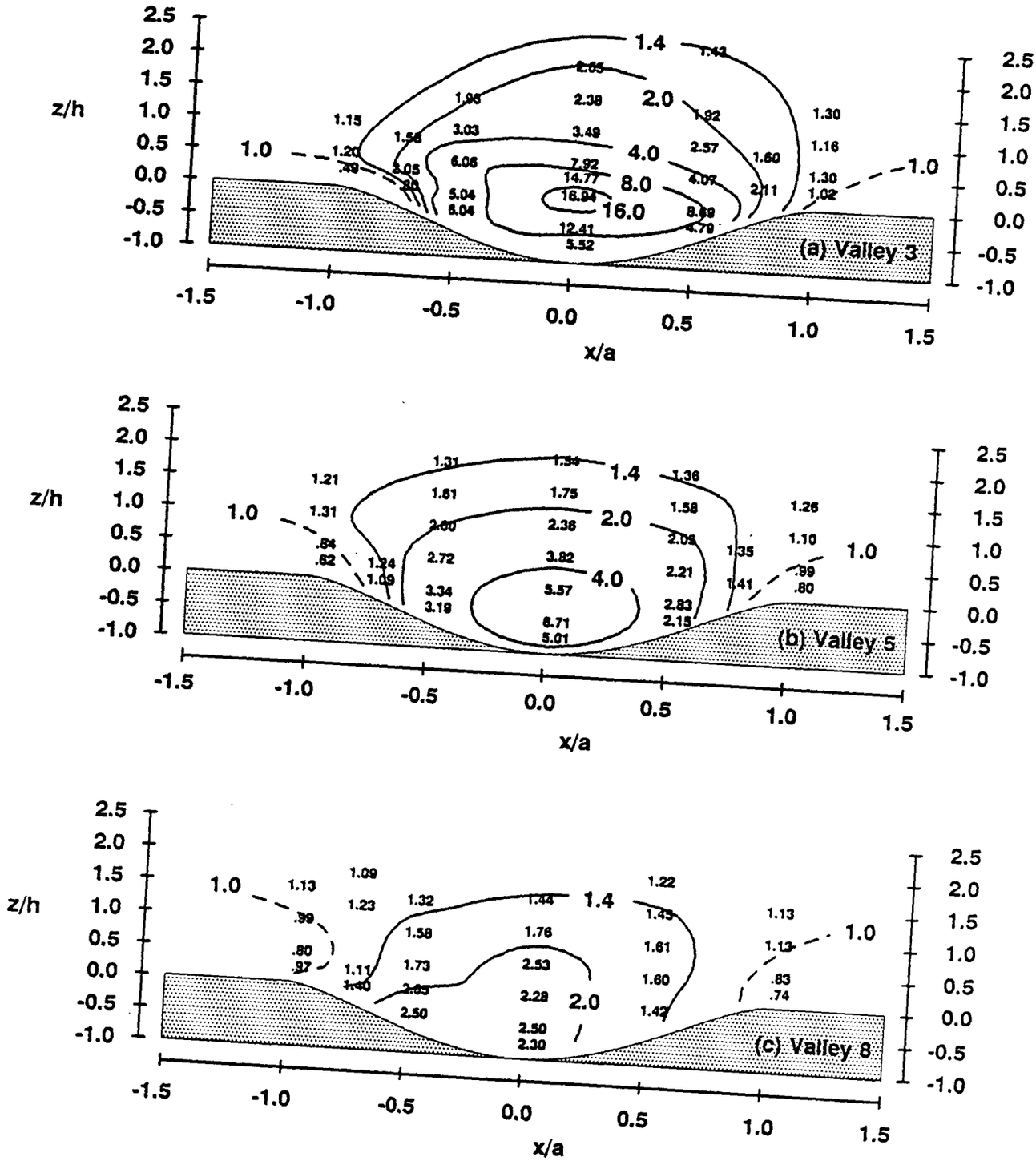

Figure 25. Contours of constant terrain amplification factor derived from experimental measurements.

from a source of the same height on flat terrain. For a stack height 3 times the valley height, A = 2.25 (a 125% excess concentration). This is, of course, an overestimate, because it does not account for the vertical rise provided by the airflow (see streamline patterns at z = 2h in Fig. 18).

Application of the data in Fig. 25 is straightforward. Let us consider a source which is located in the center of a rather broad valley, say one similar in shape to valley 8; and the height of the source is half the valley height. Figure 25c suggests that the maximum glc would be about 2.5 times that expected from a source of the same height but located in flat terrain. On the other hand, if the valley were considerably narrower, say close to valley 5, Fig. 25b suggests the maximum glc would be about 7 times as large as that from the same source in flat terrain. Although precise interpolation of these results for valleys intermediate in shape and slope to those examined here may be difficult, the results may allow us to place some useful limits on the effects of valleys of intermediate shape and slope.

Figure 26 shows the loci of source positions leading to the same locations of maximum glc. These loci have been identified by marking them with the position of the maximum glc (in valley heights from the centers of the valleys). Note that the "undisturbed" or flat-terrain loci (dotted lines) are simply parallel, nearly straight, diagonal lines. Within the valley, these loci are distorted, as shown by the solid lines. The diagrams may be used as follows: for any given source position, we may plot that position on the diagram, then follow the locus to the ground; the intersection of that locus with the ground is, of course, the location of the maximum glc. Conversely, from a knowledge of the location of the maximum glc, we may use these diagrams to determine the line along which the source was positioned. These loci become highly distorted near the valley centers, and the steeper the valley, the higher the distortion. As the distance (both longitudinal and vertical) from the valley center increases, these loci gradually relax to their undisturbed or flat-terrain values.

We have thus far discussed primarily the locations and values of the maximum glcs. It is also instructive to examine the area of coverage in the crosswind direction. Figure 27 shows the lateral plume widths measured downwind of sources of the same height (H_s = h/4) placed in the center of each of the three valleys. These distributions were measured at the same downwind distance in each case (x_s = $6H_s$). It may be seen that the lateral widths of the plumes increase quite strongly as the steepness of the valley increases.

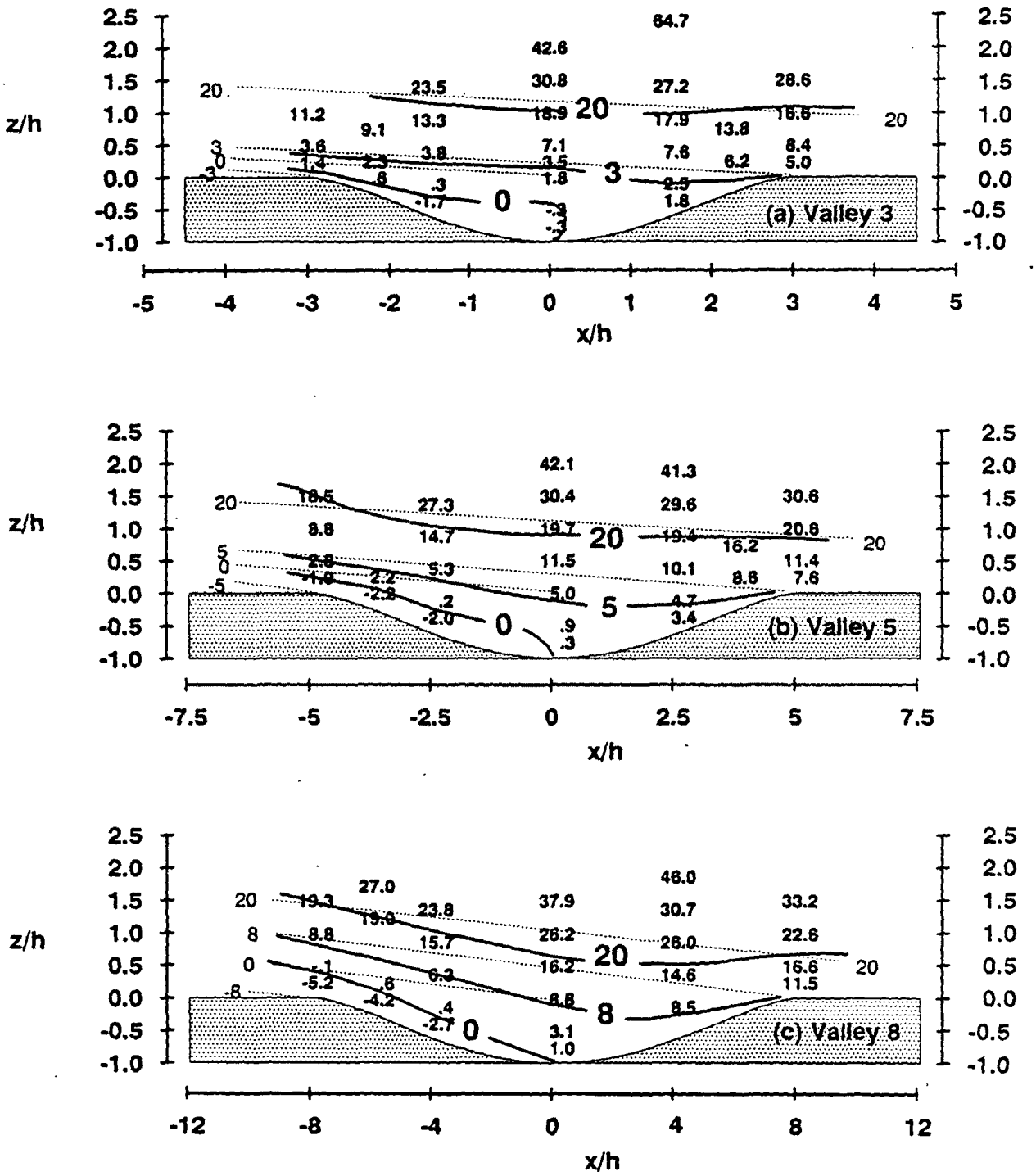

Figure 26. Distance in valley depths from the valley center to the location of maximum ground-level concentration. Flat terrain values are indicated as dotted lines.

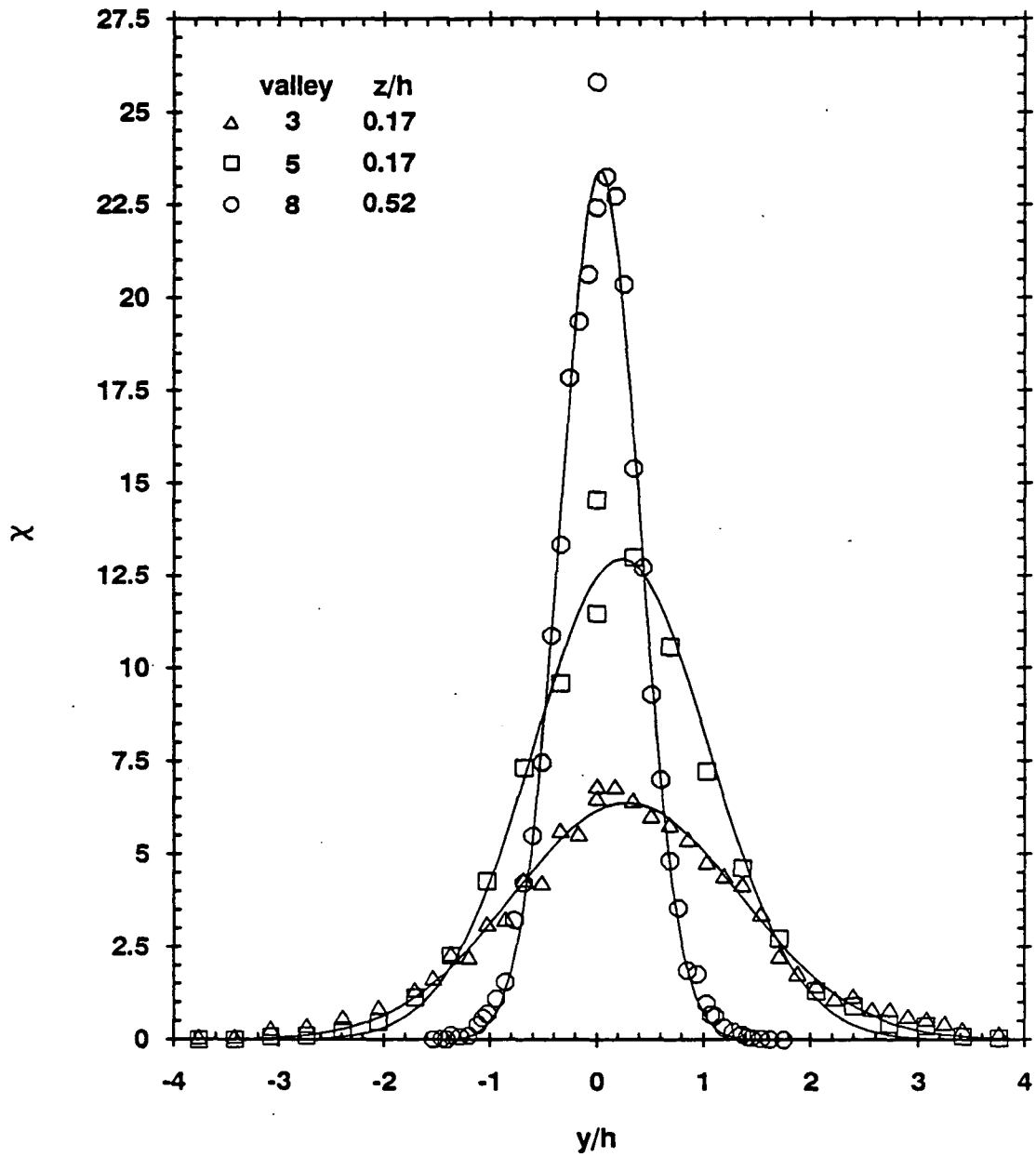

Figure 27. Lateral concentration distributions measured $6H_s$ downwind of stacks of height h/4 placed in the center of each of the three valleys. Solid lines are Gaussian curve fits.

Whereas a lateral profile was not measured at the same downwind distance in flat terrain, we may use an interpolation formula that fits the measured data quite well (see Section 4) to estimate $\sigma_y/h = 0.19$. By comparison, the corresponding values are nearly twice as large in valley 8, 4.5 times as large in valley 5, and 6 times as large in valley 3. This is due, of course, to the much reduced transport speeds and the greatly enhanced local turbulence intensities. In valley 5, the transport speed is extremely slow and the turbulence intensity is very large. Thus, the plume is wafted around in all directions as it is gradually transported from the source to the measurement point. In the case of valley 3, the measurement point is quite close to the reattachment point, so that the plume is actually transported upstream (in the mean) and recirculated within the separation/reattachment zone before reaching the measurement location. Note that the best-fit Gaussian curves shown on the figure actually fit the measured distributions quite well; this matches our common observation that lateral concentration distributions are almost always Gaussian in shape.

4. NUMERICAL MODEL AND COMPARISONS WITH EXPERIMENTAL RESULTS

One of the main purposes of the experimental study described in earlier sections was to test the applicability of a diffusion model for the evaluation of maximum glcs resulting from elevated continuous point sources placed in a curvilinear neutral atmospheric boundary layer. The model described here uses as input parameters data from wind-tunnel measurements of wind velocities and turbulence characteristics to calculate the entire flow field. This flow field is then applied in the numerical solution of the diffusion equation. Such a model was previously developed by Berlyand *et al.* (1975), primarily for evaluation of pollutant dispersion in complex terrain, on the basis of measurements of flow structure in a wind tunnel where direct measurements of pollutant dispersion were inaccessible.

The present version of the model does not incorporate a longitudinal diffusion term, and therefore does not calculate the spread of pollutants in separated flows. Thus, no attempt is made to apply the model to valley 3, and calculations were made only for valleys 5 and 8.

Application of the diffusion equation to the calculation of the spread of pollutants over flat terrain may be of interest in and of itself, because it provides additional information on the applicability of the gradient transport theory of turbulent diffusion (K-theory). Some of the assumptions involved in the development of K-theory are not strictly satisfied for elevated point sources, especially near to the source. However, since the interest here is primarily in computing glcs, K-theory is applied to elevated point sources.

4.1. Calculations of dispersion over flat terrain

Modeling the spread of pollutants over homogeneous flat terrain is based on a numerical solution of the diffusion equation for an elevated continuous point source,

$$u \frac{\partial \chi}{\partial x_s} = \frac{\partial}{\partial y} \left\{ k_y \frac{\partial \chi}{\partial y} \right\} + \frac{\partial}{\partial z} \left\{ k_z \frac{\partial \chi}{\partial z} \right\}, \tag{1}$$

where χ is the pollutant concentration, u is the mean velocity, k_y and k_z are the eddy diffusivities in the crosswind and vertical directions, x_s is the downwind distance from the source, and z is the height above ground.

If, as assumed by Berlyand (1975), $k_y = k_o u$ (where k_o may be a constant or a function of x_s), a separation of variables may be performed, so that Eq.

(1) may be reduced to the two-dimensional problem of diffusion from a line source,

$$u \frac{\partial \chi'}{\partial x_s} = \frac{\partial}{\partial z} \left\{ k_z \frac{\partial \chi'}{\partial z} \right\} . \tag{2}$$

χ' represents concentration in the two-dimensional problem.

Assuming reflection of pollutant from the ground surface, the boundary conditions are as follows:

$$\begin{array}{ll} \chi' = [Q/u(H_s)]\ \delta(z-H_s) & \text{at } x_s = 0 , \\ k_z \partial\chi'/\partial z = 0 & \text{at } z = 0 , \\ \chi' \to 0 & \text{when } z \to \infty . \end{array} \tag{3}$$

Here, Q is the source flow rate, H_s is the source height, and δ is the Dirac delta function. The relation between concentrations of point and line sources is given by the following expression (assuming y = 0 is a coordinate of the source):

$$\chi(x_s, y, z) = \frac{\chi'(x_s, z)}{(4\pi G)^{1/2}} \exp\left(- \frac{y^2}{4G} \right) , \tag{4}$$

where $G = \int_0^{x_s} k_o(\xi) d\xi$.

Equation (2) with boundary conditions (3) was solved numerically by a finite-difference method. To obtain a solution, values of u and k_z must be specified. As shown in Fig. 11a, the vertical profile of mean velocity may be satisfactorily approximated by

$$u = \left\{ \begin{array}{ll} \frac{u_*}{\kappa} \ln[(z-d)/z_o] & \text{when } z < h_1 \\ \frac{u_*}{\kappa} \ln[(h_1-d)/z_o] & \text{when } z \geq h_1 \end{array} \right\} , \tag{5}$$

where κ is the von Kàrmàn constant (0.4), u_* is the friction velocity, d is the displacement height, and z_o is the roughness length. In accordance with the wind-tunnel data, the various parameters were assumed to be $u_* = 0.19$ m s^{-1}, d = -0.5 mm, and $z_o = 0.16$ mm. (These values were obtained from preliminary results of the wind-tunnel measurement program and differ only slightly from the final values.) The value of h_1 was chosen to achieve the value of the free-stream velocity at the top of the boundary layer (4 m s^{-1}).

For k_z, it was assumed as is commonly done that $k_z = k_h$, where k_h is the eddy diffusivity of heat, and also that $k_h = \alpha k_m$, where k_m is the eddy diffusivity of momentum. In earlier works, it was generally assumed that α = 1.35, but according to more recent data (Kader and Yaglom, 1972; Snijders *et al.*, 1983), it appears more appropriate to assume α = 1.15. The latter value was used in the present study.

k_m was related to the turbulent kinetic energy (per unit mass) through

the following (Berlyand, 1975):

$$k_m(z) = \kappa\, C_1^{1/4}\, E(z) \int_0^z \frac{d\xi}{[E(\xi)]^{1/2}}\,, \tag{6}$$

where C_1 is a constant, and $E = (1/2)\,(\overline{u'^2} + \overline{v'^2} + \overline{w'^2})$. $C_1 = 0.025$ was chosen as the best-fit to the linear growth of k_m in the lower part of the boundary layer with $u_* = 0.19$ m s^{-1}.

Figure 28 shows the profile of $k_m(z)$ as calculated by Eq. (6). As might be expected, k_m increases almost linearly with height in the lower levels (as is commonly observed in the neutral atmosphere), then begins to decrease toward zero. This decrease seems to be a peculiarity of wind tunnel flows, because atmospheric observations suggest a constant value may be more appropriate.

k_m was also evaluated using the more usual relation $k_m = -\overline{u'w'}/(du/dz)$, where $-\overline{u'w'}$ is the Reynolds stress that was also measured in the wind tunnel. The profile calculated using this method was approximated as follows

$$k_m = \left\{ \begin{array}{ll} \kappa u_* z & \text{when } z \le h_2 \\ 0.818\ \kappa u_*(1-z) & \text{when } z > h_2 \end{array} \right\}. \tag{7}$$

Here, z must be measured in meters, and the value of h_2 was specified as 0.45 m. Using Eq. (7), k_m also tends toward zero at the top of the boundary layer, although Eq. (6) gave larger values at those heights. Because all source heights were substantially smaller than the boundary-layer depth, this difference has no practical significance.

Calculations of pollutant diffusion [solutions of Eq. (2) with boundary conditions (3)] were made with the use of Eqs. (6) and (7).

Difficulties are encountered with K-theory in the specification of the parameter k_y. In this case, it is helpful to use assumptions from the statistical theory of turbulent diffusion on the root-mean-square particle displacement in the lateral direction, σ_y. k_y may be related to σ_y through the well-known equation $k_y = (1/2)\, d\sigma_y^2/dt$. Taylor (1921) showed that the mean-square particle displacement is given by

$$\sigma_y^2(t) = 2\,\overline{v'^2} \int_0^t \int_0^{t'} R_L(\xi)\, d\xi\, dt', \tag{8}$$

where $R_L(\xi) = \overline{v'(t)\, v'(t+\xi)} \Big/ \overline{v'^2}$ is the Lagrangian velocity auto-correlation function. Because direct measurements of R_L are very difficult,

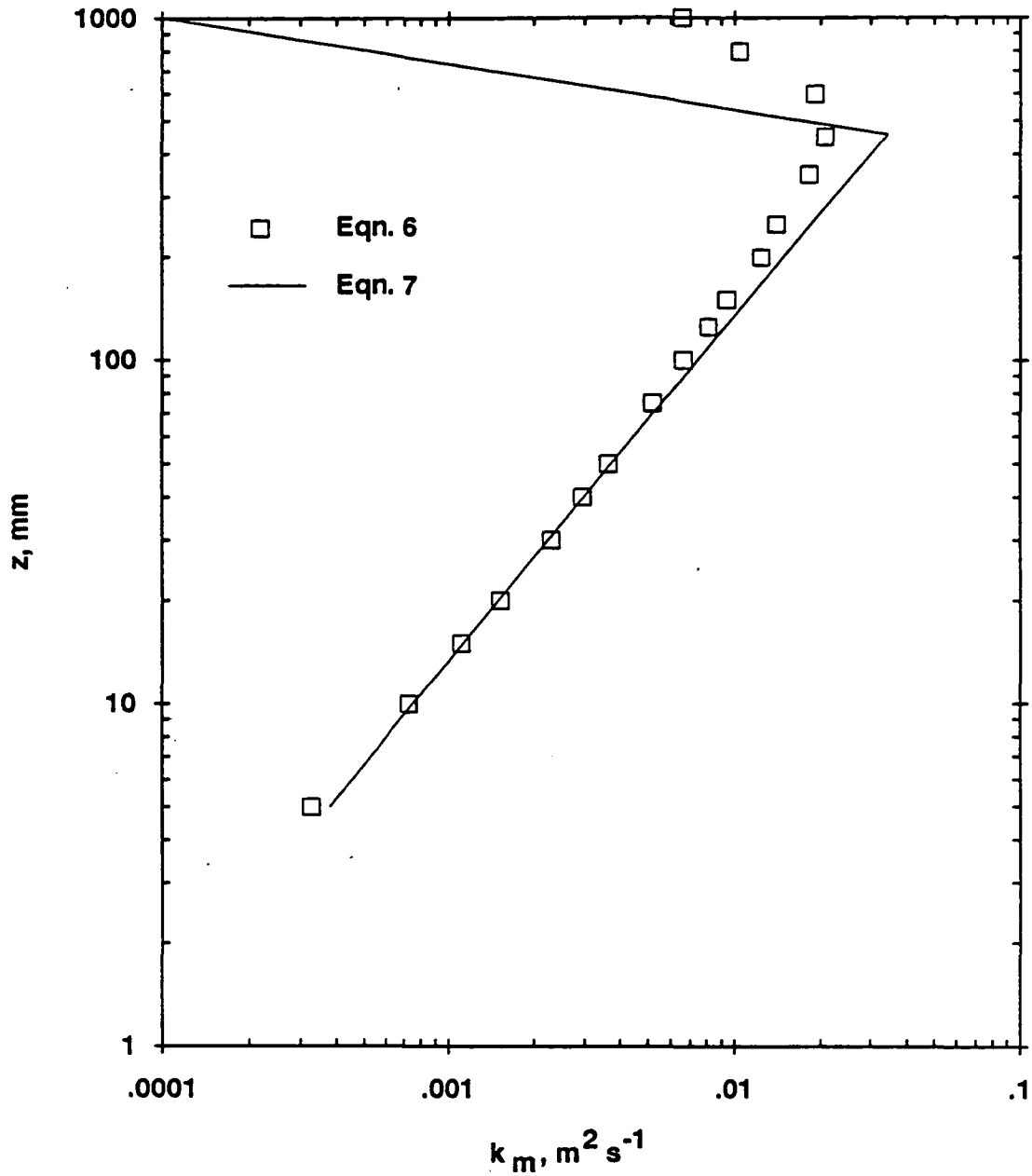

Figure 28. Vertical profile of eddy diffusivity k_m in flat terrain.

we have chosen to use known asymptotes of σ_y. As $t \to 0$, $R_L \to 1$, and as $t \to \infty$, $R_L \to 0$. Therefore,

$$\sigma_y = \left\{ \begin{array}{ll} \sigma_v t & \text{when } t \to 0 \\ \sigma_v \sqrt{2T_L t} & \text{when } t \to \infty \end{array} \right\}, \tag{9}$$

where $T_L = \int_0^\infty R_L(\xi)d\xi$ is the Lagrangian integral time scale.

Because K-theory provides a Eulerian description of diffusion, it is necessary to transform (9) into Eulerian form. For this purpose, it is usual to apply the hypothesis of "frozen" turbulence and rewrite (9) as

$$\sigma_y = \left\{ \begin{array}{ll} \sigma_\theta \, x_s & \text{when } x_s \to 0 \\ \sigma_\theta \sqrt{2Lx_s} & \text{when } x_s \to \infty \end{array} \right\}. \tag{10}$$

Here, $\sigma_\theta = \sigma_v/U$, U is the characteristic mean wind velocity, $x_s = Ut$ is the distance downwind from the source, and $L = UT_L$. It was assumed that $U = u_f(H_s)$, the velocity over flat terrain at the source height.

In the full-scale, near-neutral atmosphere, for downwind distances up to about 10 km from the source (much larger than the distance to the maximum glc), a nearly linear growth of the crosswind spread of plumes with downwind distance is usually observed (Hunt, 1980). Because of the finite width of the wind tunnel, the low-frequency, large-scale lateral wind fluctuations are absent, and a transition from linear to square-root growth in plume width clearly begins. Therefore, in the present study, an interpolation formula was used which accounts for both asymptotic limits:

$$\sigma_y = \left[\frac{2\sigma_\theta^2 \, L \, x_s^2}{x_s + 2L} \right]^{1/2}. \tag{11}$$

From the wind-tunnel measurements, we have determined $\sigma_\theta = 0.14$ and $L = 0.4$ m.

Formula (11) is very close to the more usual equation derived by using an exponential shape for the autocorrelation function (Pasquill, 1974):

$$\sigma_y^2 = 2 \, \sigma_\theta^2 \, L^2 \left[x_s/L - 1 + \exp(-x_s/L) \right]. \tag{12}$$

Figure 29 compares the interpolation curve corresponding to Eq. (11) with experimental values of σ_y obtained from lateral concentration profiles measured downwind of sources of different height in the wind tunnel.

For source heights less than 400 mm, the results of the numerical solution of the diffusion equation showed only a small difference (in the range of 4%) between values of maximum glcs, χ_{mx}, when either Eq. (6) or Eq.

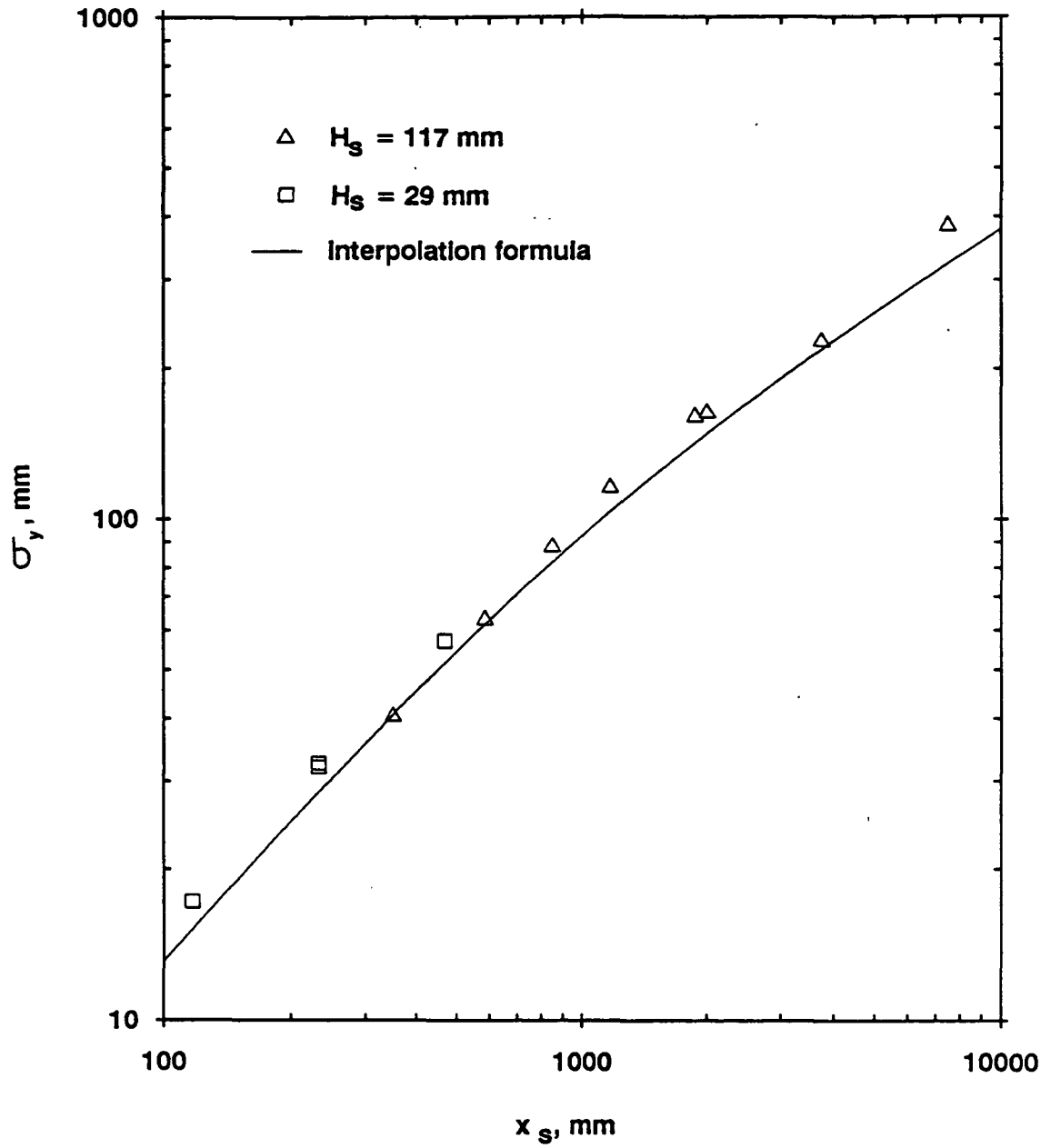

Figure 29. Growth of lateral plume width in flat terrain: comparison with interpolation formula (Eqn. 11).

(7) was used. The differences between the downwind distances from the source to the point of maximum glc, x_{mx}, however, were larger, and they increased more rapidly with height. For example, when H_s = 351 mm, the difference was about 16%.

Comparison of the calculations [using Eq. (6)] with the experimental results showed that the differences in χ_{mx} did not exceed 10% for the range of source heights between 117 and 234 mm. At the lower stack heights of 29 and 59 mm, the calculations were overpredictions of 14% and 11%, respectively. For the taller stacks of heights 293 and 351 mm, the calculations were underpredictions of 20% and 21%, respectively. With source heights between 29 and 293 mm, the differences in x_{mx} were less than 12.5%. For the stack height of 351 mm, the calculated x_{mx} was 17% larger than measured. Comparison of calculated and measured vertical concentration profiles downwind of an elevated point source show that the calculations overpredict the vertical spread of pollutants near the source. On the other hand, the experimental source was not, in fact, a "point" source. Its diameter (10 mm) was not small compared with the smallest source height (29 mm). Consequently, the behavior of the plume in this case could differ significantly from what might be considered a true point source.

Calculated and experimental values of χ_{mx} and x_{mx} and their dependence on source height are presented in Figures 30 and 31. Figure 32 shows the interrelationship between χ_{mx} and x_{mx}.

4.2 Calculations of Dispersion near Valleys

4.2.1 Generation of flow fields

As mentioned above, the model uses experimental data to reconstruct the entire flow field for use in the solution of the diffusion equation. The principal feature of the flow field is that it should be mass consistent, that is, it should satisfy the continuity equation. This problem was solved through the use of variational analysis techniques. A similar approach, initially based on the work of Sasaki (1958, 1970a, 1970b), has been used in regional-scale air-pollution modeling when the meteorological data in the region being investigated is taken as input information (Dickerson, 1978; Sherman, 1978; Pepper and Baker, 1979).

Before considering the mean wind field generation using wind-tunnel measurement data, let us consider how this wind field may be used in the solution of the diffusion equation. The diffusion equation may be written in

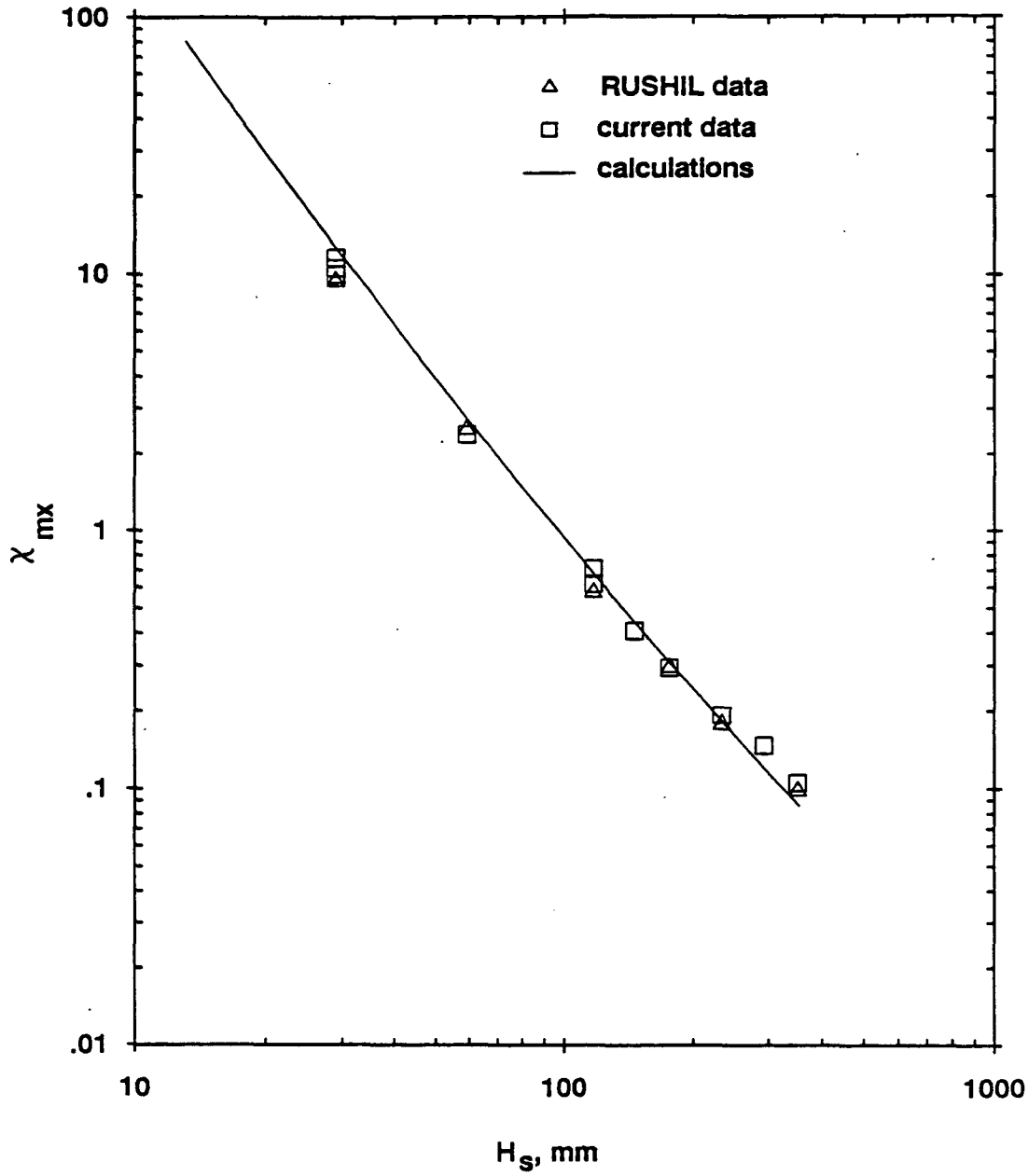

Figure 30. Dependence of χ_{mx} on source height H_s in flat terrain.

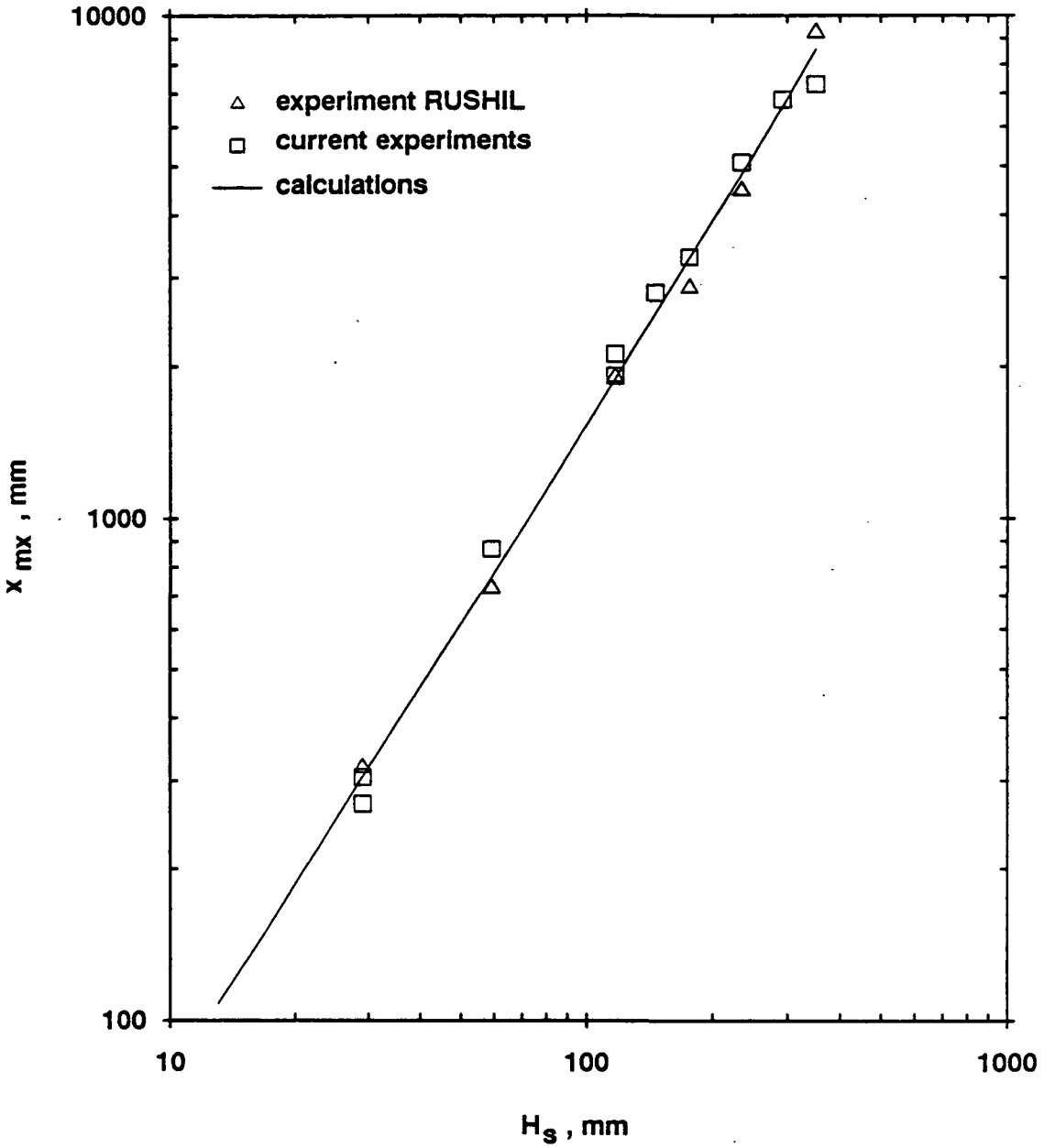

Figure 31. Dependence of x_{mx} on source height H_s in flat terrain.

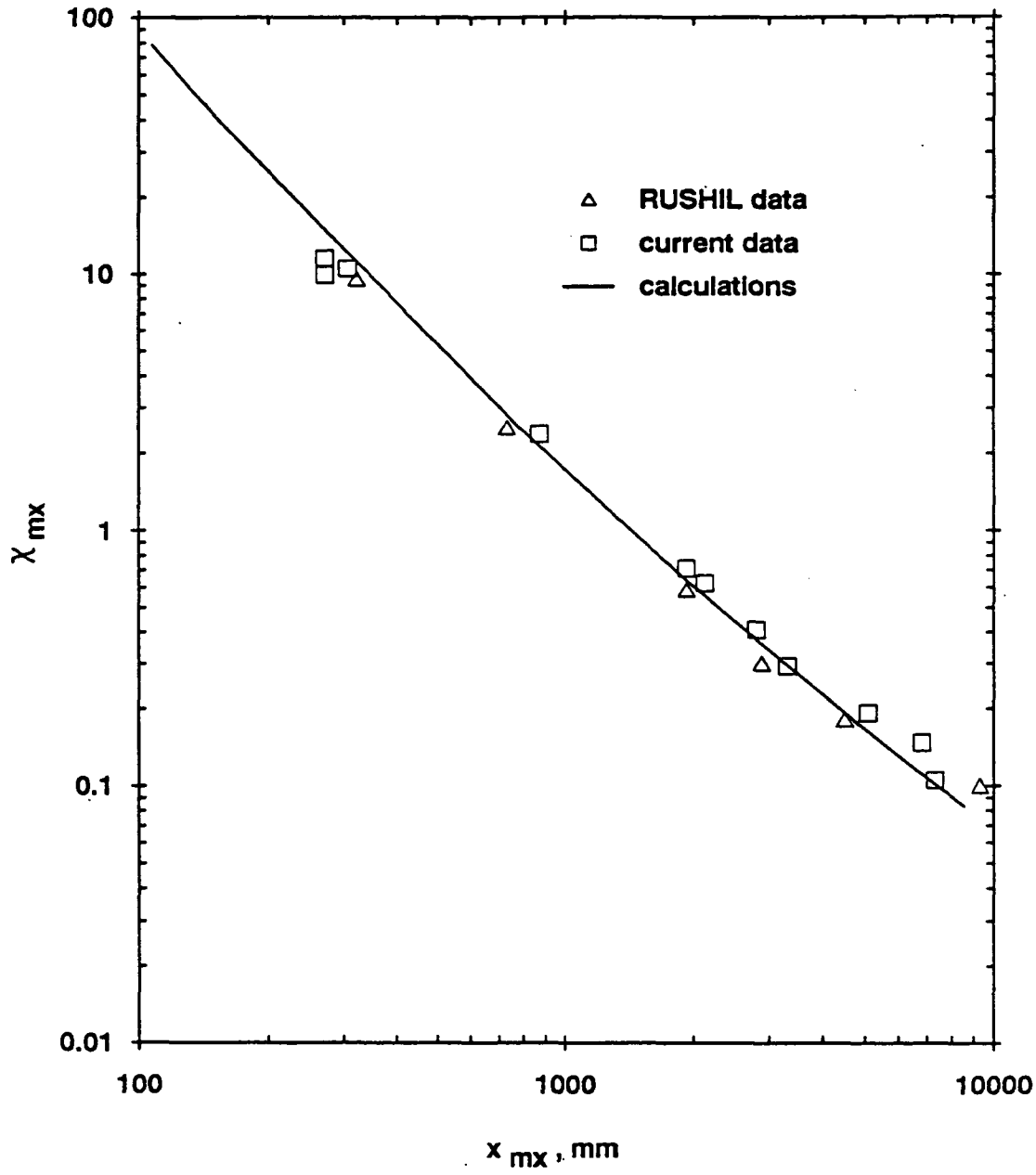

Figure 32. Relation between χ_{mx} and x_{mx} in flat terrain.

the following form

$$u \frac{\partial \chi}{\partial x} + w \frac{\partial \chi}{\partial z} = \frac{\partial}{\partial y} \left\{ k_y \frac{\partial \chi}{\partial y} \right\} + \frac{\partial}{\partial z} \left\{ k_z \frac{\partial \chi}{\partial z} \right\} , \tag{13}$$

where w is the vertical component of the mean velocity and all other notations are the same as used above. This form of the diffusion equation may be used if the slope of the terrain is small to moderate and only if the flow does not separate. In the case of complex terrain, the concentration from a point source may be related to the concentration from an infinite line source χ' using the same expression (Eq. 4) as in flat terrain. The concentration χ' will be the solution of the diffusion equation

$$u \frac{\partial \chi'}{\partial x} + w \frac{\partial \chi'}{\partial z} = \frac{\partial}{\partial z} \left\{ k_z \frac{\partial \chi'}{\partial z} \right\} . \tag{14}$$

To simplify the problem, it is convenient to transform the solution domain to a half-plane. For this purpose, the following substitution of variables may be used

$$x' = x, \quad z' = H[z - h(x)]/[H - h(x)] , \tag{15}$$

transforming the area $(-\infty < x < \infty) \times [h(x) \leq z \leq H]$ to the strip $(-\infty < x' < \infty) \times (0 \leq z' \leq H)$. Here h(x) is the valley depth (≤ 0), and H is the level above which the influence of the valley on the flow structure is not important. Within the strip $0 \leq z' \leq H$, Eq. (15) may be rewritten as

$$\hat{u} \frac{\partial \chi'}{\partial x'} + \hat{w} \frac{\partial \chi'}{\partial z'} = \frac{\partial}{\partial z'} \left\{ \hat{k}_z \frac{\partial \chi'}{\partial z'} \right\} , \tag{16}$$

where $\hat{u} = \frac{H - h(x')}{H} u$; $\hat{w} = w + \frac{z' - H}{H} u \frac{dh}{dx'}$; and $\hat{k}_z = \frac{H}{H - h(x')} k_z$.

The quantities $\hat{u}$ and $\hat{w}$ are defined such that they satisfy the equation

$$\frac{\partial \hat{u}}{\partial x'} + \frac{\partial \hat{w}}{\partial z'} = 0 , \tag{17}$$

provided the initial components of velocity u and w satisfy the continuity equation

$$\frac{\partial u}{\partial x} + \frac{\partial w}{\partial z} = 0 .$$

To generate a mass-consistent flow field with measured data, we consider the solution of Eq. (16) for the diffusion problem formulated above. In this case, the task is reduced to minimization of the functional

$$I(\psi) = \iint_{\mathbb{R}} dx'\, dz' \left[\left(\frac{\partial \psi}{\partial z'} - a \right)^2 + \left(\frac{\partial \psi}{\partial x'} + b \right)^2 \right] . \tag{18}$$

Here, ψ is the stream function of the flow, $\partial\psi/\partial z' = \hat{u}$, $\partial\psi/\partial x' = -\hat{w}$. The stream function ψ, which minimizes the functional I, corresponds to the flow for which values of $\hat{u}$ and $\hat{w}$ are closest to the corresponding measured values a and b (in the mean-squared sense) within the domain $\mathbb{R}$. The latter should be chosen in such a way that perturbations of the flow on its boundary $\partial\mathbb{R}$ could be assumed equal to zero.

The Euler equation for the variational problem under consideration is

$$\frac{\partial^2 \psi}{\partial x'^2} + \frac{\partial^2 \psi}{\partial z'^2} = \frac{\partial a}{\partial z'} - \frac{\partial b}{\partial x'} . \tag{19}$$

Introducing the stream function of the approach flow $\psi^o(z')$ and quantities ψ' and a' as follows

$$\psi = \psi^o(z') + \psi'(x',z'); \quad a = d\psi^o/dz' + a' , \tag{20}$$

it is possible to rewrite Eq. (19) as

$$\frac{\partial^2 \psi'}{\partial x'^2} + \frac{\partial^2 \psi'}{\partial z'^2} = \frac{\partial a'}{\partial z'} - \frac{\partial b}{\partial x'} . \tag{21}$$

The function $\psi = \psi^o + \psi'$ minimizes the functional (18) if the function ψ' is the solution of Eq. (21) with the boundary condition

$$\psi'|_{\partial\mathbb{R}} = 0 . \tag{22}$$

This boundary value problem, Eqs. (21) and (22), which is actually the Dirichlet problem for the Poisson equation, was solved numerically using a finite difference method. Since the domain $\mathbb{R}$ may be chosen to have a rectangular shape, a direct method with the fast Fourier transform technique (Ogura, 1969) was used for the solution. Calculations have been made for valleys 8 and 5 described in Section 2.

In principal, the technique used above allows reconstruction of the mean wind field for recirculating flows. However, the form of the diffusion equation (13) is not appropriate for application to separated flows, because the longitudinal diffusion term is omitted. From the wind-tunnel data, the flow clearly separated and a recirculation region was formed within valley 3. Hence, the mean wind field was not generated for valley 3.

The results of the flow field generation for valleys 5 and 8 are presented in Tables 1 and 2. These tables show values of longitudinal mean velocities at some typical locations near the valleys. Measured values of wind speed over flat terrain as calculated with the log-law wind profile (Eq. 5) are also included in the tables for comparison. All of the flow measurements in valley 8 were made with the hot-wire anemometer; whereas those measurements at lower levels in valley 5, where the turbulence intensities were high, were made with the pulsed-wire anemometer.

Table 1 shows measured and calculated values for valley 8 with differences that do not exceed 6%. Table 2 shows similar differences for valley 5 at locations x/a = -1.0 and x/a = 1.0. However, for position x/a = 0.0, the differences are noticeably larger and average about 10%. The larger differences at this position may be partly due to the method of obtaining the measured values. The mean longitudinal velocities obtained from the pulsed-wire anemometer were used in conjunction with the flow directions indicated by the hot-wire anemometer.

Figures 18b and c showed the calculated streamlines for valleys 5 and 8, respectively. The streamline pattern for valley 8 is asymmetric; for valley 5, the asymmetry is even stronger. A hint of a stagnation zone is seen near the bottom of valley 5.

4.2.2 Calculation of eddy diffusivities

Crosswind dispersion was calculated by using Eq. (9). The diffusion equation gives an Eulerian description of diffusion and, in the case of a continuous source, time is not explicitly included in the equation; therefore, the hypothesis of "frozen" turbulence was used as in the flat terrain calculations. It was assumed that the typical speed of pollutant transport u_s is equal to the speed of the mean flow along the streamline which passes through the source position. Since the mean flow velocity over complex terrain differs from that over flat terrain, the time of pollutant transport to a given distance will also differ.

Under the above assumptions, the time t of pollutant transport to a distance x_s downwind of the source is

$$t = \int_0^{x_s} \frac{dx'}{u_s(x')} . \tag{23}$$

Substituting this into Eq. (9) gives an expression for σ_y as a function of

downwind distance. The eddy diffusivity k_y is determined through σ_y in the same way as for flat terrain.

Table 1. Values of mean longitudinal velocity (m s^{-1}) near valley 8

Height above the ground (mm)	Flat terrain	upstream edge x/a = -1.0		center x/a = 0.0		downstream edge x/a = 1.0	
		meas	calc	meas	calc	meas	calc
5	1.61	2.09	1.97	1.21	1.14	2.12	2.00
15	2.11	2.55	2.46	1.36	1.30	2.86	2.70
30	2.43	2.85	2.79	1.59	1.56	3.05	2.90
50	2.66	3.08	3.00	1.89	1.88	3.17	3.04
75	2.85	3.22	3.16	2.17	2.18	3.21	3.13
100	2.98	3.33	3.25	2.42	2.40	3.30	3.22

Table 2. Values of mean longitudinal velocity (m s^{-1}) near valley 5

Height above the ground (mm)	Flat terrain	upstream edge x/a=-1.0		center x/a = 0.0		downstream edge x/a = 1.0	
		meas	calc	meas	calc	meas	calc
5	1.61	2.21	2.10	--	0.11	2.47	2.33
15	2.11	2.63	2.56	0.26	0.27	2.97	2.79
30	2.43	2.95	2.87	0.53	0.58	3.00	2.86
50	2.66	3.11	3.04	0.87	0.97	3.06	2.97
75	2.85	3.26	3.17	1.25	1.47	3.18	3.12
100	2.98	3.30	3.27	1.87	1.96	3.29	3.21

Equation (10) shows that for flat terrain σ_y is proportional to $\sigma_\theta \approx \sigma_v/u_f(H_s)$. (Note that in complex terrain, $U = u_s$). For more convenient comparison of formulas for flat and complex terrain, Eq. (20) may be rewritten in the form

$$t = \sigma_\theta x_1 , \tag{24}$$

where $x_1 = \int_0^{x_s} \frac{u_f(H_s)}{u_s(x')} dx'$. In this case, by using Eq. (24), Eq. (10) can be

rewritten as

$$\sigma_y = \left\{ \begin{array}{ll} \sigma_\theta x_1 & \text{when} \quad x_1 \rightarrow 0 \\ \sigma_\theta \sqrt{2\ L\ x_1} & \text{when} \quad x_1 \rightarrow \infty \end{array} \right\} . \tag{25}$$

When calculating pollutant dispersion over flat terrain it was assumed, as is usually suggested for Gaussian-type diffusion models, that σ_θ does not depend on source height. Wind-tunnel measurements (Khurshudyan *et al.*, 1981) support this assumption. Nevertheless, in complex terrain the distortion of turbulent flow characteristics near the ground may noticeably change the situation. Only a few measurements of σ_v had been made in the wind tunnel at the time the calculations were made. Therefore, the values of σ_θ used in Eq. (25) were chosen by comparing values of σ_y calculated from this formula with those obtained from measured lateral profiles of concentration. Direct measurements of σ_v showed that at the center of valley 5 and at heights below 100 mm, values of σ_v are about twice those for flat terrain.

When comparing calculated and measured values of σ_y, it is best to incorporate the finite size of the release. The finite size of the source can be accounted for to some extent by determining the distance a virtual point source would need to be located upstream of the true source position to produce a similar plume. By measuring lateral and vertical profiles of concentration near the source over flat terrain, this distance was determined to be approximately 26 mm. For sources near the valley, the distance from the real source to the virtual source would likely depend on the source location. Since no evaluations were made of the virtual source distances for sources within the valleys, the calculations were made by using distances from the center of the true source. For that reason, calculated values of σ_y are given below for ranges of x_s corresponding to positions where measurements were made. For valley 8 with a source height of 29 mm at position x/a = 1.0, the measured $\sigma_y(x_s = 176 \text{ mm}) = 23$ mm. The calculated values of σ_y for this source location are $\sigma_y(176 \text{ mm}) = 19$ mm, $\sigma_y(199 \text{ mm}) = 22$ mm, and $\sigma_y(211 \text{ mm}) = 23$ mm. For the source at position x/a = 0.0, all other parameters the same, the measurements give $\sigma_y(88 \text{ mm}) = 23$ mm and the calculated values are $\sigma_y(88 \text{ mm}) = 17$ mm, $\sigma_y(111 \text{ mm}) = 22$ mm, and $\sigma_y(123 \text{ mm}) = 24$ mm. All calculated values of σ_y were obtained by taking $\sigma_\theta = 0.14$, as was the case for flat terrain. The comparison of values of σ_y obtained from model calculations and from measurements provide insufficient evidence for changing σ_θ for valley 8. For

the case of valley 5 with a source height of 29 mm at position x/a = 0.0, the measurements of σ_v suggest using σ_θ = 0.28. Corresponding calculations give σ_y(88 mm) = 78 mm, σ_y(99 mm) = 86 mm; the measurements gave σ_y(88 mm) = 78 mm. These comparisons show that the model used for calculating crosswind pollutant spreading predicts satisfactory values of σ_y.

The vertical eddy diffusivities k_m were calculated directly by using Eq. (6) with the lower limit of integration changed to h(x), the local depth of the valley. Because σ_v measurements from the wind tunnel were not available at the time of calculations, it was assumed that $\sigma_v(x,z) = 0.72\sigma_u(x,z)$ for turbulent energy calculations. This relationship was derived under the assumption that the ratio of σ_u to σ_v near valleys would be the same as over flat terrain, where measurements in the lower part of the boundary layer gave $\sigma_u = 2.5u_*$ and $\sigma_v = 1.8u_*$. In Figures 33 and 34, vertical profiles of k_m for typical locations relative to a valley are presented and compared with the profiles over flat terrain. The calculated values of k_m were generally increased near the valleys as compared with those in flat terrain. This was especially pronounced over the bottoms of valleys. The steeper valley 5 disturbed the turbulent characteristics of the flow to a larger degree than valley 8.

When solving the diffusion equation, it was assumed that the pollutant vertical eddy diffusivity $k_{z'} = 1.15k_m$, as in the case of flat terrain.

4.2.3 Calculation of pollutant spreading and terrain amplification factors

Calculations of pollutant transport and diffusion were made by numerical solution of the diffusion equation (13) with boundary conditions analogous to those for flat terrain (the lower boundary condition was taken at z = h(x)). The diffusion equation was first solved for a line source with the result then adapted to a point source by applying Eq. (4) with calculated values of σ_y. The numerical solution of Eq. (16) was obtained by using a finite difference method. In the term $\hat{w}\partial\chi'/\partial z'$, $\hat{w}$ may be positive or negative, even at fixed x′ through its dependence on z′; thus, it is difficult to find a finite-difference scheme that is absolutely stable over the entire domain of the solution. Eq. (16) was reduced to the following equivalent form (Samarskii, 1977)

$$\hat{u}\,\frac{\partial\chi'}{\partial x'} = \frac{1}{f}\,\frac{\partial}{\partial z'}\,f\,\hat{k}_z\,\frac{\partial\chi'}{\partial z'}\,, \qquad (26)$$

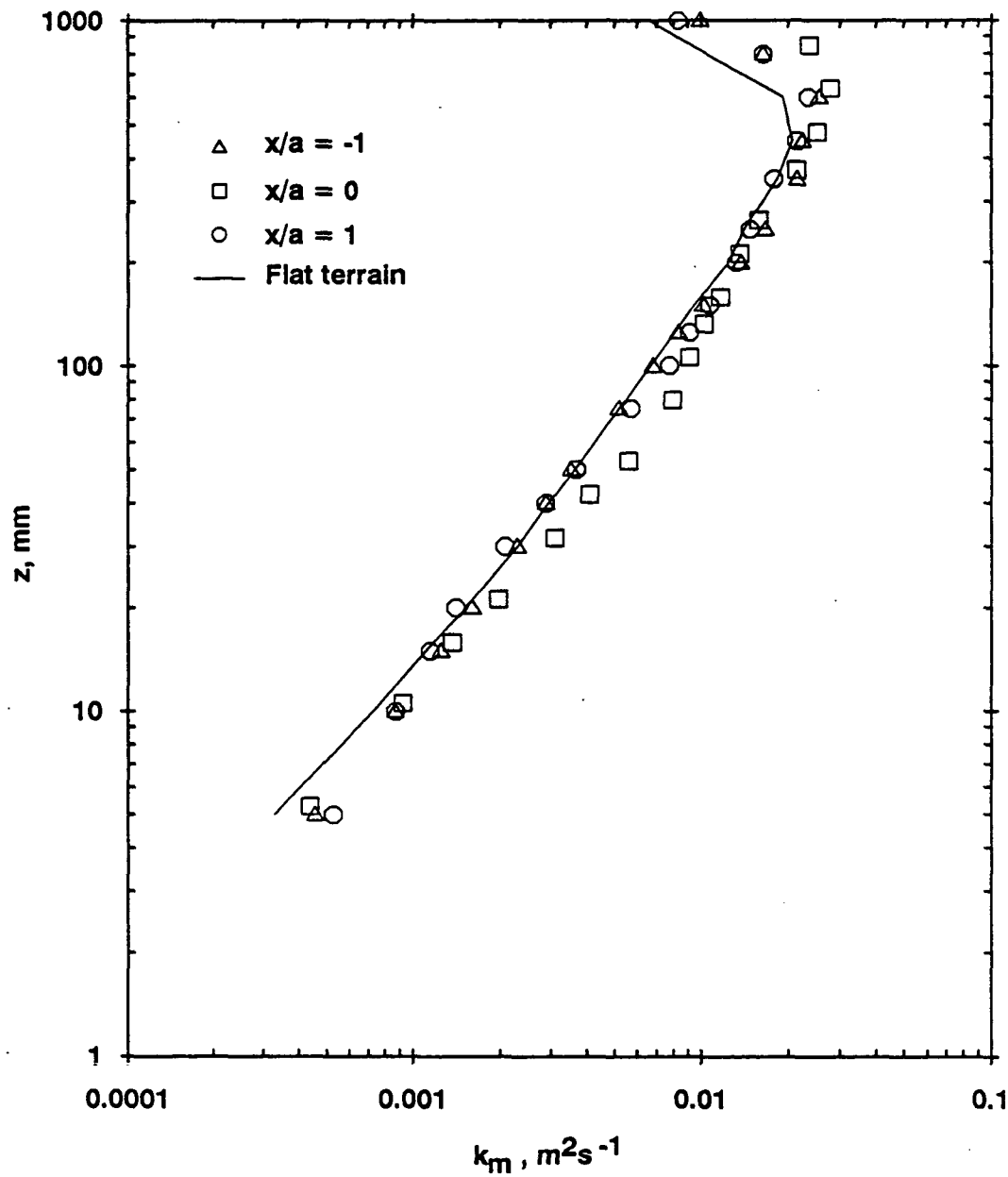

Figure 33. Vertical profile of diffusivity k_m over valley 8.

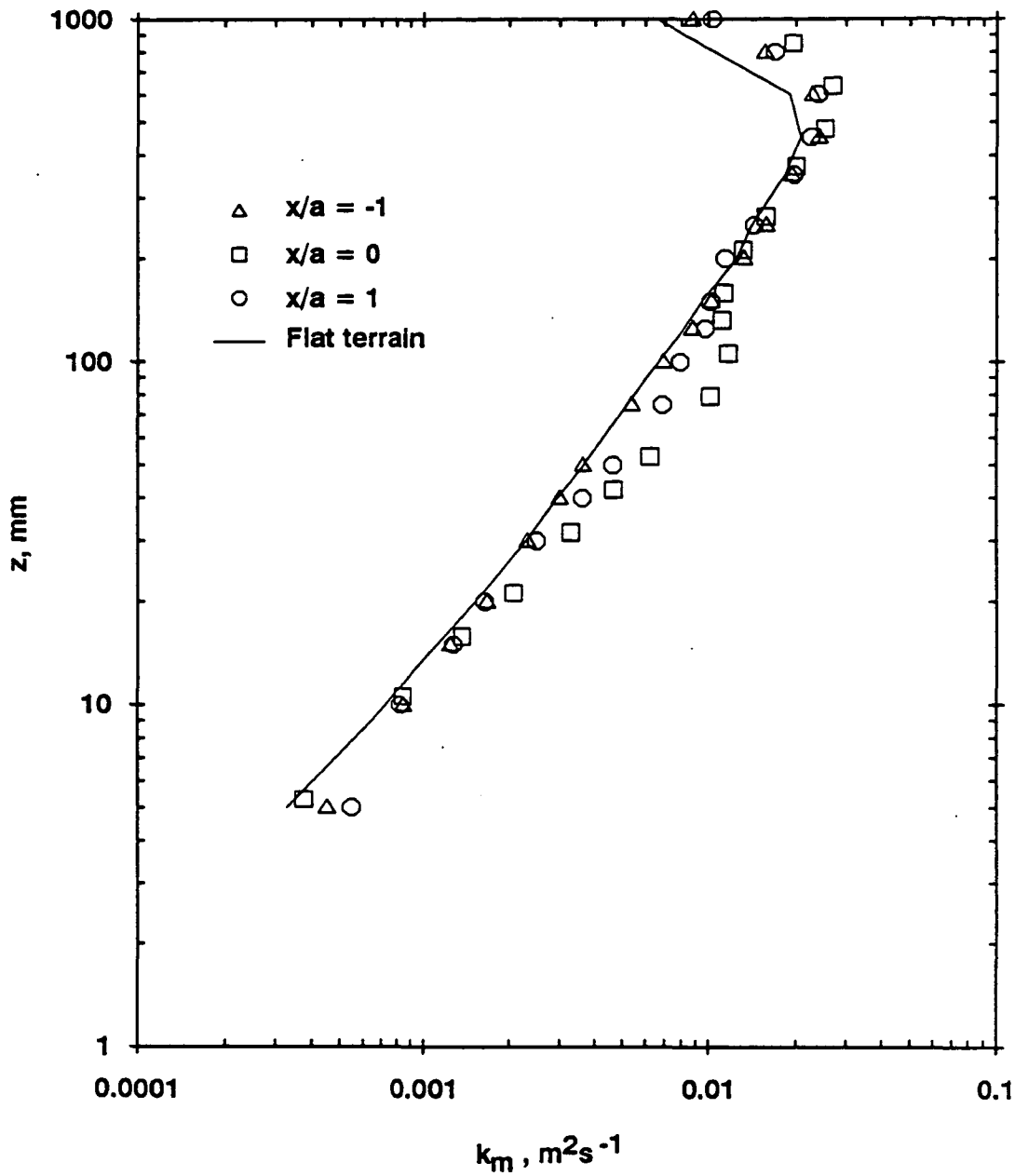

Figure 34. Vertical profile of diffusivity k_m over valley 5.

where

$$f = \exp\left(- \int_0^{z'} \frac{\hat{w}}{\hat{k}} \, dz' \right) . \tag{27}$$

Eq. (26) was solved with an explicit-implicit scheme (except for a few steps on x' near the source) which is conservative in the sense of preserving the integral horizontal pollutant flux.

By using calculated maximum ground-level concentrations χ_{mx} for sources of different heights and locations, as well as those χ^{o}_{mx} for sources situated over flat surfaces, terrain amplification factors $A = \chi_{mx}/\chi^{o}_{mx}$ were derived. Values of A depend on source height, source location relative to the valley, and the shape of the valley. Table 3 presents the calculated values of A for valley 8. For comparison, the values derived from the experimental data are shown. The agreement between calculated and experimental results is quite satisfactory in general. The discrepancies are mostly in the range of 30% and often significantly less. The same is true for the downwind distance from the source to the location of the maximum ground-level concentration. Consider the calculated values of A, shown in Table 3, when the source is located at the position one-quarter of the half-width of the valley upwind of the center of the valley. It is seen that for low sources, A is largest when the source is located slightly upwind of the valley center. For a hill, however, the largest TAFs occur when the source is located just above the downwind base of the hill. This has been discussed by Berlyand *et al.* (1983), who made theoretical calculations of flow structure and pollutant dispersion near two-dimensional valleys.

The numerical model is not strictly appropriate for calculating pollutant dispersion in flows such as measured for valley 5 in the wind tunnel. The streamlines of the flow near the bottom of the valley are severely distorted, and the wind speed close to the ground is much less than that over flat terrain. In this case, the diffusion equation without a term for longitudinal turbulent diffusion might produce large errors in the predicted pollutant spread. Moreover, the generation of the mean wind field in the stagnating flow region near the bottom of the valley demands more refined computational techniques than used for smoother flows. When there are large gradients of σ_v in the longitudinal and vertical directions, as was suggested from measurements with valley 5, the method described above for calculating σ_y should be modified in some way to incorporate the dependence of σ_v on x and z. Nevertheless, the calculations of TAFs for valley 5 were made, and the results

are presented in Table 4. It should be noted here that, according to measured data, for low sources placed near the bottom of valley 5, the values of σ_v used in the calculation of σ_y were 1.5 to 2.0 times those for flat terrain. One can see that despite the above-mentioned difficulties, the results are reasonable from a practical point of view.

Contour maps of constant TAF as predicted by the model are shown in Fig. 35. These are to be compared with the measurements shown in Fig. 25. The maps for valley 8 show generally similar overall patterns, but differ in several details. The vertical extent of the 40%-excess window (the TAF = 1.4 contour) extends to about 1.5 h from the measurements, but to only 1.25 h from the model predictions. The horizontal extent of the measured window is

Table 3. Values of TAF for sources near valley 8

Source height	Source Location											
	x/a =-1		x/a=-0.5		x/a=-0.25		x/a = 0.0		x/a = 0.5		x/a=1.0	
(H_s/h)	meas	calc	meas	calc	meas	calc	meas	calc	meas	calc	meas	calc
0.25	0.97	0.93	2.50	2.14	--	2.53	2.30	2.02	--	1.09	0.74	0.89
0.50	0.80	0.96	2.05	1.96	--	2.36	2.50	1.97	1.42	1.27	0.83	0.86
1.00	0.99	0.96	1.73	1.50	--	1.88	2.28	1.87	1.60	1.25	1.13	0.87
1.50	1.13	0.96	1.58	1.35	--	1.62	2.53	1.65	1.61	1.24	1.13	0.92
2.00	--	0.96	1.32	1.22	--	1.46	1.76	1.50	1.45	1.17	--	0.92

Table 4. Values of TAF for sources near valley 5

Source height	Source Location									
	x/a = -1		x/a=-0.5		x/a=0.0		x/a=0.5		x/a=1.0	
(H_s/h)	meas	calc	meas	calc	meas	calc	meas	calc	meas	calc
0.25	0.62	0.89	3.19	4.75	5.01	7.71	2.15	2.16	0.80	0.80
0.50	0.84	1.32	3.34	3.91	6.71	4.67	2.83	2.26	0.99	0.84
1.00	1.31	1.12	2.72	2.05	5.57	3.35	2.21	1.92	1.10	0.85
1.50	1.21	1.01	2.00	1.89	3.82	2.98	2.05	1.52	1.26	0.97
2.00	--	0.98	1.61	1.45	2.36	2.06	1.58	1.41	--	1.05

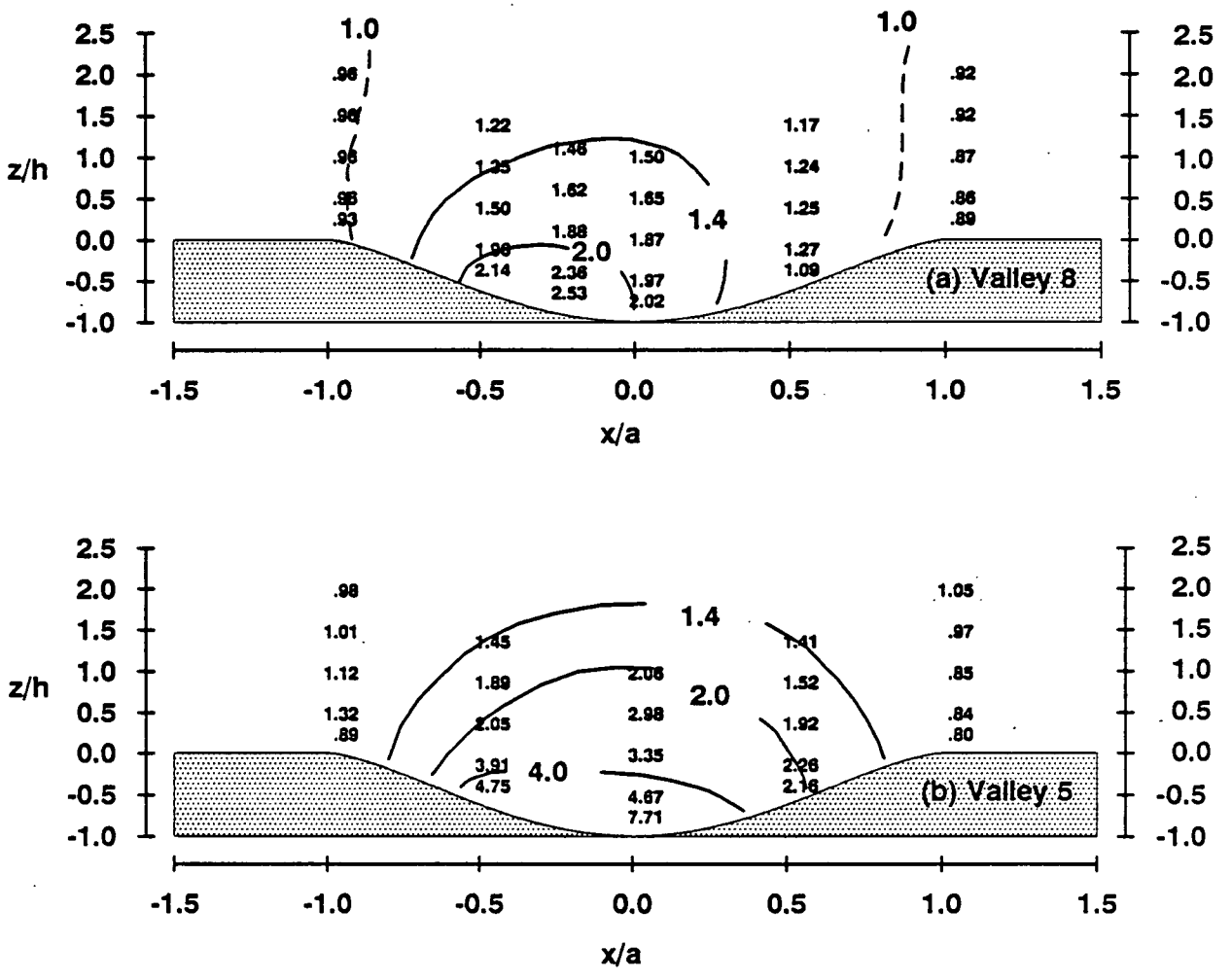

Figure 35. Contours of constant terrain amplification factor derived from model calculations.

somewhat larger than that of the model-predicted window. The model-predicted window is shifted somewhat upstream and whereas the resolution of the grid used for the experimental measurements was rather coarse, a hint of an upstream shift is also observed there. The model generally predicts larger TAFs to occur at lower elevations, whereas the measurements show elevated maxima. Both predicted and observed TAFs were generally less than unity when the source was at the upstream or downstream edge of the valley. Maximum TAF values are quite close to one another. Generally similar statements may be made when comparing the calculated and observed TAF maps for valley 5, but the differences are somewhat larger.

5. CONCLUSIONS

The laboratory work has provided a reasonable simulation of the flow structure and diffusion characteristics of the neutral atmospheric boundary layer. The model valleys were idealized in shape, but should cover the range of a majority of valleys to be found at full scale, at least in terms of the basic classes of flow structure that may be observed. Valley 8 was rather gentle in slope, and the flow over it may be characterized as relatively smooth and well-behaved. Valley 5, being steeper in slope, caused the flow to separate intermittently, but not in the mean. In valley 3, the steepest, the flow clearly separated a short distance from the upstream edge, and a recirculating flow was formed within the valley. Pollutants released at the same relative locations within each of these valleys behave very differently from one another, and the resulting surface concentration patterns are dramatically different.

The overall effects of the valleys on surface concentrations are characterized in terms of terrain amplification factors (TAFs), defined as the ratios of maximum ground-level concentrations from sources located within the valleys to the maxima that would exist from identical sources located in flat terrain. Maps of these TAFs are provided for each valley. Also provided are maps detailing the distances to locations where these maximum ground-level concentrations will occur. These maps allow a practitioner to quickly and easily assess the likely impact of a source located in a valley, and the location where that maximum impact will occur.

A two-dimensional theoretical model that uses a variational analysis technique was applied to the wind-tunnel measurements of the flow structure near the valleys to produce mass-consistent mean wind fields. Measurements of the turbulent fluctuating velocities were also used to calculate vertical and crosswind eddy diffusivities. The diffusion equation was then solved numerically to obtain maximum ground-level concentrations from elevated point sources of various heights near valleys 8 and 5, as well as over flat terrain. The calculated and measured concentrations for flat terrain showed good agreement.

Comparison of calculated and measured TAFs for valley 8 showed satisfactory agreement. Valley 5 exhibited more severe streamline distortion and a stagnation region with large fluctuating velocities near the bottom of the valley, and therefore the differences between calculated and measured TAFs

were rather significant in some cases. The absence of the longitudinal diffusion term in the diffusion equation (turbulence intensities in the bottom of valley 5 were extremely large) and the complexity of modeling eddy diffusivities in such flows affect the performance of the numerical model. A better method of incorporating the effects of crosswind dispersion should be developed, because even in these two-dimensional mean flows, turbulent diffusion is a three-dimensional phenomenon. These effects are more pronounced in the case of complex terrain.

Finally, it may be concluded that, in spite of the many problems, K-theory may be applied with a reasonable measure of success to the calculation of maximum ground-level concentrations from sources in curvilinear flows, even near rather steep obstacles. More sophisticated modeling of diffusivities and use of an elliptical diffusion equation should improve upon the present results.

REFERENCES

Arya S.P.S. and Shipman M.S. (1981) An experimental investigation of flow and diffusion in the disturbed boundary layer over a ridge, Part I: mean flow and turbulence structure. *Atmospheric Environment* **15**:1173-84.

Arya S.P.S., Shipman M.S. and Courtney L.Y. (1981) An experimental investigation of flow and diffusion in the disturbed boundary layer over a ridge, Part II: diffusion from a continuous point source. *Atmospheric Environment* **15**:1185-94.

Bearman P.W. (1971) Corrections for the effects of ambient temperature drift on hot-wire measurements in incompressible flow. *DISA Information* **11**:25-30.

Berlyand M.E. *(1975) Contemporary Problems of Atmospheric Diffusion and Air Pollution.* Hydromet Press, Leningrad, USSR 448p.

Berlyand M.E. and Genikhovich E.L. (1971) Atmospheric diffusion and the structure of the air flow above an inhomogeneous surface. Proceedings, *International Symposium on Meteorological Aspects of Air Pollution*, 1968, Leningrad, Hydromet Press, Leningrad, USSR pp. 49-69.

Berlyand M.E., Genikhovich E.L. and Gracheva I.G. (1983) The influence of thermally nonuniform complex terrain on the structure of air flow and characteristics of pollutant dispersion. *Trudy GGO*, Hydromet Press, Leningrad, USSR **467**:3-20.

Berlyand M.E., Genikhovich E.L., Gracheva I.G., Khurshudyan L.H., Nekrasov I.V. and Khudyakov G.E. (1987) Structure of atmospheric boundary layer and peculiarities of turbulent diffusion in complex and thermally nonuniform relief conditions. Proceedings, *WMO Conference on Air Pollution Modelling and its Application*, May 19-24, 1986, Document WMO/TD No. 187, Leningrad, USSR, **1**:116-24.

Berlyand M.E., Genikhovich E.L. and Khurshudyan L.H. (1975) Use of the results of modeling of an air stream in wind tunnels for the calculation of air pollution. *Atmospheric Diffusion and Air Pollution, Trudy GGO*, Hydromet Press, Leningrad, USSR (EPA Trans. TR-79-0431) **352**:3-15.

Bradbury L.J.S. and Castro I.P. (1971) A pulsed-wire technique for velocity measurements in highly turbulent flows. *Journal of Fluid Mechanics* **49**:657-91.

Castro I.P. and Snyder W.H. (1982) A wind tunnel study of dispersion from sources downwind of three-dimensional hills. *Atmospheric Environment* **16**:1869-87.

Dickerson M.H. *(1978)* MASCON – A mass consistent atmospheric flux model for regions with complex terrain. *Journal of Applied Meteorology* **17**:241-53.

EPA (1985) Guideline for determination of good engineering practice stack height (technical support for the stack height regulations – revised). EPA-450/4-80-023R, *U.S. Environmental Protection Agency*, Research Triangle Park, NC 102p.

Gifford F.A., Jr. (1975) A review of turbulent diffusion typing schemes. ATDL 75/2, *Atmospheric Turbulence and Diffusion Laboratory,* National Oceanic and Atmospheric Administration, Environmental Research Laboratory, Oak Ridge, TN 58p.

Harrison H. (1987) WYNDValley: an air quality model for near-stagnant flows in constricted terrain. EPA-910/9-87/179, *NTIS* PB 88-158968, U.S. Environmental Protection Agency, Seattle, WA 48p.

Harrison H. (1988) A user's guide to WYNDvalley 2.10. *WYNDsoft, Inc.*, 6333 77th Avenue, SE, Mercer Island, WA 98040 42p.

Hosker R.P. (1974) Estimates of dry deposition and plume depletion over forests and grassland. Paper No. I, Proceedings, *Symposium Physical Behavior of Radioactive Contaminants in the Atmosphere*, AEA-SM-181/19, International Atomic Energy Agency, Vienna pp. 291-308.

Hunt J.C.R. (1980) Recent developments and trends in physical and mathematical modeling. Proceedings, *Fifth International Conference on Wind Engineering*, Ft. Collins, CO, Pergamon Press, New York, NY **2**:957-64.

Hunt J.C.R., Puttock J.S. and Snyder W.H. (1979) Turbulent diffusion from a point source in stratified and neutral flows around a three-dimensional hill: Part I: diffusion equation analysis. *Atmospheric Environment* **13**:1227-39.

Hydromet State Committee (1987) Techniques of calculation of industrial pollutant concentrations in the atmospheric air. *All-Union Standard Document*, Hydromet Press, Leningrad, USSR 93p.

Kader B.A. and Yaglom A.M. (1972) Heat and mass transfer laws for fully turbulent wall flows. *International Journal of Heat Mass Transfer* **15**:2329-51.

Khurshudyan L.H., Snyder W.H. and Nekrasov I.V. (1981) Flow and dispersion of pollutants over two-dimensional hills: summary report on joint Soviet-American study. EPA-600/4-81-067, *U.S. Environmental Protection Agency*, Research Triangle Park, NC 143p.

Lawson R.E., Jr. (1984) Standard operating procedures for the EPA Fluid Modeling Facility. *FMF Internal Document*, U.S. Environmental Protection Agency, Research Triangle Park, NC 132p.

Lawson R.E. Jr., Snyder W.H. and Thompson R.S. (1989) Estimation of maximum surface concentrations from sources near complex terrain in neutral flow. *Atmospheric Environment* **23**:321-331.

Ogura M. (1969) A direct solution of poisson equation by dimension reduction method. *Journal of Meteorological Society*, Japan **47**, no. 4.

Paine R.J., Strimaitis D.G., Dennis M.G., Yamaotino R.J., Mills M.T., and Insley E.M. (1987) User's guide to the complex terrain dispersion model: model description and user's instructions. EPA/600/8-87/058a, *U.S. Environmental Protection Agency*, Research Triangle Park, NC **1**, 155p.

Pasquill F. (1974) *Atmospheric Diffusion*. 2nd Ed., Ellis Horwood Ltd., Chichester, John Wiley & Sons, New York, NY 429p.

Pepper D.W. and Baker A.J. (1979) Modeling pollutant dispersion over irregular terrain with second moments and cubic splines. Proceedings, *Fourth Symposium on Turbulence and Diffusion in Air Pollution*, Reno, NV, American Meteorological Society, Boston, MA.

Porch W.M., Barr S., Clements W.E., Archuleta J.A., Fernandez A.B., King C.W., Neff W.D. and Hosker R.P. (1989) Smoke slow visualization in a tributary of a deep valley. *Bulletin American Meteorological Society* **70**:30-35.

Samarskii, A.A. (1977) *Theory of Finite Difference Schemes.* Nauka Press Moscow, USSR, 656p.

Sasaki Y. (1958) An objective analysis based on the variational method. *Journal of Meteorological Society*, Japan **36**:77-88.

Sasaki Y. (1970a) Some basic formalisms in numerical variational analysis. *Monthly Weather Review* **98**:875-83.

Sasaki Y. (1970b) Numerical variational analysis formulated under the constraints determined by long wave equations and low-pass filter. *Monthly Weather Review* **98**:884-98.

Sherman C.A. (1978) A mass-consistent model for wind fields over complex terrain. *Journal of Applied Meteorology* **17**:312-9.

Shipman M.S. (1988) Fluid Modeling Facility computer user's guide. *FMF Internal Document*, Version 6, U.S. Environmental Protection Agency, Research Triangle Park, NC 96p.

Smith F.B. (1973) A scheme for estimating the vertical dispersion of a plume from a source near ground level. Proceedings, Chapter 17, *Third Meeting of Expert the Panel on Air Pollution Modeling*, Oct., 1972, N.A.T.O. CCMS, Paris, France; also Proceedings No. 14, *U.S. Environmental Protection Agency*, Research Triangle Park, NC.

Snijders A.L., Koppius A.M. and Nieuwvelt C. (1983) An experimental determination of the turbulent prandtl number in the inner boundary layer for air flow over a flat plate. *International Journal of Heat Mass Transfer* **26**:425-31.

Snyder W.H. (1979) The EPA meteorological wind tunnel: its design, construction, and operating characteristics. EPA-600/4-79-051, *U.S. Environmental Protection Agency*, Research Triangle Park, NC 78p.

Snyder W.H. (1983) Fluid modeling of terrain aerodynamics and plume dispersion -- a perspective view. Keynote Paper, Preprint Vol., *Sixth Symposium on Turbulence and Diffusion*, March 22-25, Boston, MA, American Meteorological Society, Boston, MA pp. 317-20.

Snyder W.H. and Britter R.E. (1987) A wind tunnel study of the flow structure and dispersion from sources upwind of three-dimensional hills. *Atmospheric Environment* **21**:735-51.

Strimaitis D.G., Paine R.J., Egan B.A. and Yamartino R.J. (1987) EPA complex terrain model development: final report. EPA-600/3-88/006, *U.S. Environmental Protection Agency*, Research Triangle Park, NC 463p.

Taylor G.I. (1921) Diffusion by continuous movements. Proceedings, *London Mathematical Society* **20**:196-212.

Turner D.B. (1970) Workbook of atmospheric dispersion estimates. *Office of Air Programs*, U.S. Environmental Protection Agency, Research Triangle Park, NC Pub. No. AP-26.